On the Challenges for Time-of-Flight Electron Spectroscopy at Storage Rings

Ståhlman, Christian

2014

On the Challenges for Time-of-Flight Electron Spectroscopy at Storage Rings

Christian Stråhlman

Licentiate Thesis
2014

Lund University

On the Challenges for Time-of-Flight Electron Spectroscopy at Storage Rings

Printed in Sweden by Media-Tryck, Lund, 2014

Cover design: Johan Winqvist

MAX IV Laboratory, Lund University
P.O. Box 118
SE–221 00 Lund
Sweden

http://www.maxiv.se/

ISBN 978-91-7623-165-4 (PRINT)
ISBN 978-91-7623-166-1 (PDF)

ABSTRACT

Time-of-flight (TOF) techniques for energy analysis have been common in electron spectroscopy for many decades. TOF-based electron spectrometers benefit from higher transmission and information rate compared to their main competitor: the hemispherical analyser; the drawback being their lower energy resolution. However, the advent of angle-resolved TOF spectrometers for electron energy analysis challenges this perception. State-of-the-art TOF analysers, such as the *Scienta ARTOF*, offer energy resolution comparable to the hemispherical analyser resolution, while keeping the high transmission. Electron TOF should therefore be valuable complementary instrumentation at any future high-brilliance storage rings such as MAX IV.

TOF instruments demand pulsed light with comparably low repetition rates. At storage rings they often rely on the availability of single bunch modes with lower pulse repetition rates. However, time-sharing limits the beamtime available both for timing based instrumentation and experiments, and for those demanding high intensity. Solutions to allow simultaneous operation are therefore critical for the user community. This thesis explores four classes of solutions: Accelerator adaptations, choppers, instrument gating and coincidence techniques. A review of accelerator adaptations, choppers and coincidence techniques is presented which in particular highlights future opportunities for timing based experiments at MAX IV.

With regard to gating, this thesis reports the development of an electronic gate for the ARTOF analyser. It is showed how a pulsed electric potential and a system of transmission meshes can be used to simulate single bunch operation and discard electrons which would be unresolvable in the analyser. One paper shows how a detector gate has been implemented to allow use of the instrument in hybrid mode at BESSY storage ring in Berlin. We show that detection efficiency can be increased more than ten times. A second paper discusses the necessary requirements to build a similar gate for the operation mode of the future MAX IV rings and outlines some initial experimental results.

POPULÄRVETENSKAPLIG BESKRIVNING

Den rykande startpistolen
eller
Konsten att ta tid på en flygande elektron

Flygande elektroner kan berätta mycket om hur världen sitter ihop. Elektroner som lämnar ytan av något material avslöjar både vilka atomer som finns i materialet och hur de kemiska bindingarna ser ut. Allt detta är nödvändigt att förstå när man vill utveckla nya material – till exempel för kretskort, solceller eller skärmar till smarta telefoner – eller förstå hur kemiska reaktioner går till olika miljöer – till exempel i en bilkatalysator.

Tekniken för att arbeta med de flygande elektronerna kallas *elektronspektroskopi*. När man bestrålar ett material med intensivt ljus tvingas elektronerna att flyga iväg. Deras flygriktning och fart kan berätta för oss hur materialet ser ut på mikroskopisk nivå. Elektronspektroskopi kräver därför två saker: en ljuskälla och en elektrondetektor. Den här uppsatsen handlar om mötet mellan dessa två. Å ena sidan världens skarpaste ljuskälla: den synkrotronljusproducerande lagringsringen. På andra sidan ett mätinstrument: flygtidsspektrometern. Båda dessa är mycket viktiga för elektronspektroskopin. Problemet är att de inte passar ihop.

En *lagringsring* är en partikelaccelerator där elektroner cirkulerar med nära ljusets hastighet. Medan de cirkulerar skapar de intensiva strålar av röntgenljus eller ultraviolett ljus. Vi kallar det för *synkrotronljus*. På MAX IV–laboratoriet finns tre lagringsringar där elektronerna skickas runt i grupper med tre meters avstånd. Eftersom elektronerna rör sig med ljusets hastighet är det med endast tio nanosekunders mellanrum som en elektrongrupp passerar experimentet och skickar ut en synkrotronljuspuls. Tio nanosekunder är en mycket kort tid, men andra lagringsringar kan ha ännu tätare mellan pulserna. Till exempel lagringsringen BESSY i Berlin, där avståndet bara är två nanosekunder.

Flygtidsspektrometern är ett instrument för att mäta en elektrons fart och flygriktning. Att mäta en elektrons fart med ett

Figure 1. *En tydlig startsignal är nödvändig för att ta tiden på ett lopp. Redan vid Olympiska spelen i S:t Louis 1904 blev den trefaldiga olympiska mästaren Archie Hahn skickad ur startgroparna med en startpistol. Startpistolen ger en ljudlig signal både till löparen och till tidtagaren att loppet har börjat. (Image: Public Domain)*

Figure 2. *Målgång i hundrametersloppet vid Olympiska spelen i Aten 2004. Målkameran fungerar som detektor och gör tidtagningen exakt. (Image: Public Domain)*

flygtidsinstrument är som att ta tid på en sprintlöpare på en löparbana. Banan har alltid en bestämd längd. Man ger löparen en startsignal genom att skjuta med en startpistol, vilket också är signalen till tidtagaren att starta klockan. Tidtagningen slutar när löparen går i mål, och med den uppmätta tiden kan man beräkna löparens medelhastighet. I flygtidsspektrometern är elektronen löpare, och löparbanan är ett vakuumrör. En elektron som har blivit utslagen från provet av en ljuspuls leds genom röret fram till en detektor. Det är som om ljuspulsen vore startpistol och detektorn är tidtagare.

Det är nu det blir problem. I alla elektronspektrometrar med bra energiupplösning är flygtiden minst hundra nanosekunder, ibland flera mikrosekunder. Eftersom vi inte kan se elektronen när den flyger är det enda vi kan mäta när elektronen kommer fram till detektorn. Startsignalen måste komma från ljuspulsen. Dessa pulser kommer dock mycket tätare än flygtidens längd. Det är som om startpistolen på löparbanan skulle skjutas av tiotals gånger under varje lopp. För tidtagaren blir det omöjligt att veta när löparen startade. För att tidtagningen ska fungera får det bara vara ett startskott varje lopp, på samma sätt som det bara får komma en ljuspuls varje gång en elektron flyger genom spektrometern. När varje elektron följs av massor med startskott måste vi fråga oss: Vilken är den rykande pistolen?

I den här uppsatsen diskuterar jag olika sätt att lösa problemet med den rykande startpistolen. Det finns nämligen flera. Ett av sätten är att ändra på lagringsringens inställningar så att ljuspulserna kommer mer sällan – man tvingar personen med startpistolen att skjuta mer sällan. Så gör man på många lagringsringar i världen, men det är väldigt svårt att göra på lagringsringar som MAX IV. Varje försök att ändra på hur elektronerna ligger i lagringsringen kan göra hela acceleratorn instabil. Mina kloka kollegor som är acceleratorfysiker undersöker dock om man ändå kan göra detta på MAX IV.

Ett annat sätt är att blockera majoriteten av ljuspulserna innan de kommer fram till experimentet – personen med startpistolen skjuter, men skottet hörs inte. En apparat som gör detta kallas *mekanisk slutare* (eller chopper) och är oftast ett roterande hjul med smala öppningar som låter en enda ljuspuls passera. De slutare som behövs för att passa flygtidsspektrometern kräver stor ingenjörskonst att tillverka. Det krävs ett 30 centimeter stort hjul som gör tusen rotationer per sekund och som har öppningar på några få mikrometer. Sådana slutare finns dock idag, och jag föreslår att man kan använda dessa på MAX IV.

Om man inte alls kan förändra ljusets egenskaper får man arbeta med detektorn – kan man inte stoppa startpistolen så får man stoppa löparna efter starten. Jag har tillsammans med kollegor i Berlin utvecklat två slags elektroniska grindar som hindrar elektronerna som sänds ut från provet att komma fram till detek-

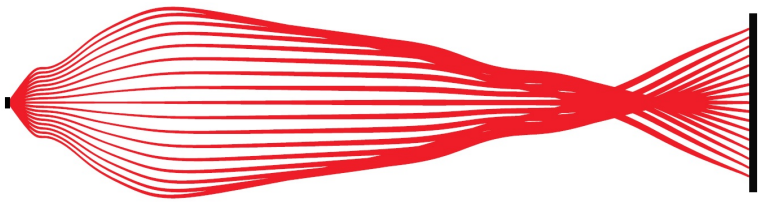

Figure 3. *De vindlande "löparbanor" som elektronerna använder i flygtidsspektrometern – från starten i en liten punkt, till målgången på den mycket större detektorn. Hela flygningen sker i ett vakuumrör.*

torn. Vi bromsar in alla elektroner som vi inte vill detektera med ett elektriskt fält och ett mikrometertunt metallnät av rent guld. Vi använder en elektrisk puls för att "öppna" grinden precis så ofta som spektrometern behöver och under den korta tiden kan elektronerna passera utan problem. Skillnaden mellan de två grindarna är att den ena (detektorgrinden) stoppar elektronerna just före målgången medan den andra (nosgrinden) arbetar precis vid startlinjen. Utmaningen för oss är att få fram en elektrisk puls som är tillräckligt stark för att blockera elektronerna som vi inte vill detektera, och samtidigt så snabb och exakt att den inte ändrar flygtiden för de elektroner som vi vill mäta. En elektrisk puls kan också skapa störande radiovågor som överbelastar detektorn. För att lösa detta var vi tvungna att studera många olika slags elektriska pulser och testa hur de påverkade spektrometern, och i slutändan lyckades vi skapa elektriska pulser som passade för lagringsringen BESSY och de synkrotronljuspulser som finns där. Tack vare vår detektorgrind kunde vi detektera elektroner 30 gånger mer effektivt. Ett experiment som annars hade tagit en hel dag kunde vi nu göra på 20 minuter. Detta gör flygtidsspektrometern mycket mer användbar på BESSY. Detektorgrindar kommer nu användas på de nya experimentstationer som byggs där.

För att få samma goda resultat på MAX IV vill vi använda nosgrinden. Det är en större utmaning eftersom de elektriska pulserna måste vara både starkare och kortare. I uppsatsen diskuterar jag hur en sådan grind kan fungera. Vi har gjort tester, men det återstår mer arbete innan den kan användas på ett riktigt experiment på MAX IV. Till nästa mätning ska jag bygga om grinden för att bättre kunna styra elektronerna. Jag kommer också att skaffa en generator för de elektriska pulserna som ger bättre och kortare pulser. Vårt mål är att grindtekniken ska kunna användas vid flygtidsexperiment på MAX IV. Med tillgång till det världsbästa ljuset och de bästa instrumenten tror vi att forskarna i Lund kan göra världsledande elektronspektroskopi.

ABBREVIATIONS

ALS	Advanced Light–Source
ARPES	Angle–Resolved Photoemission Spectroscopy
BESSY	Berliner Elektronenspeicherring-Gesellschaft für Synchrotronstrahlung m. b. H
CFD	Constant Fraction Discriminator
eTOF	Electron time–of–flight spectrometer
DLD	Delay Line Detector
FWHM	Full Width at Half Maximum
GAME	Gated ArTOF Modular Extension
HDA	Hemispherical Deflection Analyser
HZB	Helmholtz–Zentrum Berlin
MCP	Multichannel Plate
NIM	Nuclear Instrumentation Module
PPRE	Pulse Picking by Resonant Excitation
PSB	Pseudo–Single–Bunch
ROI	Region of Interest
TDC	Time–to–digital Converter
TOF	Time–of–flight
UV	Ultraviolet
VUV	Vacuum Ultraviolet

CONTENTS

Papers

CHAPTER 1

INTRODUCTION

Recent years have seen important developments in instrumentation for photoelectron spectroscopy [1]. Resolution and efficiency in electron spectrometers has increased by many orders of magnitude over the latest decades. In addition, light sources with increased brilliance are fundamental for explaining the persistent interest in electron spectroscopy as an important tool for material science.

The most common light source for photoemission experiments using X-rays and VUV light is synchrotron radiation emitted from storage rings. Storage rings have many properties suitable for photoelectron spectroscopy—high intensity, low emittance, high stability and the possibility to host and run many experiments simultaneously. It is the perfect choice for experiments asking for reliable, reproducible and (quasi-)continuous light. However, a storage ring has not been the obvious choice for experiments requiring non-continuous light in short pulses with repetition rates in the MHz range or lower, as the storage rings are optimised for high intensity and delivers light in pulses with 100–500 MHz repetition rate and 30–300 ps pulse length. For most spectroscopies, this is equal to a continuous light source.

A significant part of recent instrument development has taken place in the area of time–of–flight (TOF) based electron spectroscopy. Although TOF–spectrometers are by no means new, they are now entering areas previously reserved to hemispherical deflection analysers (HDA). This is marked for example by the novel angle–resolved time–of–flight spectrometers [2–5], which are now commercially available. Here an electrostatic lens, similar to lenses found in HDA analysers, has been extended and optimized into a complete TOF system. By utilizing a many-element cylindrical electrostatic lens and a position sensitive detector, the angle resolved TOF–instrument can determine electron energy and emission angles with resolution comparable

to or exceeding state-of-the-art hemispherical analysers. Other advancements have come in the area of magnetic bottle spectrometers [6]. For detection of ions, the TOF analyser is also an indispensable tool.

To take full advantage of recent advances in TOF–instrumentation, it is necessary to understand the present capabilities of storage rings with regard to their timing characteristics. Recent years have seen developments in accelerator and beamline technology which allow storage rings to provide light with suitable temporal characteristics for state-of-the-art electron and ion spectroscopy. It is now possible to create local single–bunch pulse structures for instruments with timing–requirements, while other beamlines simultaneously can benefit from high intensity, quasi-continuous light. This implies that timing–based instrumentation at storage rings will not be restricted to designated time with "single–bunch" delivery. Instead those instruments can be used in parallel during normal operation, without compromising high intensity light for other experiments.

The main problem facing implementation of TOF systems at storage rings is their inherent requirement for relatively low–frequency pulsed light. As TOF–systems exploit temporal dispersion of electrons in a drift tube, one needs a light source with a pulse separation close to the typical flight-time in the spectrometer. Therefore; the pulse separation must *at least* be larger than the expected temporal dispersion of the electrons in the energy region of interest. In general, high electron energy resolution can only be achieved when the time–of–flight is increased by means of strong retardation potentials [2] or magnetic fields. This increases temporal dispersion in applications where high energy resolution is demanded.

In addition, high precision timing instrumentation puts demands on the length of the light pulse; uncertainty in the time of interaction between photon and sample adds to the timing uncertainty of the instrument, namely the un-resolvable temporal dispersion of monoenergetic electrons and detection errors.

As present developments in storage ring design have a strong focus on increasing brilliance it is unlikely that future storage rings will be optimized for timing–based experiments. The vast majority of the storage ring user community today favour high intensity and have no demand for temporal resolution. New lattice designs aims at decreasing storage ring emittance even further towards the diffraction limit. A part of the time–resolved community also may find suitable light characteristics at free electron lasers. Even so, it is of great interest for the spectroscopy community to utilize also these new high brilliance light sources for timing based experiment.

This thesis attempts to give a comprehensive analysis of

solutions to the challenge facing electron time-of-flight spectroscopy at synchrotron radiation storage rings. These solutions are sought in four categories:

Accelerator adaptations — The storage ring itself can be adapted to suit the needs of timing–based instrumentation. In its simplest form this involves changing the filling pattern of the storage ring. Operation in "single–bunch" mode increases significantly the temporal distance between light pulses, in expense of mean intensity. New accelerator developments include operation in pseudo–single–bunch (PSB) modes, aiming to accommodate the needs of both high intensity experiments, and users in need for specific single bunch structures.

Choppers — Choppers are mechanic shutters in the beamline which artificially change the time structure of the light by blocking undesired pulses. They often require the storage ring to be run in certain filling modes, such as hybrid modes.

Spectrometer gating — By installing an electron "gate" on a spectrometer, one attempts to block undesired electrons from reaching the detector. In this thesis I will present development work done on the ARTOF time-of-flight spectrometer . The gating schemes have been the main focus of my experimental work. Two approaches to spectrometer gating, detector gating and front gating, are presented in Paper I and Paper II, with further discussion in Chapters 4 and 5.

Coincidence measurements — Techniques where the detection of another particle emitted from the sample is detected in coincidence with the time-of-flight electron, and where this additional electron can serve to determine the necessary start time.

The thesis is outlined as follows: Chapter 2 contains a comprehensive overview on solutions currently sought to overcome the timing restrictions at storage rings. The chapter also introduces common timing–based spectrometers used in electron spectroscopy today. The chapter is concluded with a discussion on which areas of development should be considered for MAX IV. Chapter 3 presents the ARTOF spectrometer, which was the basis for my work on spectrometer gating. Chapters 4 and 5 provide background to the papers. Here, detector gating and front gating is put into their context and additional experimental and theoretical results are presented. Chapter 6 gives a summary and outlook on the further development of instrument gating and ideas for the continuation of my PhD studies.

CHAPTER 2

USING TIMING–BASED INSTRUMENTATION AT STORAGE RINGS

This chapter will provide an overview on solutions currently sought to overcome the timing restrictions of storage rings. As noted in Chapter 1, approaches and solutions are sought along four lines: Accelerator adaptations, choppers, spectrometer gating and coincidence measurements. This chapter will however start with an overview of common timing–based spectrometers used in electron spectroscopy today. To facilitate a deeper discussion on which solutions should be sought, a classification of spectrometers will be proposed according to their inherent demands for timing. This will allow for a deeper discussion on which solutions should be sought for each category of instrumentation.

The chapter concludes with a discussion on how combinations of different approaches can be successfully utilised and how the electron spectroscopy community can benefit from the strengths of new timing–based spectroscopic techniques. In particular, opportunities for the MAX IV Laboratory will be raised.

2.1 Spectrometers and their Requirements for Timing

A photoelectron measurement aims in measuring electron distributions in energy, direction of movement, start position and start time [2]. To these one can also add the electron spin [7, 8]. Energy and direction of movement (E, v_x, v_y) can be combined to give a full representation of the electron momentum in three dimensions (p_x, p_y, p_z) or a representation using energy and emission angles (E, θ, ϕ). The latter representation forms the basis for angle–resolved photoelectron spectroscopy (ARPES).

Figure 2.1. *The ARTOF 10k. (©VG Scienta AB. Reproduced with permission.)*

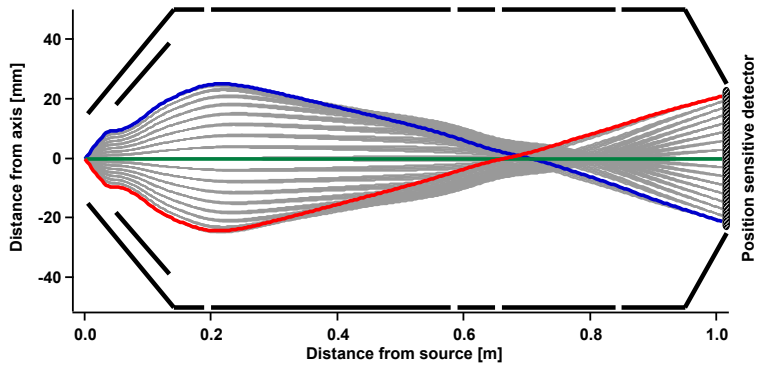

Figure 2.2. *Schematic illustration of typical flight paths for electrons through the ARTOF lens. Here, the instrument works in angle–resolved mode (angle–to–point). It is obvious that monoenergetic electrons traveling on the outer paths have longer flight times than centred electrons.*

Electron TOF (eTOF) was first developed and used by Bachrach *et al.* at SPEAR [9]. An important eTOF instrument was later developed by Hemmers *et al.* [10] which has served as a model for many types of eTOF currently in use at storage rings and free electron lasers (see e.g. Refs. [11, 12]). These eTOFs use a compact design where electrons fly through a field–free tube, preceded by a short electrostatic lens. The energy resolution is limited by the use of a field–free drift region, but the concept has often been applied in coincidence setups due to its relatively high transmission. The instrument of Hemmers *et al.* was first implemented at the Advanced Light Source (ALS), USA, with the storage ring operating in "two–bunch mode" where pulses were separated by 328 ns [10]. Electrons with 5 eV kinetic energy or higher could be separated in this time–window. The bunch length in two–bunch mode was 82 ps, which is negligible compared to other timing errors originating from detector and electronics.

Several types of eTOF instruments exist on the market today. The instruments manufactured by *VG Scienta AB* (Scienta ARTOF 10k and Scienta ARTOF-2) are solely used for the work in this thesis [3, 4]. Since all instruments differ in geometry and instrumental properties, only part of the discussion is applicable to other TOF lens solutions such as e.g. the THEMIS spectrometers manufactured by *Specs GmbH* [5].

The ARTOF instrument, depicted in Figures 2.1 and 2.2, consists of an electrostatic lens and a position sensitive detector. The lens images the sample area on the detector with spatial or angular resolution. Its ability to record both time–of–flight and

detector hit–position allows for a transformation where energy and angular information can be extracted from the data. Using a lens instead of a field–free region as a drift–tube prolongs flight–times and allows for a much higher energy resolution than earlier eTOF-instruments. The ARTOF cover a 30°cone of the sample volume within one measurement, similar to hemispherical analysers. The main advantage of the ARTOF is however that it can give 300 times higher electron transmission than hemispherical analysers due to its slit-less design [13].

The over-all time–resolution is defined as a convolution of the light pulse length and the precision of the acquisition electronics. As noted, the time-resolution of a TOF instrument sets the limit for achievable electron energy resolution. It has been found that very high resolution can be achieved with a ∼100 ps light pulse [3]. Constrains on repetition rate is determined by the flight–time in the lens. In all TOF-spectrometers higher energy particles travel faster than those with lower energy, thus the requirement for repetition rate varies between different electron energy windows. In the ARTOF-lens, 10 eV electrons require slightly less than 1000 ns to reach the detector, whereas 1 eV electrons could require 3000 ns or more, depending on the width of the energy window [3].

The timing constraints of the light source originate from the notion that each detected electron must be assigned to a specific light pulse to determine the flight–time. As flight-times are in the 1 μs range, light emitted with the single–bunch frequency of many storage rings ($\sim$ 1 MHz) provides in most cases suitable time structure for eTOF–experiments.

The magnetic bottle spectrometer is a time–of–flight electron spectrometer where electrons are collected by an inhomogeneous magnetic field. Their flight–time is prolonged by means of a long solenoid magnet. A schematic picture of a magnetic bottle spectrometer is displayed in figure 2.3. As the electrons are made to perform helical motion around the magnetic field lines of the solenoid magnet, their travelled distance increases, and therefore also their time–of–flight. The very long flight–time increases directly energy resolution of the instrument. Another benefit of the instrument is its very high collection efficiency. Due to a conical permanent magnet pole close to the interaction region, almost all electrons, independent of which direction they are emitted, are guided into the spectrometer. The magnetic bottle spectrometer is particularly well suited for electron coincidence experiments; recently even for experiments with simultaneous electron and ion detection [14]. However, no position or angular information can be extracted from data.

The long flight–times put hard restrictions on the repetition rate of the light source. The flight–times in a long spectrometer (for example see Ref. [6]) can be many μs . A realisation of

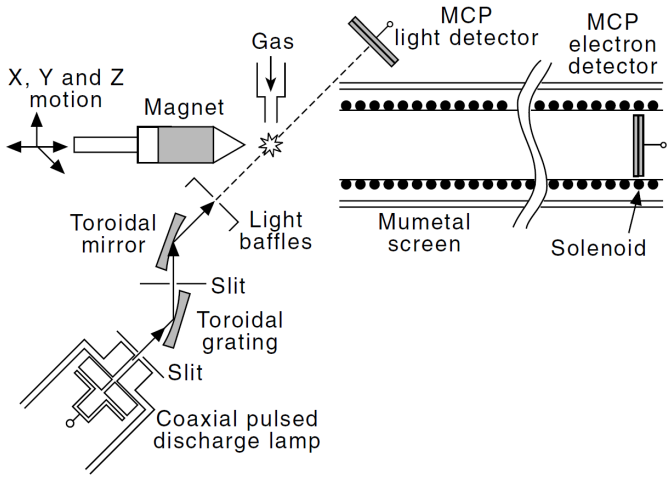

Figure 2.3. *Schematic drawing of the magnetic bottle spectrometer developed by Eland et al. [6]. The prolonged flight time and high collection efficiency stems from the solenoid magnet surrounding the drift tube, in combination with the conical permanent magnet placed close to the interaction region. (©John Eland, Department of Chemistry, Physical and Theoretical Chemistry Laboratory, Oxford University. Reproduced with permission.)*

such a magnetic bottle spectrometer was done by Eland *et al.* [6]. A further developed version of this spectrometer [15] is adapted for use at a storage ring with a flight–time typically longer than 1 μs . These flight–times are considerably longer than the single–bunch frequency of typical storage rings. A shorter spectrometer can be constructed to reduce the flight–time, at the expense of resolution [16]. Requirements on the light pulse length depend on spectrometer design and electron energy. For fast electrons the pulse length can become the limiting factor for achievable energy resolution. For example, Eland *et al.* used a 20 ns pulse during home lab experiments and noted that energy resolution was limited by the light pulse for electron energies above 20 eV [6]. Typical pulses from a storage ring are significantly shorter. Combined with large temporal difference between expected flight–times; the length of typical storage ring pulses is insignificant for instrument resolution and the only remaining challenge is to reduce the repetition rate of the light pulses.

TOF is also common for ion mass spectrometry and a number of different instruments exist for this kind of spectroscopy [17]. The fundamental difference when it comes to timing is the

relatively large mass of any ion compared to an electron. Therefore flight-times are expected to be much larger in ion-TOF setups compared to similar eTOF. In principle it is possible to use a spectrometer at a light source and use the time-reference of the light pulse as a trigger. In practice this is never done at storage rings due to the very low repetition rate required from the light source. Instead ion-TOF–instruments are either parts of a coincidence setup or the time-of-flight measurement is initiated by a separate pulsed extraction field which acts as an external trigger [18]. With this external field all timing of the instrument can be referenced to the trigger and there is no need to employ the time-structure of the light source. This kind of externally triggered extraction potentials are most common for ion detection since slow ions stay in an interaction region for a longer time, allowing enough time for a pulse to be applied.

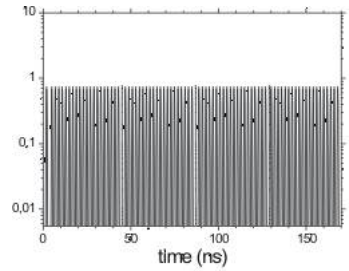

Figure 2.4. *Multi–bunch mode.*

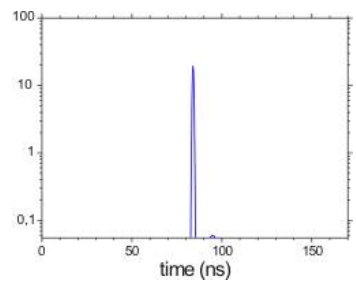

Figure 2.5. *Single–bunch mode.*

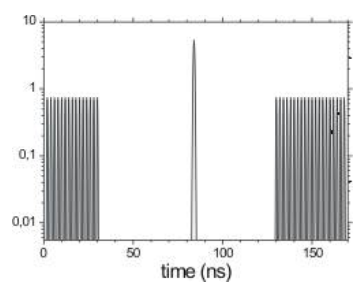

Figure 2.6. *Hybrid mode.*

2.2 Storage Ring Light Sources

2.2.1 Fundamental Temporal Properties

Light emitted from a storage ring has a temporal profile which is a replica of the electron bunch structure in the storage ring. The duration of the light pulses scale with the spatial length of the electron bunch (electron bunch length divided by the speed of light) and the intensity of each light pulse is proportional to the stored charge in the electron bunch. Electron bunches follow the so called closed orbit, which is divided into a fixed number of evenly spaced 'buckets', which represents a volume traveling along the closed orbit where an electron bunch can reside. The spacing of these buckets is determined by the frequency of the RF–system [19].

Two temporal properties of the light source have to be considered in timing–based spectroscopies: The length of the light pulse (pulse length) and the frequency of the pulses (repetition rate). As explained earlier, requested repetition rate of the instrument is closely related to the expected time-of-flight, whereas pulse length contributes to the energy resolution of the instrument.

The overall bunch structure is often manipulated by different injection schemes, where we can distinguish between multi–bunch modes (Figure 2.4), single–bunch (Figure 2.5) and hybrid modes (Figure 2.6). The most straight–forward way to store electrons in the storage ring is to fill each bucket with an equally large number of electrons (the multi–bunch mode)[1]. For most users, multi–bunch light is perceived as continuous and is often

[1] This has e.g. been the standard operating modus for the MAX I [20], MAX II [21] and MAX III [22] storage rings.

	Circumference [m]	Revolution period [ns]	Bucket separation [ns]	
MAX II	90	300	10.00	[21, 26]
MAX IV (3 GeV ring)	528	1760	10.00	[27]
MAX IV (1.5 GeV ring)	96	320	10.00	[27]
BESSY II	240	800	2.00	[28]
ALS	196.8	656	2.00	[29]
ASTRID2	45.7	152	9.52	[30]
ESRF	844.4	2817	2.82	[31]
SOLEIL	354.1	1181	2.84	[32]
Spring-8	1436	4790	1.97	[33]
SLS	288	961	2.00	[34]

Table 2.1. *Relevant properties of some of the storage rings referred to in the text.*

referred to as quasi-continuous. Multi–bunch modes provide the highest intensity and shortest pulse separation achievable for a storage ring. Modern storage rings optimized for high intensity therefore favour multi–bunch operation. Another cause for multi–bunch operation is the use of Landau cavities at storage rings optimized for low–emittance. These cavities primarily increase stability of the electron beam as well as elongating the bunches [23, 24]. The latter effect increases the lifetime of the beam due to a reduction of Touschek scattering[2]. Since the cavities in the storage ring lattice are driven, partly or fully, by the current passing through them, uneven filling patterns reduces the stabilizing effect of the Landau cavities [25].

In multi–bunch operation light is emitted in equally sized pulses separated by the time set by the RF–system. RF–systems with 500 MHz frequency are used at the vast majority of storage rings for synchrotron radiation, giving 2 ns bunch separation. Exceptions are the present and planned storage rings at the MAX IV Laboratory in Lund, Sweden [26, 27], the ASTRID2 ring in Aarhus, Denmark [30], and the planned Solaris-ring in Krakow, Poland [35], where 100 MHz and 105 MHz RF is utilized respectively, giving 10 ns and 9.5 ns pulse separation.

While the multi–bunch mode is optimized for high intensity, the achievable temporal information is very limited. In current practice, no instrumentation using the timing of the light can be operated successfully in multi–bunch. Only timing–based instrumentation with external timing (such as pulsed extraction fields) can be operated.

[2] The Touschek effect describes loss of electrons in the storage ring due to particle scattering. It is the major effect limiting lifetime of stored beams in typical modern storage rings [19].

The opposite approach to multi–bunch mode is to fill only one single bucket with electrons, which is referred to as single–bunch operation. In this mode the total intensity of the light is reduced because of the much lower ring current. This can be exemplified by the single–bunch mode at BESSY II in Berlin, Germany, which yields a total current of 20 mA, while the multi–bunch mode is run with 300 mA current [36]. Single–bunch operation is thus not attractive for experiments where intensity is crucial. The temporal separation of light pulses is however much increased in single–bunch operation, as the repetition rate equals the revolution frequency of the electron bunch (large rings give low repetition rates, and vice versa). Where multi–bunch light had 2–10 ns between pulses, single–bunch increases spacing to hundreds of ns, or even several μs.

Some facilities do not use a single–bunch mode directly, rather a "few–bunches" mode. For example the Advanced Light Source (ALS) at Berkeley, USA, regularly uses a two–bunch mode with 328 ns pulse separation. The European Synchrotron Radiation Facility (ESRF) in Grenoble, France, has opted for four–bunch and 16–bunch modes. Since these rings are very large, the few-bunch repetition frequency still is similar to single–bunch operation in smaller rings.

The single–bunch frequency is the hard limit for the lowest achievable repetition rate for a storage ring (provided no manipulation of the closed orbit is performed). Instruments requiring repetition rates lower than ∼1 MHz, such as magnetic bottles and some ion–TOF instruments, require further manipulation of the light for their proper functioning. These "sub-single–bunch–requirements" can often be addressed by choppers or by the more exotic accelerator modes outlined below.

The category of instruments benefitting from "single–bunch–requirements" includes most electron-TOF, among which you find angle–resolved TOF instruments.

Table 2.1 outlines the most important timing properties for some storage rings. These examples show that there are many filling patterns which can be utilised. Nevertheless, there is a conflict between timing–based experiments, where low repetition rate is preferred, and experiments where high photon flux is desirable. It is also not possible to create single–bunch modes with pulse separations longer than the revolution period. Especially for small rings, these separations are often too short for timing–based spectroscopies.

2.2.2 Pseudo–Single–Bunch and Resonant Pulse–Picking

Operation in pseudo–single–bunch (PSB) is an attempt to simultaneously address the requirements set by the photon–hungry

experiments and timing experiments. PSB has been implemented at the Advanced Light Source (ALS), USA [37, 38] and more recently also at SOLEIL, France [39, 40]. A fundamentally different approach (resonant pulse picking) has been developed at BESSY, Germany [41]. Both approaches uses additional components in the accelerator lattice to displace or excite electrons in one single bunch, causing light to be emitted spatially separated from the light emitted by the other bunches. A collimator in the beamline allows only the separated light to pass.

PSB operation at ALS starts from a hybrid mode where one bunch, called camshaft bunch, is isolated from the bunch train by a 100 ns window, requiring a dedicated hybrid injection scheme. The PSB scheme involves a vertical displacement of the camshaft bunch by a fast kicker magnet. As the camshaft bunch gets a vertical displacement when it reaches the insertion device, the light will likewise be emitted with a vertical displacement. It is easier to achieve complete spatial separation of the PSB light and the full intensity light with a vertical displacement since the vertical dispersion of electrons generally is smaller than the horizontal dispersion, the drawback being that the vertical direction often is used for photon monochromatic in the beamline. An increased emittance in this plane would decrease energy resolution in the beamline.

The PSB scheme requires a short pulse, high repetition rate kicker magnet in the storage ring lattice. A sudden kick from the magnet sends the camshaft bunch on a trajectory separated from the ideal orbit of the machine. The displaced bunch will have an oscillatory motion relative to the bunch train orbit. This implies that the vertical displacement of the camshaft bunch will be different for all insertion devices along the storage ring. The kicker magnet can be tuned to provide the maximum displacement in one or a few insertion devices, but not all beamlines can be served with PSB simultaneously.

ALS has also developed a "kick–and–cancel" scheme for PSB, although with a lower frequency than normal single–bunch [37]. In this scheme the camshaft bunch is kicked to a displaced orbit where it remains for some turns before it is kicked back to the ideal (reference) orbit. With this scheme, one can make sure that the displaced bunch only passes the undulator with a specific displacement once every kick. Therefore the PSB frequency, as seen by the beamline, can be decreased to any fraction of the single–bunch frequency; from hundreds of kHz down to a few Hz. The maximum repetition rate in this scheme is limited by the performance of the kicker magnet, 1.5 MHz, which is sufficient to make a kick every second revolution [37]. The ability to create pulsed light with any fraction of the single–bunch frequency is very attractive to instruments with sub-single–bunch requirements. On the other hand, if the repetition rate can be made high

enough, it can also be an option for instruments requiring otherwise single–bunch mode.

The approach implemented at BESSY uses a feature dubbed *pulse picking by resonant excitation* (PPRE) [41]. A single bunch on the closed orbit is subject to a quasi–resonant excitation of incoherent betatron oscillations. The kick is provided by a stripline kicker, causing the bunch to increase its emittance. As the excited bunch passes an insertion device, light from the excited bunch is emitted with much higher emittance than normal bunches, causing a much larger beam size. The "edge" of this beam can be separated in the beamline. This effect will be present in all beamlines each revolution. Resonant pulse picking is thus a global feature, affecting the whole ring, compared to ALS PSB which is localized to some beamlines. Since pulse picking at BESSY is using a stripline kicker similar to stripline kickers in the transverse feedback system, a hybrid mode might not be required for this solution. The limiting factor is the rise and fall times of the stripline kicker and the required excitation magnitude, which is significantly smaller than in ALS PSB operation. However, the ring must have bunch–by–bunch monitoring abilities.

The BESSY approach has some benefits compared to ALS PSB. Since the vertical dispersion is untouched, the vertical plane can more easily be used as the dispersive plane for monochromatisation. Furthermore, the single–bunch light can be made to follow the beamline's optical axis if a small lattice bump is provided prior to the undulator. However, limitations are present since only a fraction of the light from the excited bunch is collected by the beamline. Resonant pulse–picking will have much lower intensity than ordinary single–bunch light and it cannot be used in bending magnet beamlines. Resonant pulse–picking provides light with single–bunch repetition rate, while the frequency at ALS can be tuned.

The particular benefit of any PSB operation is the combination of single–bunch–like light for some experiments, while others benefit from (almost) full intensity quasi-continuous light. The exact characteristics of the underlying hybrid mode must be carefully considered. For the ALS approach, a hybrid bunch must be sufficiently separated to allow the magnet kick to act on it without inflicting on the orbit of other bunches. Both ALS and BESSY operate in hybrid modes where more than 15 % of the total multi–bunch intensity is compromised by the hybrid window. For small rings, where the single–bunch repetition rate is just a few hundreds of ns, it may not be possible to create a hybrid mode without losing a majority of the intensity.

2.2.3 Short pulses

The duration of a light pulse at a beamline is directly linked to the length of electron bunches in the storage ring. The so called *natural bunch length* is a property of the lattice parameters and the RF system [42]. The bunch length can then be elongated by Landau cavities to increase lifetime and beam stability.

Short pulses has not been a major feature at modern storage rings, as they are at other light sources such as free-electron lasers and short–pulse lasers. In the last few years, however, many synchrotron radiation facilities have investigated and developed operation modes where very short pulses can be created in the storage ring.

In timing–based instrumentation the precision by which the times can be determined is a significant contribution to the overall resolution of the instrument. If the light pulse is used as a start trigger, the length of the light pulse translates to achievable resolution. It is thus of interest to keep bunch length limited compared to other sources of error, such as detector resolution and temporal broadening of monoenergetic particles in TOF instruments.

Most of the modern storage rings with 500 MHz RF (or similar) have electron bunch lengths ranging from tens up to hundreds of ps (see table in Ref. [43])[3]. Compared to several microseconds long flight-time, typical storage ring pulses are appropriate as start triggers. On the other hand, long pulse lengths may compromise timing resolution for angle-resolved TOF instruments. The ARTOF reports good performance at 100 ps [3]. At MAX IV, where bunch lengthening is applied in the storage ring to increase beam stability and lifetime [27], the several hundred picoseconds long bunches must be more carefully considered.

Short pulses are required in many kinds of time–resolved photoelectron spectroscopies (tr-PES). In these applications the short pulses are motivated by the time-scales of the physical and chemical dynamic processes under study. Requirements for time–resolved photoelectron spectroscopy using synchrotron radiation have been covered in a recent review by Yamamoto and Matsuda [43]. Their findings will not be repeated here.

There are different approaches to achieve short pulses in storage rings [44]. Many facilities use so-called ”low–alpha optics” [45] to create short bunches. The length of these bunches can typically be reduced from tens of ps down to a few ps [46]. Ultra-short photon pulses in storage rings can also be created with femto–slicing techniques [47, 48]. Other possible solutions include using cavities and higher order RF systems to shorten

[3] Bunch lengths are given as rms-values.

bunches; a reversed, but similar operation to the bunch elongation performed by Landau cavities. MAX IV Laboratory is currently establishing a so-called Short Pulse Facility [49] which will utilize the short electron bunches from the 3 GeV linear accelerator directly to create short (∼100 fs) hard X-ray light pulses in beamlines separated from the storage rings.

It can be concluded that pulse length in general is not a restriction for proper use of timing–based instrumentation at storage rings. While many attempts to reduce pulse lengths exist at storage rings, they are first and foremost aimed at time-resolved experiments covering short time dynamics, and there is no actual demand from the instrument point of view for shorter pulses. It should be noted however that instrumentation using timing is often convenient to use in tr-PES because of their often high transmission. Light-sources optimised for time–resolved experiments are still often suitable for instrumentation using timing, as long as the available intensity is sufficient.

2.3 Choppers

Previous sections showed that certain filling patterns of storage rings have little value for timing–based instruments. For example, the ARTOF will work well in single–bunch but is practically useless as a standalone instrument in multi–bunch mode. This applies to all experiments with sub-single–bunch requirements even in single–bunch modes.

Choppers are used to tackle this temporal problem by physically blocking or deflecting undesired light in the beamline. The aim of a chopper at a storage ring is typically to transmit only one single light pulse from the ring[4]. Design of choppers is faced with a number of challenges: For transmission of a single pulse the opening time must not exceed twice the temporal distance between two adjacent pulses. If the chopper is used in hybrid modes, the opening time should be shorter than the hybrid window. The transmission of pulses should then be repeated with a frequency suitable for the experiment. This frequency may range from single shots delivered on demand up to a few MHz.

Another figure of merit for the chopper is its attenuation, i.e. how much of the desired light is transmitted through the chopper during operation. To this end one must consider the beam size relative to the openings of the chopper, since transmission increases if the chopper can be placed where the beam is small.

For efficient use at a storage ring it should be possible to synchronize the chopper to the delivery of pulses. Each storage ring references their RF frequency to a timing signal in order to keep

[4] There are also chopper solutions where the aim is to transmit a bunch train of a specified length.

	Type	Window [ns]	Rep. rate [kHz]	Sync.	
Plog-maker et al	Parallel (disc)	750	9.7–78	Yes	[53]
Ito et al	Perpendicular (hamster wheel)	350	80.1	No	[54]
ESRF	Perpendicular (tunnel)	200	0–3	Yes	[55]
Buffalo-1	Parallel (disc)	3520–2110	13.6–22.6	Yes	[56]
McPher-son	Perpendicular (tunnel)	2450	2.7	Yes	[57]
Jülich MHz	Parallel (disc)	141	1250	Yes	[58, 59]
DIA-MOND	Parallel (disc)	3700	0-0.05	Yes	[50]

Table 2.2. *Properties of some choppers, including their type (parallel or perpendicular), timing constraints and if they are synchronized to the light pulses.*

the buckets in phase within the ring. This signal is sometimes called the ring (master) clock. A chopper's rotating element(s) can thus be continuously synchronized to the same clock governing the movement of electron bunches in the ring. Recently developed choppers for storage rings have this ability. However, some jittering of the rotation frequency is always present. Inability to keep very precisely to the reference time can hinder good performance.

During the last decades a number of chopper designs have been developed. In general these can be divided into two groups: Those based on rotating absorbers and those based on rotating deflectors [50]. The latter works by means of deflection or diffraction of the beam by a rotating crystal [51] or mirror [52]. During rotation the light is repeatedly focused onto a slit located at some distance (could be several meters) from the rotation axis. This type of chopper can be optimized for very short time windows (down to tens of nanoseconds). However, this requires a significant distance between rotation axis and the slit. If only one deflecting/diffracting surface is present the repetition rate is equal to the relatively low rotation frequency, which limits their applicability for instruments with single–bunch demands.

Absorption choppers have been further developed during the last years. Table 2.2 shows performance data for some recent mechanical absorption choppers. These choppers fall into two categories [60]; rotation axes aligned parallel or perpendicular to the beam (see Figure 2.7). The difference in performance can be seen from the geometrical analysis made by Cammarata *et al.* [55] where it is pointed out that the perpendicular tunnel al-

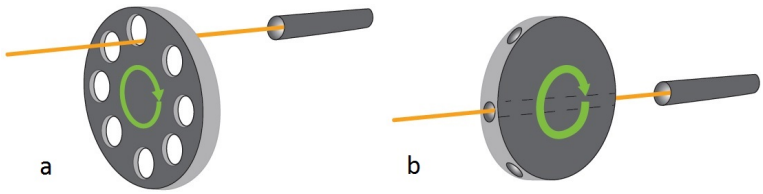

Figure 2.7. *Choppers of the (a) parallel and (b) perpendicular type.*

lows for a shorter time window than parallel slots for any given slot size. The limiting factor, both for repetition rate and window time, is the achievable rotation frequency. However, parallel choppers using rotating discs can host a much larger number of slots, thus increasing the possible repetition rate. The repetition rate for a slotted parallel chopper is given by the number of (equidistant) slots times the rotation frequency. The time window is limited by the width of the slots and achievable rotation frequency, while repetition rate is only limited by the number of slots.

A very favourable situation for synchrotron users would be if the beamlines hosted a chopper solution capable of isolating one light pulse from an accelerator mode optimized for high–intensity light. The timing experiments could then be run in parallel with high–intensity–experiments. At present, there is no chopper developed which can isolate one single bunch from a 500 MHz (or even 100 MHz) bunch train. However, some solutions exist where choppers are used to isolate hybrid bunches [55, 58]:

A chopper system for the beamline ID09B at ESRF was developed by Cammarata *et al.* [55]. ID09B is a hard x-ray beamline for time-resolved experiments in macromolecular crystallography and liquids. The system consists of three parts: A heat–load chopper, a millisecond shutter and a high–speed chopper. The high–speed chopper allows to create a 300 ns opening window with 3 kHz frequency, which is sufficient to isolate the hybrid bunch in ESRF's most common hybrid mode (the so–called "7/8+1"). In this mode one hybrid bunch resides within a 352 ns window in the multi–bunch train. Although this setup is creating a single light pulse usable for sub-single–bunch instrumentation, 1 ms or more between pulses is far too long for efficient operation of the spectroscopy instrumentation we have outlined in earlier sections[5]. To increase the pulse frequency to 100 kHz or more would not be possible with the used design due to me-

[5] Flight times in the 1 μs regime.

chanical restrictions of the rotating chopper.

The *Jülich MHz–chopper* is to this day the only chopper capable to a repetition rate in the MHz range. The parallel slotted disc chopper was constructed for the BESSY storage ring to extract single bunches from the hybrid mode [58, 59]. The hybrid mode at BESSY has a single bunch residing in a 200 ns window which is repeated every 800 ns (1.25 MHz). The chopper consists of a slotted disc, 338 mm in diameter, rotating at $\sim$ 1 kHz. The 1252 slots are 0.15 mm wide, allowing for a 141 ns window at the desired 1.25 MHz repetition rate. Presently an updated version of the chopper is manufactured for use at BESSY[6]. The chopper is designed with ring clock synchronization, which is a necessary feature in hybrid mode extraction. To withstand the large rotation speed, the outer edge of the disc is only 0.5 mm thick. This limits the chopper to soft X-ray and VUV beamlines, since the X-ray attenuation otherwise would be too small.

The Jülich MHz–chopper also represents to this day the chopper with the shortest available time window. Thus, choppers are only a possible solution to single–bunch or sub-single–bunch instrumentation if a hybrid mode exists where the hybrid window is at least 150 ns[7]. Many larger storage rings have this available already, but at smaller storage rings hybrid modes with such large hybrid windows would significantly reduce total intensity. On the other hand, the Jülich MHz–chopper design paired with single–bunch operation even in such a small ring would allow for use of single–bunch instrumentation.

Beside hybrid mode extraction, many choppers have been developed for simply lowering the single–bunch (or few–bunch) frequencies to better suit sub-single–bunch instrumentation. These choppers have lower requirements both concerning window opening and repetition rate, and simpler designs can be utilized. One chopper scheme for sub-single–bunch use has been designed by Plogmaker *et al.* [53] and is currently in use at BESSY. The principal design aim of this chopper is to decrease the pulse frequency from 1.25 MHz in BESSY single–bunch mode to 10–100 kHz, a frequency suitable for the magnetic bottle spectrometer. They utilized a solution with two spinning discs mounted on a joint axis. Each disc has a set of equally spaced apertures along the periphery of the disc. The discs can be rotated relative to one-another and thus the effective opening, as defined by the overlap of the apertures, can be changed. The rotation of the disc can be synchronized to the ring clock to make sure there is synchronization between chopper and the light pulse. From this setup they managed to extract a single light pulse at 9.7 kHz

[6] This chopper will have narrower slots, thus even further limiting the time window.

[7] Updates in progress may reduce this window a bit further.

and 78 kHz respectively while BESSY operated in single–bunch mode. The authors also report that they have created μs bunch trains from a multi–bunch source, and point to the future possibility to use the chopper in hybrid–bunch extraction at BESSY, although this would require an opening window smaller than 200 ns.

A chopper of the perpendicular type intended to gate a magnetic bottle spectrometer has been designed by Ito *et al.* [54]. This utilizes a "hamster wheel" design mounted on a turbo–pump motor equipped with magnetic bearings. It has shown a 350 ns opening window with 80 kHz repetition frequency. However, there is no synchronization between the synchrotron light pulses and the chopper rotation which forbids exact determination of the repetition frequency. The authors however show that for their application, this was not necessary. A prerequisite for asynchronicity to be a feasible solution is that the pulses are equidistant and with low repetition rates, which is the situation for single–bunch modes in larger storage rings.

2.4 Gating and Instrument Adaptations

The purpose of the electron gate is to block unwanted electrons from reaching the detector. Gating of electron spectrometers is the experimental focus of this thesis. Our novel outcomes are further discussed in Chapters 4 and 5, where two approaches to spectrometer gating are introduced. This section will thus only introduce the general ideas behind instrument adaptations for timing–based spectroscopies.

While accelerator modes and choppers aims to prevent interaction between light and sample, instrument gating filters out unwanted electrons *after* the interaction, e.g. photoemission. The goal is to allow only electrons originating from a certain interaction event to reach the detector. When this is achieved, the selected interaction time stamp is simply used as start signal for the time analysis. The benefit of electron gating compared to light choppers is that electrons can be very easily deflected using electric and magnetic fields, as they are charged particles. To create pulsed electromagnetic fields with fast rise times and high repetition rates is much easier than any physical blocking with the same temporal properties. The complication is to create a gate which is efficiently rejecting unwanted electrons while leaving accepted electrons undisturbed. Even slight field errors in an instrument can introduce large deviations in electron speed and direction. Also, the gating must be introduced in the instrument at a position where the temporal dispersion of the electrons has not yet exceeded the repetition rate of the incoming light. If gating is performed after that point, it will not be possible

to distinguish between electrons created in subsequent events. To achieve high selectivity, the gate should be close to the sample. On the other hand, the effect of field errors is minimized if the gate is close to the detector; these conditions are unfortunately contradictory.

This thesis will discuss both gating at the detector (detector gating, see Chapter 4) and gating close to the sample (front gating, see Chapter 5). Some experiments have also been reported where detector gating has been used to study time–resolved effects on semiconductor surfaces [61–64]. In these pump–probe experiments, the detector gate is synchronized with the laser to allow detection of electrons emitted from the relevant probe. In a study by Takahashi *et al.* a detector gate was used in a hemispherical analyser to gate electrons with ∼10 eV kinetic energy [64]. They report using a 5–6 V gating pulse, 50 ns long, applied to the front side of the MCP. They achieve as low as 5 ns opening and closing time of the detector[8]. In a similar experiment, they applied a gating pulse to the sample area to induce an electric field dependent energy shift to the emitted electrons. Those electrons emitted while the gating pulse was applied will arrive at the detector with lower kinetic energy and become distinguishable from electrons emitted at a different time.

2.5 Coincidences

Timing can be used in coincidence measurements if one uses detection of a particle in a non-time–dispersive instrument as a start trigger for detection in the other timing–based instrument. The assumption is that the coincidence is "true", meaning that the two emitted particles originate from the same event. One example is studies of Auger decay where the emission of a low energy photoelectron is coincident with a high energy Auger electron. Then, recording in one detector can serve as trigger for the temporal analysis of a second electron. Another example is spectrometry of ionized molecules or atoms where at least one electron is always emitted coincident to the creation of a positive ion [65]. The field of coincidence spectroscopy is large, and only a few examples highlighting the important temporal schemes will be mentioned here.

Ion-TOF-spectrometers can be mounted with an electron detector opposite to it (see for example [66]). Following photoionization, the light electron hits the detector while the much heavier ion moves only a very short distance. If the interaction re-

[8] The total 10 ns gate time makes this a possible solution for 100 MHz storage rings such as MAX IV. The gate time is considerably smaller than chopper opening times. However, the applied pulse amplitude is low and limits its applicability.

gion is situated in a permanent electric field, the ion will move into the ion-TOF and subsequently hit the ion detector [67]. The time–of–flight is simply given by subtracting the time of electron detection from the ion detection. If ions are extracted by a pulsed electric field, the electron detection can serve as a start trigger also for the extraction pulse [68]. In any case, two concerns must be raised: First, the detection efficiency must be large to ensure that a significant amount of coincidences are recorded. Otherwise, if only one particle is detected, the amount of noise increases. Second, a significant amount of coincidences must be "true". When the event rate is increased, the probability of false coincidence detection increases. Coincident detection of non-coincident particles skews the TOF-analysis and introduces noise in the data [65].

The two main classes of electron energy analysers are eTOF-instruments and hemispherical analysers (HDA) [2]. The latter is not a time-dispersing element. Rather, the TOF of electrons through a HDA is almost constant [69]. This property can be used in experiments where a HDA and eTOF(s) are used in a coincidence setup [11, 70]. Compared to electron/ion–coincidence spectroscopy, the coincident particles' speeds are in the same order of magnitude. Thus, the temporal dispersion of monoenergetic electrons in the HDA becomes significant. Since HDA detection acts as a start trigger, the temporal error is propagated to the eTOF-detection. Calculations show that these errors amount to 1-10 ns for a typical HDA [69]. The error can be made smaller using higher pass energy; or, under some conditions completely removed exploiting the time structure of the multi–bunch mode (see Section 2.6.1).

2.6 Discussion

While many new technologies have arisen on how to exploit timing–based instrumentation at storage rings, the challenge remains how to combine these developments into useful solutions. High–brilliance storage rings offer new opportunities for the spectroscopy user communities. At the same time, great over-all benefits can be achieved if high intensity experiments and timing–based instrumentation can be used simultaneously.

Single–bunch modes are successfully implemented at many storage rings, and they are often useful for timing–based instrumentation, but constitute a great intrusion to other types of experiments. Single–bunch modes also differ in usability depending on the size of the storage ring.

The greatest opportunity for timing–based instrumentation at storage rings are those accelerator and chopper schemes which allow the storage ring to be run with high current and de-

liver high intensity light at the same time as single–bunch light can be delivered on demand at certain experiments. The recent development of a MHz chopper which allows to pulse–picking a single–bunch pattern from a hybrid mode is a very significant achievement. This scheme allows single–bunch instrumentation to be used at dedicated beamlines while all other experiments can use multi-bunch light with limited effect on the total intensity. The MHz chopper scheme is limited only by the availability of a suitable hybrid mode. Current MHz chopper reports a window limit below 200 ns, which excludes hybrid mode solutions at very small rings. However, schemes to reduce the repetition rate of single–bunch modes at these rings can be useful for some instrumentation.

Pseudo–single–bunch (PSB) holds similar promises as MHz choppers; the possibility to create simultaneously single–bunch operation for some beamlines and high intensity for others. The work done at BESSY and ALS show that different approaches exist and have proven successful. Depending on chosen solution, the PSB can to some extent be adapted to single–bunch or sub-single–bunch requirements. The approach is however more intrusive on the machine, and disturbances to beam stability must be carefully considered. Most PSB operation will require hybrid mode[9] , and the size of the hybrid window is determined by the mode of excitation.

Recent theoretical and practical investigations at MAX IV Laboratory has highlighted how the use of passive Landau cavities in the ring lattice hinders or complicates the use of single–bunch modes and hybrid modes. As Landau cavities are an integral part in the MAX IV accelerator concept, and many existing laboratories with timing capabilities has opted to implement similar lattices in order to reach low–emittance, there is a potential risk that such modes may suffer from the update. In this regard, PSB and resonant pulse picking have a particular advantage since they involve displacement or excitation of charged bunches rather than a reduction in current. These potential benefits and threats should be carefully considered at MAX IV, as well as other facilities undergoing lattice updates.

2.6.1 Opportunities for MAX IV

When MAX IV is inaugurated in 2016, it will be the brightest storage ring light source in the world. With two storage rings (Figure 2.8), MAX IV will cover a broad range of photon energies with outstanding beam properties. The larger 3 GeV ring will have an emittance below 0.3 nm rad, while the smaller 1.5 GeV ring

[9]The possibility of multi–bunch mode PSB will be discussed in the next section.

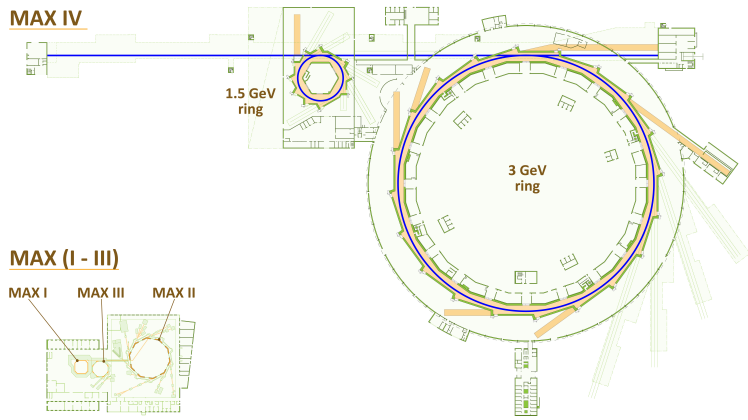

Figure 2.8. *The storage rings at the MAX IV Laboratory. (©Johnny Kvistholm, MAX IV Laboratory)*

	3 GeV ring	1.5 GeV ring	SPF
Revolution period	1760 ns	320 ns	
Bunch separation	10 ns	10 ns	10 ms
Natural bunch length (FWHM)	~70 ps	~120 ps	~100 fs
Bunch length with maximum elongation (FWHM)	~470 ps	~470 ps	

Table 2.3. *Temporal properties of the MAX IV rings. Expected pulse lengths are given both as natural bunch lengths and with maximum elongation due to Landau cavities. The ultimate performance of the ring should be in between these values. Note that bunch lengths have been converted from rms-lengths to FWHM-times. [49, 71–74]*

reaches approximately 6 nm rad [27]. The outstanding properties of the 3 GeV ring are possible due to many novel features in the accelerator, among which one finds a multi-bend achromat lattice, very small vacuum chambers and damping through harmonic Landau cavities. All of these accelerator features are aimed at creating a small electron beam with high stability. As a secondary effect of the optimization for high brilliance, MAX IV has some unique temporal properties, summarised in Table 2.3. The large bunch separation (10 ns) has already been mentioned. In addition, MAX IV will display exceptionally long pulses as a consequence of the bunch stretching introduced by Landau cavities.

In addition to the two storage rings, MAX IV will include a short pulse facility (SPF), where 100 fs hard X-ray pulses will be

created with 100 Hz repetition rate [49].

When comparing the temporal properties of the MAX IV storage rings with 500 MHz facilities, it should be noted that equal current implies five times higher charge per bunch in the MAX IV ring; thus increasing also the intensity of each emitted light pulse. Any isolation of one bunch at MAX IV thus would give a high intensity even without increasing the charge in one bucket[10]. MAX IV rings are also planned to run with 500 mA current in top-up mode, which is higher than many comparable storage rings.

Although MAX IV was never intended to be a storage ring for timing–based experiments, its unique temporal characteristics gives opportunities to exploit accelerator modes, choppers, gates and coincidence schemes to allow timing–based instrumentation. Recently, parts of the MAX-lab user community have raised an interest in using timing–based instrumentation at MAX IV. The first community to express an interest in timing capabilities was for electron and ion spectroscopy[11]. These included ion-TOF instruments and magnetic bottle spectrometers at the FinEstBeaMS beamline at the 1.5 GeV ring [75]. This beamline will have open ports, why there is also a possibility to later include other electron spectrometers would the need arise. A community using the ARTOF [4] has also indicated interest in using this instrument at MAX IV.

Some of the following opportunities for timing should be considered at the MAX IV Laboratory:

Single bunch mode — The Detailed Designed Report [27] does not suggest that other accelerator modes than multi–bunch are considered. The accelerator design is also not particularly well suited for single–bunch operation. This is due to the passive Landau cavities used to elongate bunches. "Passive" cavities imply that their properties are driven by the current passing through them. When the current is reduced, as is necessary in single–bunch, the elongating and stabilizing effect disappears. Consequently, the nominal single–bunch charge (5 nC, 15 mA) could be harder to sustain. Without cavities, bunches will approach the natural bunch length.

[10] The general approach in single–bunch mode or hybrid mode is to fill the camshaft bunch with a much higher charge than a typical bunch in the bunch train.

[11] At a later stage, other communities have expressed similar interests. These include a wide range of photon energies, repetition rates and pulse lengths; both at the 3 GeV ring and the 1,5 GeV ring. These demands are presently being collected by a working group from the user community. Meetings and workshops will be held to investigate demands and possibilities further. The discussion in this thesis is however limited to demands put by electron and ion spectroscopy.

If a single–bunch mode would be developed at the 1.5 GeV ring, it would have a 330 ns repetition rate (3.0 MHz). Compared to many other rings with dedicated single–bunch modes (see table 2.1), this is a quite high repetition rate. Nevertheless, it is sufficient for most applications of the ARTOF [3]. Since transmission of this instrument is significantly higher than that of a HDA, a net gain in transmission would be expected even with a lower intensity of the single bunch. Ovsyannikov *et al.* [4] have identified low dose electron spectroscopy as one area where angle-resolved time–of–flight spectrometers are beneficial. Studies of sensitive and fragile systems require very small light intensities and consequently need high transmission instruments for an efficient data collection; such low dose studies using ARTOF has been reported from BESSY [13]. Since single–bunch repetition rate at BESSY is 1.25 MHz, a 3.0 MHz single–bunch rate would theoretically increase the collection efficiency by a factor 2.5, given that the same dose is applied during a shorter time.

Time-resolved photoelectron spectroscopy (tr-PES) has been pointed out as a strong case for the ARTOF. These experiments are of two types: those occurring on a long time-scale (compared to the repetition rate of the light) where the time–evolution is directly observable in the spectra, and pump–probe experiments. The former would benefit from the high single–bunch repetition rate of MAX IV, since the repetition rate sets the time resolution. The latter, however, has a severe drawback at MAX IV due to the long bunches.

Resonant pulse picking — The outcome of resonant pulse picking is similar to a single–bunch mode, both in terms of repetition rate and reduced intensity. The benefit would be the simultaneous operation of high–intensity experiments and experiments with single–bunch requirements. A particularly intriguing possibility is to operate resonant pulse picking without hybrid mode (in order to run MAX IV in stable operation at full intensity). The 10 ns repetition rate of MAX IV would be an advantage in this regard. Due to the intrinsically lower horizontal emittance of MAX IV 3 GeV ring compared to BESSY, one could possibly expect a more efficient separation of resonantly excited light from the multi–bunch train.

Choppers — To allow for instrumentation with sub-single–bunch requirements, MAX IV will have to make use of choppers. All choppers currently in use at storage rings require dedicated single–bunch or hybrid modes. Two chop-

pers have reported window times below 330 ns: The ESRF chopper and the Jülich MHz chopper. The former is a hard X-ray chopper and offer features which are not necessary at the small ring, which is intended for soft X-rays/VUV. It also shows a repetition rate which is at least one order of magnitude lower than optimum for any magnetic bottle spectrometer. However, would low frequency requirements arise at the large ring, this chopper paired with a hybrid or single–bunch mode would be a viable alternative. Using a modified version of the Jülich MHz chopper could satisfy the users of sub-single–bunch instrumentations at the large or small ring, given that a single–bunch mode is available. It would require either that the present disc is run at a slightly lower frequency[12] or that a new disc is fabricated with slot positions tailored for MAX IV. The latter would allow use of long magnetic bottles.

Since no single–bunch or hybrid modes are presently planned at MAX IV, one should also consider what could be done under normal multi–bunch conditions. Especially, I have looked into the possibilities provided by of the Jülich–type MHz chopper. At present, this chopper shows a 141 ns window, optimised for single–bunch selection from the hybrid mode at BESSY. We have explored if a combination of two such choppers, where one is run at a small delay, could create an effective window less than 20 ns. Such a setup would allow selection of a single–bunch from the 100 MHz multi–bunch train directly. However, the placing accuracy of the slot edges is 10 μm , and with circumferential speed of the disc, 1060 m/s, this implies a temporal error close to 10 ns. The cumulated error of two edges (opening and closing) is thus already close to 15 ns, to which one should add jittering, physical deformation of the spinning disc and ring clock errors. In addition, the small window would only allow the light beam to be 10 μm in size, as the adjacent pulses would otherwise "leak" through the chopper.

Irrespective of the possibility to pick a pulse from a 10 ns window, a combination of two MHz choppers could theoretically decrease the time window to some value close to 50 ns. This would open up the possibility for a hybrid mode with a much smaller window; a removal of 6 out of 32 bunches in the small ring. While a 141 ns window in the small ring would reduce the intensity to 55 % , and compromise beam stability, a 50 ns window would mean that only six buckets would have to be emptied and 80 % of the

[12] Reducing rotation speed by 20 % would allow selecting every third single–bunch and mimic $\sim$ 1 MHz repetition rate.

intensity could remain. If such a scheme could be created, it would open up for simultaneous single–bunch and high intensity instrumentation at the small ring. However, such an approach would necessarily need a careful review of instrument performance, and might prove quite expensive compared to other solutions.

Coincidences with HDA — Coincidence experiments using HDA in coincidence with eTOF instruments can benefit from the temporal properties of MAX IV – without any changes to the timing properties. Electron coincidence spectroscopy has been used for many years to disentangle effects in photoemission experiments where more than one electron is emitted. A coincidence spectrum substantially increases the amount of information drawn from the experiment. One example is where coincident monitoring of inner-shell photoionization followed by Auger decay allows disentangling the Auger spectrum into contributions from individual intermediate (singly charged) states, which otherwise overlap in the same energy region.

An issue in electron coincidence experiments is to achieve reasonable resolution while keeping a high transmission in the electron spectrometers. High transmission is of particular importance in coincidence experiments, since it reduces the number of false coincidences. In recent publications, Lupulescu *et al.* [76] and Arion *et al.* [70] showed how the ARTOF can be used to achieve high transmission, while keeping the high energy resolution of the HDA. The detection of an electron in the HDA is used as a start trigger for the ARTOF instrument. The measurement uncertainty is determined by the temporal dispersion of detected electrons in the hemispherical analyser, which is ~ 6 ns for 200 eV pass energy [76]. This time-reference broadening accounts for half of the total timing error and becomes even more dominating if the pass energy is reduced. The 500 MHz RF system at BESSY gives no possibility to eliminate this error by assigning electrons to specific light pulses. However, at MAX IV the 100 MHz RF system makes this possible as long as the temporal broadening in the HDA is less than 10 ns. We can thus find the arrival time of the light pulse, and directly use it as a reference for the ARTOF. The instrument resolution then equals the stand–alone resolution at a pulsed source. It would also allow us to further reduce the pass energy of the HDA. A study by Kugeler *et al.* [69] suggests that the pass energy can be set below 20 eV before time dispersion exceeds 10 ns. The 100 MHz system; unique for MAX IV, the Solaris-ring in Poland and the Astrid-ring in Aarhus; allows a substantial improve-

ment of resolution in both channels, while preserving high transmission. Put into practice, this electron coincidence scheme would provide users at MAX IV with the highest resolution achievable at any storage ring in the world.

CHAPTER 3

ANGLE–RESOLVED TIME–OF–FLIGHT SPECTROSCOPY

3.1 Background

Two types of electron spectrometers dominate at brilliant VUV and X-ray light sources: the hemispherical deflector electrostatic analyser (HDA) and time-of-flight (TOF) based analysers [2]. The fundamental difference is their means to analyse the energy of the electron. The HDA records the spatial dispersion of electrons with different energies traveling through an electrostatic field. The TOF–system on the other hand measures the time it takes for the electron to travel from the sample to the detector, i.e. the electron speed.

Both TOF and HDA analysers become more sophisticated by the introduction of imaging detectors. An imaging detector can give information on the position where the electron hits the detector plane; this is in addition to the detection of the time [2]. Introducing an imaging detector in the field-free TOF–system gives the possibility to record directions of movement as a function of hit positions. Angular directions $[\theta, \phi]$ (see Figure 3.1) can be uniquely determined from detector positions $[x_{\mathrm{det}}, y_{\mathrm{det}}]$. This feature is exploited e.g. in COLTRIMS [77].

There are many practical problems associated with the field–free TOF–system. Electrons are light particles and will reach very high speeds even at modest kinetic energies. Therefore the time-resolution of the light source and the detector must be very high. In addition, with high speed electrons the acceptance of the analyser is reduced to a very small solid angle [2]. To avoid this problem, flight times must be increased; either by increasing the length of the flight path or by reducing the electron speed in a predictable manner. A solution using the former approach

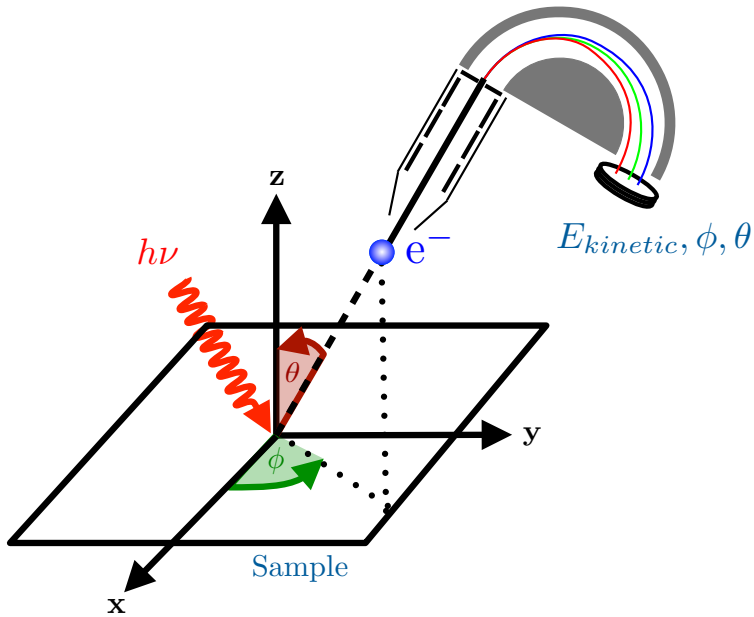

Figure 3.1. *Angles of emission from a sample as they are defined in an ARPES experiment.* (x, y, z) *in this case is the Cartesian coordinate system with reference to the sample and should not be confused with the detector coordinates defined with reference to the detector surface.*

is the magnetic bottle spectrometer [6, 78, 79] where a magnetic field is used to make the electrons follow a long helical trajectory through the flight tube before hitting the detector. This gives higher energy resolution and very high collection efficiency, but all angular information is lost; it is thus not possible to reconstruct the initial electron momentum. The other solution is to use an electrostatic lens system where a large acceptance angle can be focused on the detector while angular information is preserved. Electrostatic lenses have for a long time been an integral part of the HDA [80, 81]. The lens system preceding the actual hemisphere section serves multiple purposes. It is used to retard or accelerate the electrons to achieve higher energy resolution, and to distribute them over the entrance slit of the hemisphere [2]. One can distinguish between two important lens modes: The imaging mode—where electrons are distributed over the length of the entrance slit according to their initial positions—and the angle–resolving mode—where they are distributed according to their take-off angle.

It is in principle possible to remove the hemispherical analyser and use the time-of-flight for energy discrimination. In-

Figure 3.2. *The ARTOF–2 spectrometer. (Published with permission from VG Scienta AB.)*

stead of focusing electrons to a slit, the electrons can be focused on a detector surface. Wannberg [2] shows that for angle-resolving lens, there is a correlation between measured time-of-flight (t) and detector position ($x_{\mathrm{det}}, y_{\mathrm{det}}$) on one hand, and electron energy (E_{kin}) and take-off angles (θ, ϕ) on the other. Another way of putting this is that we can define a transformation matrix where the conversion is a three dimensional function [3][1]

$$E_{\mathrm{kin}} = E_{\mathrm{kin}}(x_{\mathrm{det}}, y_{\mathrm{det}}, t) \quad (3.1)$$

$$\phi = \phi(x_{\mathrm{det}}, y_{\mathrm{det}}) \quad (3.2)$$

$$\theta = \theta(x_{\mathrm{det}}, y_{\mathrm{det}}, t) \quad (3.3)$$

Time-to-Energy–conversion and Position-to-Angle–conversion now come together. This constitutes the basis for Wannberg's proposal for an angle-resolved time–of–flight system.

3.2 The ARTOF instrument

This section outlines the features of the *ARTOF* spectrometers manufactured by *VG Scienta AB*. A presentation of the instrument with first results was published by Öhrwall *et al.* [3]. An update with recent developments was later published by Ovsyannikov *et al.* [4]. The content of this Section has been drawn from these publications unless otherwise stated. *VG Scienta AB* is now also manufacturing an updated version of the ARTOF instrument—the ARTOF-2—featuring an improved lens system which reduces the detection of unwanted fast electrons and allows larger energy windows.

The lens design takes its starting point in the lens used for the hemispherical electron analyser Scienta SES-200 [81]. This lens was cylindrically symmetric and consisted of five lens elements

[1] The original article contains a typographical error in this equation.

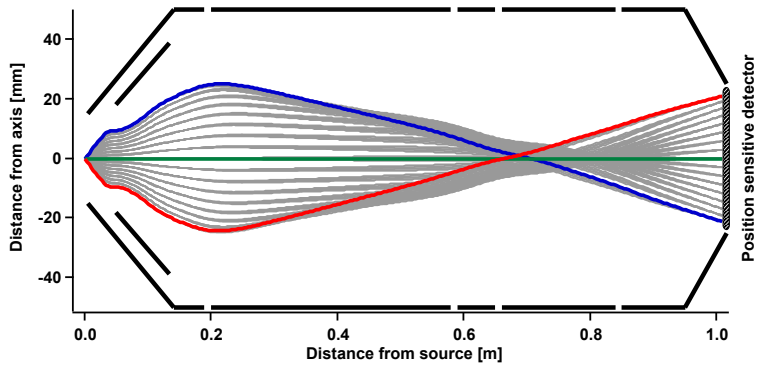

Figure 3.3. *Simulated trajectories through the ArTOF lens. Here a* ±15° *fan of* 10 eV *electrons is focused on the detector with the lens in angle resolved mode. Note that the x and y-scales are different.*

[80]. It could operate in angle–resolved and imaging modes. Figure 3.3 shows a schematic drawing of the five lens elements of the ARTOF lens and a simulation of electrons traveling through the lens in angle resolving mode. In this mode the electrons are distributed on the detector according to their emission angle. Electrons follow quite complicated trajectories which must be calculated using electrostatic simulations. It should be noted that a parallel–to–point transformation takes place early in the lens and a focal plane is created. This focal plane is imaged to the detector with the remaining part of the lens [2].

The lens accepts electrons in a selected energy window, typically 10 % of the centre energy. The voltages in each lens element are chosen to optimise the lens focus for this energy. Due to chromatic aberrations, the resolution of the instrument decreased as energies depart from the centre energy. Far from the centre energy, the transformation matrix becomes degenerate and an assignment of electron energies is no longer possible.

The ARTOF allows detection of electrons within a ±15°emission cone. The transmission of the instrument is thus much higher than for hemispherical analysers at comparable energy resolution. The ratio can be estimated by comparing the area of a circle with diameter equal to the length of the entrance slit to the area of the same slit [4]. For high resolution experiments, where the HDA slit would typically be very narrow, this can imply up to 300 times increase in transmission. Electrons entering the lens are retarded to prolong flight time, and to increase energy resolution. The lens also acts as an energy filter where low energy electrons are not accepted.

A *RoentDek* position–sensitive delay–line–detector is utilized

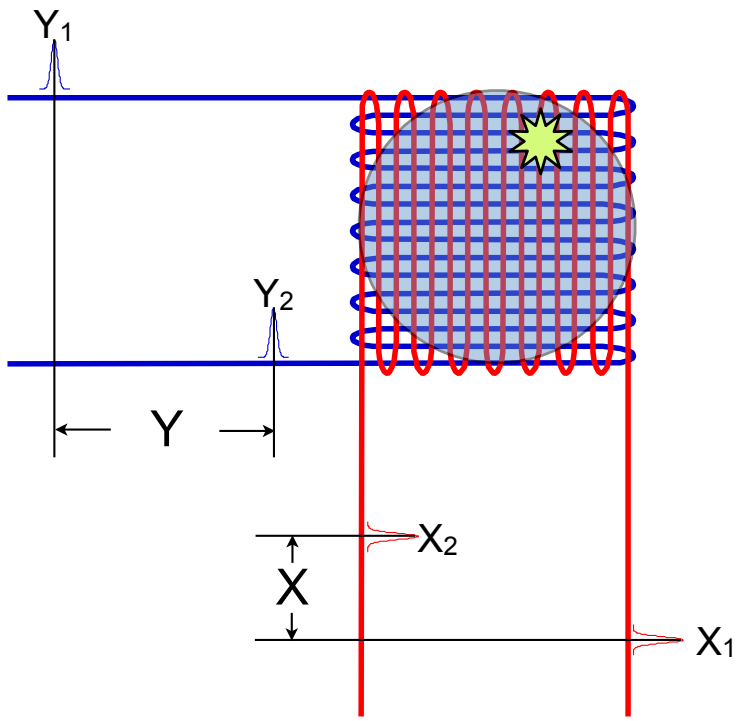

Figure 3.4. *Schematic depiction of the delay–line detector from above. Impinging electrons create an MCP avalanche which induces a signal on the delay-lines. The signal travels in both directions through the meandering delay-line and can be picked up by a TDC. The relative timing of the two signals determines the hit position on the detector. Two delay-lines give the position in two dimensions.*

for time and position detection. A 40 mm Chevron-type MCP–stack precedes the delay lines (figure 3.4). Position is determined by comparing relative times of the signals from the delay–lines. The detection time can be determined either by the MCP-signal or by the mean arrival time of the delay–line pulses. The MCP signal is, however, the most precise due to its short rise time. In total the detector produces five signals which are preamplified outside the vacuum. These preamplified signals are sent to the constant fraction discriminators (CFDs) where they are transformed to NIM-pulses. The pulses are fed into a time-to-digital converter (TDC) from which they can be read by the computer.

The timing at the detector is critical for the instrument: Energy resolution is related to time resolution in a complicated way.

The energy resolution can be estimated using the formula [4]

$$\Delta E = \sqrt{(\alpha E^{3/2}\Delta t)^2 + (\beta \Delta d^{\gamma} E)^2} \tag{3.4}$$

where Δt and Δd are the time-resolution for the electronics and the detector, and α, β, γ are properties of the transformation matrix for the selected centre energy E.

To assure ultimate resolution, the sample must be placed in the focal spot of the lens which is situated along the ARTOF axis at a predetermined distance from the first lens element. This implies that the ARTOF axis, the light beam and the sample must coincide in one point in space.

The ARTOF must also be calibrated to the timing of the light source. If the ARTOF is used with a suitable pulsed light source (storage ring in single–bunch mode), the acquisition should be synchronized to its internal time reference (ring clock). Scattered photons from the sample or sample holder can be used as an absolute time–stamp.

The high transmission and data acquisition rate gives rise to extensive amounts of data. Each event is stored as a vector with the x, y and t coordinates. The analysed data is consequently stored as a vector with E, ϕ and θ coordinates. The initial analysis can be performed with software provided by the manufacturer. In addition, we have used a set of scripts developed within the ARTOF project to analyse data, for example, in **k**-space. These extensions provide means of analysis for ARPES and other applications, some of which will be mentioned in the last section of this chapter.

3.3 Timing and the Cause for Instrument Gating

The ARTOF is a timing–based instrument with single–bunch requirements, as outlined in the previous chapter. The flight–times for analysable electrons span from a few hundreds of nanoseconds up to 3 microseconds [3]. Due to scattered photons and high energy electrons from higher order light, a single light pulse can be expected to give rise to TOF detections in a time-range starting from a few ns (photons) up to microseconds. To avoid overlaps the ideal light–source should have a pulse separation which just slightly exceeds this range.

We have proposed ARTOF gating as a tool at storage rings lacking required characteristics. The purpose of a gate is to deflect undesired electrons by means of electric fields. Accepted electrons are those which can be unambiguously assigned to a specific light pulse (i.e. a known t_0). Those electrons which overlap remain unresolvable.

The temporal properties of the light source determine which gate solutions can be applied. Figure 3.5 shows a TOF spectrum

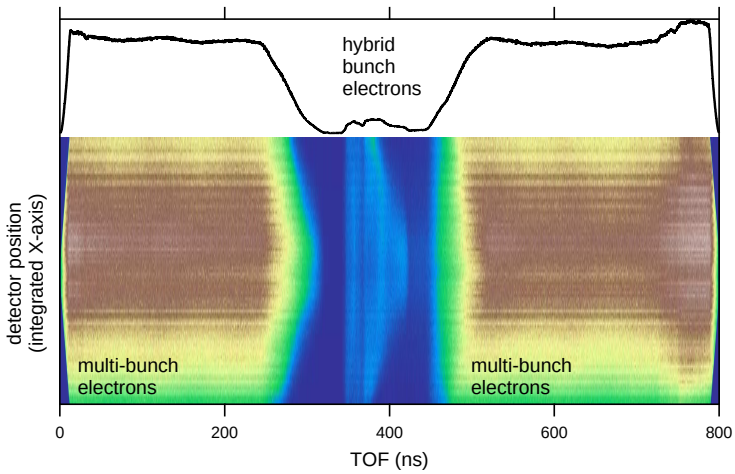

Figure 3.5. *Typical TOF spectrum acquired in hybrid mode at BESSY. The graphene valence band is measured with $h\nu = 180$ eV and the instrument optimized for recording $E_{kin} = 175$ eV. Electrons generated by the hybrid bunch are clearly separated from the multi–bunch electrons by the 216 ns hybrid window.*

acquired at BESSY when it was operated in hybrid mode. The electrons generated by the hybrid bunch arrive at the detector temporally separated from the electrons generated by the multi–bunch train. However, most detections are unresolvable. Under these circumstances, the electron spectrum can be analysed from the hybrid electrons and all other electrons can be disregarded. However, it is disadvantageous to have a large background of undesired electron detections since these overloads the MCP detector. Hence, the acquisition time for an electron spectrum increases by more than an order of magnitude compared to single–bunch operation. This problem can be tackled by detector gating. By means of a pulsed electric field close to the detector one closes the detector when the multi–bunch electrons are expected. This is the basic idea for our studies on detector gating in Chapter 4. This gating scheme is applicable for hybrid modes where the temporal dispersion of hybrid electrons fits within a sufficiently large window. It cannot be applied directly under multi–bunch conditions, or when the temporal dispersion exceeds the hybrid window. The latter problem arises for detection of very slow electrons. Alternatively, gating can be performed prior to the lens. The temporal dispersion increases as an electron travel through the lens; therefore an early gate allows removing electrons originating from light pulses with short temporal separation. This is the basic idea for our studies on front

gating in Chapter 5. This is required if gating should be possible in any multi–bunch operation, like the 100 MHz operation at MAX IV.

3.4 ARTOF applications

The benefits in ARTOF applications stem from its high transmission in combination with high energy resolution. A good overview of ARTOF application areas is given in Ref. [4].

The ArTOF allows mapping of the whole momentum space in three dimensions (3D-ARPES). For example, the study by King *et al.* [82] shows 3D-ARPES on Bi_2Se_3. In this study, the sample was cleaved and the evolution of band structure was studied in real time. This was made possible due to the high transmission of the instrument, allowing a large fraction of the emitted electrons to be measured in a short time, also, the whole 3D momentum space is monitored in a single run.

ARTOF opens up for experiments with very low radiation doses: In single–bunch modes, the sample is irradiated with a much lower mean intensity. This would typically be a drawback since fewer electrons are emitted, but this is rather a benefit for radiation sensitive samples. A study by Vollmer *et al.* presents results of low dose spectroscopy on organic crystals (rubrene). Here, photon flux was kept at 10^8 photons/s, and still the band structure could be obtained in 20 minutes. [13]

It was discussed in Section 2.5 how TOF instruments increase the true coincidence rates in electron–electron coincidence experiments. These types of experiments benefit strongly from higher transmission, and the ARTOF has been successfully implemented in such setups [11, 70].

At SPring-8, beamline BL07LSU is featuring an ARTOF instrument for pump–probe experiments together with a laser source [83]. Similar to low–dose experiments, the high transmission is a benefit since repetition rates are low for high laser energies.

In summary, ARTOF instruments have in a short time found application areas where hemispherical analysers previously were the only viable alternative. Especially the high transmission compared to other high resolution instruments benefits the whole user community. These two classes of electron analysers are, however, complementary and can both be widely applied at storage rings.

CHAPTER 4

DETECTOR GATING

The detector gating scheme is one of the two realisations of ARTOF gating which have been explored within the ARTOF development project. The detector gate solution, also called the *Gated ARTOF Modular Extension (GAME)*, was developed particularly for BESSY hybrid mode operation. We have presented our successful operation of the GAME in Paper I. The design was made within the ARTOF development project in collaboration with *VG Scienta AB* in 2012 and was implemented and tested at BESSY during 2013 and 2014.

4.1 Physical design

The ARTOF uses a commercially available delay-line detector from *RoentDek GmbH*, consisting of two Chevron stacked MCP plates followed by two delay lines and an anode. As noted in the

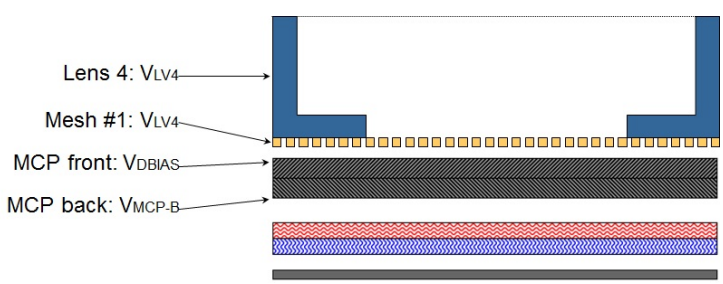

Figure 4.1. *Schematic side-view of the delay line detector in its original setup. Electrons impinge on the mesh from above. The lens axis is normal to the gold mesh.*

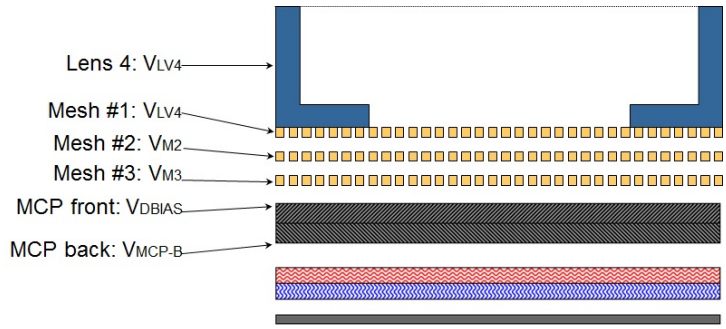

Figure 4.2. *Schematic side-view of the delay line detector with added gating meshes. The MCP and delay-lines have been moved 20 mm further away from the lens.*

previous chapter, an electron hitting the detector generates five signals, one from the MCP stack and one signal from each end of the two delay-lines. In non-gated operation, the MCP signal provides for the arrival time of the electron, while the hit coordinates are deduced from the delay-line signals. Figure 4.1 shows the non-gated detector where the MCP stack is preceded by a gold mesh kept to the same potential as the last lens element of the electron lens. For detector gating, depicted in Figure 4.2, we introduced two additional meshes between the last lens element of the analyser and the MCP. With this addition, the MCP and delay-lines were moved to a position further away from the source point (where the light interacts with the sample). Both meshes were connected in vacuum to a voltage feed-trough. To achieve gating we applied a high constant deflection potential together with a low voltage gate pulse to the M2 mesh. A high voltage source, identical to the power supplies commonly used for the lens elements of the ARTOF, feeds a tuneable negative potential V_{nej} to the M2 mesh. This potential acts as an energy filter and allows passage of only the electrons with kinetic energies higher than $-q\,V_{\mathrm{nej}}$. To achieve gating, we add a pulsed gating potential V_{gate} sufficient to deflect all electrons. The gate characteristics is altered by changing the potential V_{nej} as well as the gating pulse length, amplitude and repetition rate. For pulse generation we use a ±10 V function generator which is coupled to M2 through a high-capacitance coupling capacitor (Figure 4.3). The circuit acts as a high-pass filter, adding the pulse as a variable signal on top of the constant V_{nej} potential. Electrons with lower kinetic energies will always be deflected by the gate if a sufficient V_{nej} potential is applied. As the filter potential is set to deflect all electrons with energies lower than the region of interest, the

function generator signal is fed through the coupling capacitor, creating a (maximum) 20 V increased potential on M2. By this scheme, the mesh can be made into an efficient gate for electrons with energies between $-q\,V_{\mathrm{nej}}$ and $-q(V_{\mathrm{nej}}+V_{\mathrm{gate}})$. It allows us to use a pulse generator with limited amplitude, which makes the instrument simple and has a limited effect of the read-out of the detector. However, electrons with higher kinetic energies will not be gated by this scheme. These electrons are mostly easy to recognise since they are always faster and arrive earlier to the detector than the electrons within the energy window. The problem with high energy electrons arises when fast electrons from the multi–bunch train overhauls the preceding electrons before detection[1]. This is a fundamental restriction to the GAME and could only be practically solved by increasing the gate amplitude or making the hybrid window longer in the storage ring.

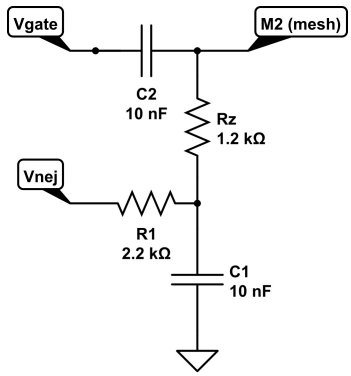

Figure 4.3. *Circuit feeding the potential V_{nej} and the gate pulse V_{gate} to the M2 mesh. The signal is transmitted through the C2 capacitor, acting as a high pass filter.*

4.2 Electronic pulsing

A pulsed electric potential very close to the detector introduces disturbances to the signal readout. In normal operation of the detector, the detector timing signal is read from the potential drop occurring when an electron impinges on the MCP surface and causes an electron avalanche. The amplitude of this signal is several orders of magnitude lower than the amplitude of the gate pulse. Considering that the mesh assembly acts as a parallel plate capacitor, it is obvious that high frequency signals on M2 will extend to the neighbouring meshes and the MCP. Even if only a fraction of the signal is transmitted, its high amplitude will overshadow the true MCP signal and prevent its use. In some cases false signals could be introduced also as far as the delay-lines. To circumvent this problem we took a number of steps and precautions:

- The time-of-flight must not be extracted from the MCP signal. A timing signal could also be deduced from the combined detection of four delay line signals. Since the delay lines have a fixed length, the total delay of the two signals in each line is constant. Therefore, the mean arrival time of the four DLD signals has a constant delay to the time of detection. By utilizing this, the use of the MCP signal can be circumvented. In the current detector setup the timing resolution of the delay lines is slightly worse than the MCP signal (a few hundred ps). However, changing from MCP to DLD timing has implications on the internal logic of the experiment since the MCP signal normally

[1] In operation at the beamline we always expect higher-order light to create fast electrons. These are most likely to overhaul the slower electrons.

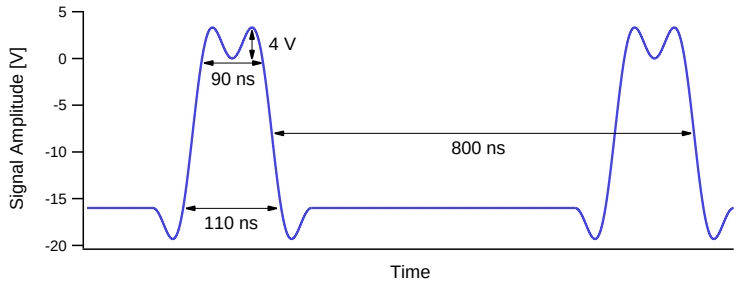

Figure 4.4. *Custom made gate pulse with 20 V amplitude as defined in eqn. 4.1. Each of the pulses is triggered by the 1.25 MHz ring clock signal. Since the full width of the gate pulse is 300 ns (measured from start to end of the oscillation), the intermediate space is filled by a constant negative potential which keeps the gate closed. As indicated, we achieve a 90 ns fully open window with 10 ns rise and fall times. The oscillation of the gate function has 4 V amplitude at 20 V gate potential.*

is used as start time trigger for the DLD signals. To facilitate a pure DLD operation, we had to develop MCP-signal-independent data acquisition schemes.

- We used the M3 mesh as an extra shield for the detector. We wanted to have a large grounded element between the pulsed mesh and the MCP to avoid extensive transmission of signal to the detector. M3 was grounded through a short in-vacuum coaxial cable connecting the mesh and the grounded vacuum feed–through.

- We shaped the gating pulse to minimize the crosstalk between M2 and neighbouring meshes. Figure 4.4 shows the function at its maximum amplitude. To make the longest possible time window we wanted to keep the rise and fall times short. We also had to consider that the pulse should have few high frequency Fourier components to avoid transmission of signals to the MCP. After a trial including the eight Fourier components, we settled with a function only including first and third order components. The function is given by

$$V(t) = \frac{2V_{\text{gate}}}{\pi}\left(\sin\frac{\pi t}{150\text{ ns}} + \frac{1}{3}\sin\frac{3\pi t}{150\text{ ns}}\right) - \frac{V_{\text{gate}}}{2} \qquad (4.1)$$

where t is an arbitrary time parameter. The function is set to trigger on the signal from the ring and run for one period (200 ns) before settling on a constant negative potential. The signal is repeated with 1.25 MHz repetition rate

(the single bunch frequency). The highest frequency component in this function is 10 MHz; this was found to allow operation with $V_{\text{gate}} = 20$ V and DLD referencing. The function with eight components can be used for similar operation, but only up to $V_{\text{gate}} < 10$ V. The custom-made gate pulse has approximately 10 ns rise and fall time, which is sufficient for most applications.

Tuning the GAME hardware and the proper gate pulse is a complex task and there is room for further improvements. For future development we should seek a deeper theoretical understanding of the signal handling in the GAME. The possibility to include a band pass filter to the MCP has not been studied yet. Furthermore, a better ground connection to M3 could be achieved in vacuum to allow for better shielding. Shapes of potential elements can possibly be developed further to minimize the signal transmission between detector elements by controlling the capacitance with geometry.

4.3 Time-of-flight Errors induced by Detector Gating

Consider an electron emitted from the sample with kinetic energy U_0. The sample is grounded, i.e. sample potential $V_{\text{sample}} = 0$ V. The electron kinetic energy at any given point with potential V is

$$U_{\text{kin}} = U_0 + q\,V \tag{4.2}$$

where q is the unit charge[2]. While traveling through the lens, any point with potential $V < U_0/q$ is unreachable for the electron. Thus, when the detector is surrounded by a volume where $V_{\text{gate}} < U_0/q$, the electron cannot reach the detector.

A schematic picture of the original setup of the detector is given in Figure 4.1. The gold mesh is kept in physical contact with the last lens element of the ARTOF lens, and thus shares the same potential. A potential V_{LV4} is fed to the last lens element. A strong positive potential V_{DBIAS} is fed to the MCP. The mesh and the MCP are parallel surfaces, producing a homogeneous electric field

$$\mathbf{E} = -\frac{V_{\text{DBIAS}} - V_{\text{LV4}}}{d_0} \cdot \hat{\mathbf{r}} \tag{4.3}$$

where d_0 is the distance between the potential surfaces and $\hat{\mathbf{r}}$ is the spatial unit vector along the lens axis. To determine the electron's time-of-flight through the detector, i.e. from the mesh to the MCP, we have to consider the electron's speed at the mesh

$$v = \sqrt{2U_{\text{kin}}/m} = \sqrt{2(U_0 + q\,V_{\text{LV4}})/m} \tag{4.4}$$

[2] Note that the electron is a negatively charged particle with charge $-q$.

and the impinging angle θ relative to the lens axis. The electron will be accelerated by the **E**–field before reaching the MCP. Due to the direction of the field vector along the lens axis, the velocity component $\mathbf{v}_{\parallel}$ parallel to the lens axis will increase while $\mathbf{v}_{\perp}$ remains unchanged.

To find an approximate value of the impinging angle θ we can consult published particle trajectories [3]. Figure 3.3 (see Chapter 3) suggest that electrons, before reaching the detector, pass through an intermediate focus approximately 200 mm from the detector prior to traveling on almost straight lines to the detector with 20 mm radius. This corresponds to a maximum impinging angle $\theta_{\max} \approx 0.1$ rad. This small angle justifies the approximation $|\mathbf{v}| = |\mathbf{v}_{\parallel}|/\cos\theta \approx |\mathbf{v}_{\parallel}|$. Therefore, for the time-of-flight calculation, we can regard the electron as impinging parallel to the lens axis.

The time-of-flight of a charged particle in a homogeneous electric field is well known [84].

$$t = \frac{\sqrt{2m(U_{\text{kin}} + qEd_0)}}{qE} - \frac{\sqrt{2mU_{\text{kin}}}}{qE}. \tag{4.5}$$

Substituting equation (4.2) and equation (4.3) in equation (4.5), and setting $d = d_0$, the non-gated case becomes

$$t_{\text{nogate}} = \frac{\sqrt{2m(U_0 + qV_{\text{DBIAS}})}\cdot d_0}{q(V_{\text{DBIAS}} - V_{\text{LV4}})} - \frac{\sqrt{2m(U_0 + qV_{\text{LV4}})}\cdot d_0}{q(V_{\text{DBIAS}} - V_{\text{LV4}})}. \tag{4.6}$$

The gated detector, pictured in Figure 4.2, has been extended with two additional meshes. The first mesh (M1) still maintains a physical connection to the last lens element. The MCP has been moved 20 mm back from its original position. Since the length of the flight paths through the detector is increased, and the gate includes decelerating elements, the time-of-flight, t_{gate}, must be larger than t_{nogate}. This increased flight-time must be considered while processing the measured data.

The gated detector produces three regions of homogeneous electric fields separated by the meshes. We can apply equation (4.5) to each region. Using the notation given in Figure 4.2 we have

$$\begin{aligned}
t_{\text{M1–M2}} &= \frac{\sqrt{2m(U_0 + qV_{\text{M2}})}\cdot d_1}{q(V_{\text{M2}} - V_{\text{LV4}})} - \frac{\sqrt{2m(U_0 + qV_{\text{LV4}})}\cdot d_1}{q(V_{\text{M2}} - V_{\text{LV4}})} \\
t_{\text{M2–M3}} &= \frac{\sqrt{2m(U_0 + qV_{\text{M3}})}\cdot d_2}{q(V_{\text{M3}} - V_{\text{M2}})} - \frac{\sqrt{2m(U_0 + qV_{\text{M2}})}\cdot d_2}{q(V_{\text{M3}} - V_{\text{M2}})} \\
t_{\text{M3–MCP}} &= \frac{\sqrt{2m(U_0 + qV_{\text{DBIAS}})}\cdot d_3}{q(V_{\text{DBIAS}} - V_{\text{M3}})} - \frac{\sqrt{2m(U_0 + qV_{\text{M3}})}\cdot d_3}{q(V_{\text{DBIAS}} - V_{\text{M3}})}
\end{aligned} \tag{4.7}$$

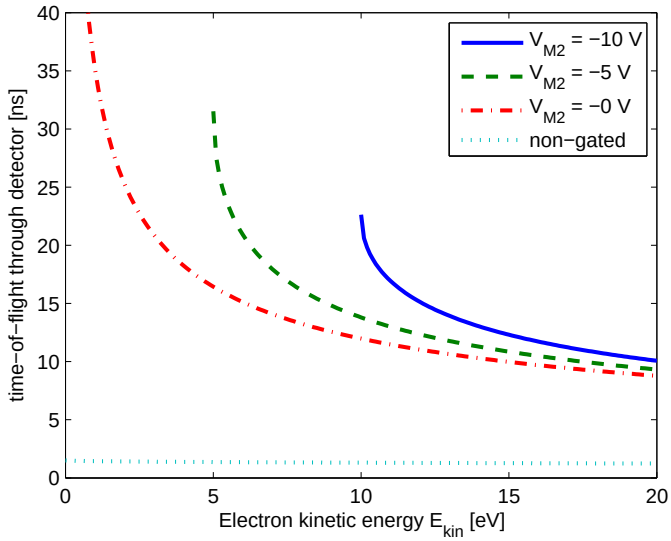

Figure 4.6. *Time-of-flight for electrons with a range of kinetic energies E_{kin} traveling through the gated detector with different gating potentials. $V_{\mathrm{M2}} = 0$ V correspond to the field free case. Note the sharp edges at the cut-off potentials.*

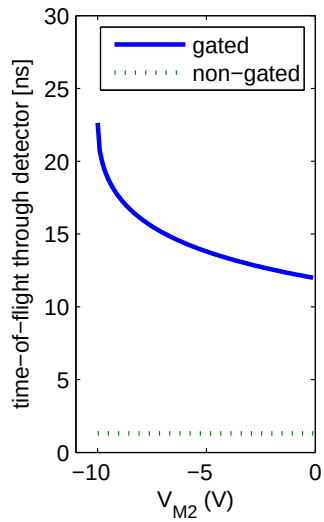

Figure 4.5. *Time-of-flight for 10 eV electrons traveling through the gated detector (blue) for different potentials V_{M2} on the gating mesh M2. The time-of-flight for 10 eV electrons in the non-gated detector is given for reference (green).*

where d_1, d_2, d_3 are the lengths of each of the regions (the distances between the meshes). Summing up the flight times gives the total time-of-flight between the last lens element and the MCP detector.

$$t_{\mathrm{gate}} = t_{\mathrm{M1-M2}} + t_{\mathrm{M2-M3}} + t_{\mathrm{M3-MCP}}. \tag{4.8}$$

To calculate the increase in flight time induced by the gate we need to evaluate the difference $\Delta t \equiv t_{\mathrm{gate}} - t_{\mathrm{nogate}}$. A gate setup with $d_0 = d_1 = d_2 = d_3 = 10$ mm could be used as a benchmark to estimate the magnitude of Δt. We apply a high positive potential on the MCP ($V_{\mathrm{DBIAS}} = +500$ V), and keep all other potentials to ground. Then $t_{\mathrm{gate}} = t_{\mathrm{M3-MCP}}$ and the increase in flight-time equals the field-free flight from M1 to M3 in the gated detector.

$$\Delta t = \frac{2d}{\sqrt{2U_{\mathrm{kin}}/m}} \tag{4.9}$$

For $U_{\mathrm{kin}} = 10$ eV, a typical kinetic energy for an electron impinging on M1, we find $\Delta t = 10.6$ ns. This is a significant increase in flight time.

In real gating, one might want to decrease the kinetic energy even further with the gating mesh (M2). A potential $V_{\mathrm{M2}} = -5$ V

on M2 adds an additional 2 ns to the flight time. Figure 4.5 illustrates the increasing time-of-flight as a stronger deflection potential on M2 is introduced. As the deflection potential approaches the cut-off potential the increase in time-of-flight rises above 20 ns.

As noted earlier, the perpendicular component $\mathbf{v}_\perp$ of the electron velocity is not affected by the electric fields. Nevertheless, the final position on the detector is indeed affected due to the increased flight-time. This spatial change is determined by

$$\mathbf{r}_{\text{gate}} - \mathbf{r}_{\text{nogate}} \equiv \Delta\mathbf{r} = \mathbf{v}_\perp \cdot \Delta t \tag{4.10}$$

where $\mathbf{r}_{\text{gate}}$ and $\mathbf{r}_{\text{nogate}}$ are the hit positions on the detector in the gated and non-gated case, respectively. Reviewing again the trajectories in Figure 3.3, it can be easily seen that increased flight-time will also increase the spread of electrons on the detector, as the electrons radiates from the intermediate focus. These shifts in positions cause an additional complication to the gate. In the non-gated, angular resolved mode of the lens, the electrons originating from the sample are focused parallel-to-point[3] to the detector. When the detector is displaced, it is also positioned out of focus of the lens. This problem could however be circumvented by an adaptation of the lens focus to the new detector position (by changing potentials of the lens elements) and an updated transformation matrix (equation (3.3)). Secondly, the decelerating potential on the M2 mesh effectively "elongates" the lens by increasing the flight-time. This elongation is dependent on the gating potential, as can be seen in Figure 4.5, but also on the kinetic energies of the electrons. Keeping in mind that a range of electron energies should be readily detected, it must also be noted that the flight-time is not linear with regard to the electron energy. Figure 4.6 reflects this phenomenon.

While Δt can be calculated analytically, there is no possibility to analytically determine the position deviation for each combination of electron energy and initial angle. Such analysis must therefore be executed with the aid of simulations performed by the manufacturer.

4.4 Experimental results

The results our gating is presented in Paper I and will only be discussed briefly here.

The main figure of merit for detector gating is the detection efficiency; defined as the number of detected electrons originating from the selected camshaft bunch and arriving in the analysis

[3] Monoenergetic electrons emitted with identical angles, but from different sample points, are focused to the same point on the detector.

time window, hence electrons within the selected energy window. These electrons represent the effective counts, which are compared to the total number of all detector counts. The detection efficiency is increased in two steps; by introducing the constant potential V_{nej} and by the gate pulse. To quantify this effect, we made three sets of measurements on a bilayer graphene sample, using 185 eV light and the centre energy of the lens at 175 eV, thus measuring parts of the valence band. The first measurement had no constant voltage applied, resulting in 300 effective counts/s out of a total count rate of 90,000 counts/s (efficiency: 0.3%). The application of a constant potential $V_{\mathrm{nej}} = 164\,\mathrm{eV}$ gives 600 effective counts/s at a 72,000 counts/s total (efficiency: 0.8%). Finally, the application of the gate pulse at 20 V amplitude gives 5,000 compared to 65,000 counts/s (efficiency: 8%), increasing the efficiency by an order of magnitude. The latter efficiency increase is expected at BESSY, since roughly 10% of the total current in the ring is due to the camshaft bunch. Figure 4.7 shows the full time-of-flight spectrum acquired with and without the gate pulse applied. The energy analysis of the electrons in the analysis window (Figure 4.8) reveal that the kinetic energy spectrum is undisturbed by the gate pulse.

The constant potential V_{nej} introduces a clear cut-off with a characteristic cone–shape which can be clearly seen even without an applied gate pulse. Figure 4.9 shows flight time vs. detector position for four different deflection potentials. Electrons with longer flight times are accepted at the centre of the detector, while electrons at the periphery have a more restricted acceptance. We would expect the opposite behaviour if the cut–off was uniform with regard to the electron energy. An electron hitting the detector close to its edge has a longer flight time than an equally energetic electron hitting the centre. Therefore, this effect must have a different origin. We have not conclusively established why this phenomenon appears. It is known from the properties of the lens that electrons hitting the detector in the periphery will have lesser impinging angles towards the mesh ensemble. Since electrons with initial kinetic energies close to the cut off potential will be decelerated to very low velocities, it is possible that those with smaller impinging angles are more likely to be deflected by the constant potential. This feature has implications on the energy analysis, since we can see that electrons are deflected even if their kinetic energy should be sufficient to clear the deflection potential. We can conclusively state that the cone edge have a well-defined shape and magnitude, and moves along the TOF-axis proportionally to the magnitude of the potential. This implies that no effect should be present at a sufficiently low deflecting potentials.

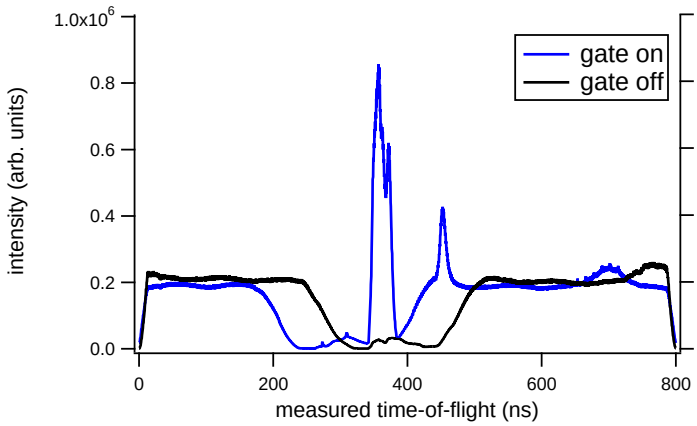

Figure 4.7. *Full measured time-of-flight spectrum on graphene valence band with (blue) and without (black) gate enabled. The spectra have been normalised to the (apparent) background level of the multibunch electrons. The gate pulse was delayed to match the desired temporal window for gating the electrons originating from the hybrid bunch. The graph clearly shows how the analysable electrons originating from the camshaft bunch are enhanced.*

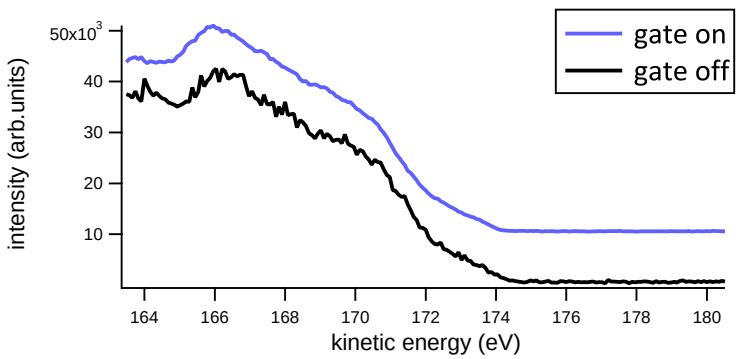

Figure 4.8. *The graphene valence band spectrum obtained with and without gating during 10 minutes measurement. The statistics of the former in much higher, although all features of the spectrum are preserved.*

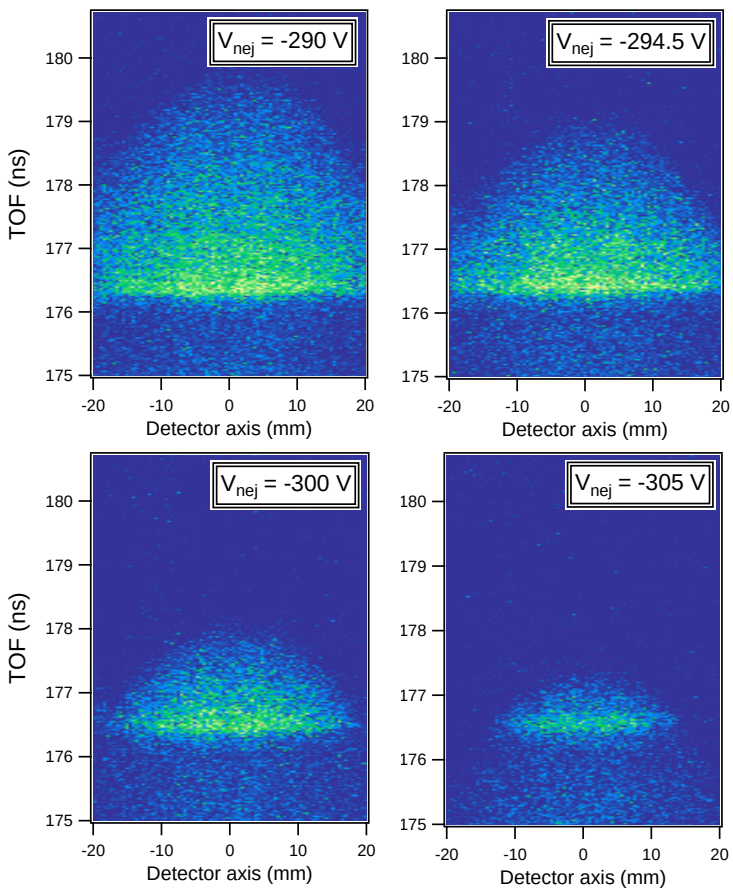

Figure 4.9. *Measured graphene valence spectra for four different V_{nej} deflecting potentials. These spectra were measured with* 320 eV *photon energy and the lens focused at* 310 eV *electron kinetic energy, measured for five minutes each. The analysable window of the spectrometer is 30 eV and extends from 168 ns to 192 ns. The spectra clearly show the cone–shape of the cut-off, and its movement along the time axis as the deflecting potential increases.*

4.5 Discussion

In conclusion we have shown that it is possible to gate the multi-bunch electron pulses in an ArTOF spectrometer, thus allowing using effectively the signal originating from the camshaft pulse(s). The efficiency of the detection has been shown to increase with at least one order of magnitude. Detector gating is restricted to hybrid modes. This gating scheme should be useful for operation at BESSY together with a mechanical chopper [59] or resonant pulse picking [41]. A plan to utilize this combination is currently pursued at BESSY where both choppers and pulse picking will be commissioned soon.

Several issues however remain for the future: We have seen that high energy contributions in the photon beam decrease the efficiency of the gate. This could be improved with a photon energy filter in the beamline. The parameters of the lens should be further optimized to account for focusing conditions at relevant gating potentials, in order to fully preserve the resolution of the instrument. This must include a full implementation of the gating scheme in the lens transfer matrices. Here, the variability of the gating pulse should be taken into account. The theoretical framework in this chapter shows that there are still many factors to consider in order to preserve the excellent resolution of the instrument.

We intend to study the influence of the gating pulse to the detector to allow for higher gate amplitude. One option which has not yet been pursued is to introduce a signal handling scheme where gate pulse noise is filtered from the MCP response before reading in the CFD. The physical design of the mesh ensemble could possibly be changed to further reduce the signal transmission from mesh to detector. One should also consider to move the gate mesh to the front of the ARTOF spectrometer, as will be described in Chapter 5, in order to allow for much higher gate amplitude and also to allow for gate operation for smaller hybrid windows.

CHAPTER 5

FRONT GATING

The front gating scheme is the second of the two realisations of ARTOF gating which have been explored within the ARTOF development project. The front gate solution was developed particularly with operation at MAX IV in mind; namely to multi–bunch operation with 10 ns pulse separation. The theoretical and methodological framework is outlined in Paper II, which was presented at the *Synchrotron Radiation Instrumentation* conference in Lyon, July 2012. During the time past, the front gating scheme was adapted to allow for proof-of-principle tests to be made at BESSY in hybrid mode. Although front gating and detector gating have been developed in parallel, detector gating was prioritised due to its direct applicability to BESSY operation. Initial tests with a mounted front gate were performed at BESSY in March 2014.

This chapter presents the current state of front gate development. It shows how the front gate has been realised together with results from initial tests. Although the front gate measurements have not showed conclusive results yet, they can provide a base for further development. It is my aim to proceed with front gating development in the coming year.

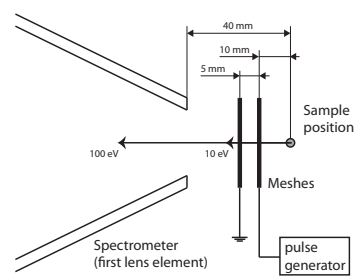

Figure 5.1. *The conceptual design of the electronic gate. The mesh closest to the sample is connected to a fast pulse generator. The second mesh shields the entrance to the spectrometer from the gating potential. The annotations refer to the setup intended for the ARTOF 10k, where lens-to-focus distance was 40 mm. The distance travelled by a 10 eV, and a 100 eV, electron in 10 ns is indicated.*

5.1 Physical design

The original design considerations for the front gate were presented in Paper II. In its most simple form, it consists of two consecutive high transmission meshes placed in front of the first lens element of the ARTOF (see figure 5.1). A sufficient negative potential is applied to the mesh closest to the sample. The purpose of this gating potential is to deflect all electrons away from the lens when the gate is closed. The second mesh, which is grounded, has two functions: Firstly, it protects the spectrom-

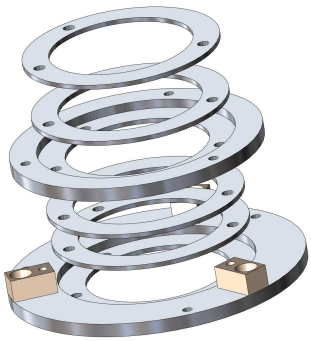

Figure 5.2. *Exploded view of the front gate designed for use with ARTOF 10k and ARTOF-2. The meshes were glued between the thinner rings and mounted to the holder. The lower mesh holder was fastened with screws directly on the first lens element.*

eter from the gating potential, whereas the gating potential otherwise would leak into the lens and obstruct its focusing condition. Secondly, it increases the available ramp–up time for the gating potential. When the gate is closed, no electrons from the interaction region are able to reach the spectrometer. To open the gate, the potential is reduced to zero (ground) allowing for undisturbed passage of electrons.

Since the publication of Paper II, the conceptual design was developed into the front gate seen in figure 5.2. The gold meshes were fixed between two stainless steel rings with UHV-compatible silver–glue. The meshes were straightened to assure high flatness. Two stainless steel holders were created for the mesh rings. These were separated with isolating spacers made from UHV-compatible PEEK plastic. The inner holder could be mounted directly on the spectrometer nose by removing the nose cap and using the existing mount. The design was made to fit both ARTOF 10k and ARTOF2.

The high transmission gold mesh was acquired from *Precision Eforming* (28 wires/cm, 18 μm wire diameter, and 90 % transmission efficiency). Effective diameter for both meshes was 32 mm. They were mounted with 8 mm separation, which was sufficient to prevent sparks from the high–voltage loads.

A second design was developed for use with the ARTOF 10k pre-lens[1]. Due to the smaller nose and a shorter lens-to-focus distance, it was used without holders. The outer mesh diameter had to be reduced to allow for the light beam to pass the gate without being blocked. Effective diameters were 15 mm and 35 mm. A photograph of the mounted front gate for the pre-lens is seen in figure 5.3.

The inclusion of additional electrostatic elements to the lens system will inevitably disturb the trajectories of electrons. Even slight changes in arrival times, arrival positions or focus conditions can have substantial effects on resolution in a precision instrument. Therefore, precautions must be made to ensure that these disturbances are kept to a minimum and become predictable. Changes of original trajectories can be tolerated if a renewed calculation of lens potentials can account for them. In this respect, front gating constitutes a stronger disturbance to the instrument than detector gating; the reason being that the disturbing element is placed very early in the lens, thus allowing a directional error to propagate over the full trajectory.

When no gate is mounted to the spectrometer, the electric field at the nose is determined by its shape and the applied potential to the first lens element (L1). The front of an electrostatic

[1]This lens was constructed at Uppsala University for use together with the prototype version of the ARTOF 10k. Sone Södergren, Uppsala University, is acknowledged for providing details of the design.

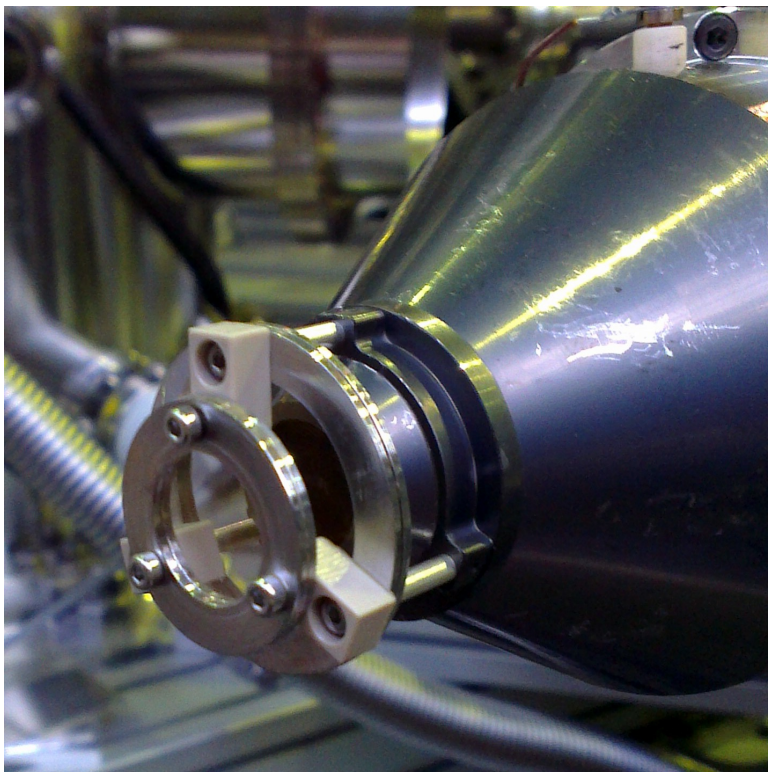

Figure 5.3. *Front gate mounted on the pre-lens. The gate was elevated from the lens using aluminium spacers since the lens geometry did not allow a direct contact mount.*

lens for electron spectroscopy is typically grounded [2]. The beginning of L1 is located a few mm inside the spectrometer opening. Usually an accelerating potential is applied to L1; this potential increases collection efficiency since a larger emission cone can be accepted by the instrument. Figure 5.4 shows an electrostatic simulation of the front gate mounted on the pre-lens (as depicted in figure 5.3). For this simulation the SIMION software [85] was utilized. In this geometry, L1 is situated >20 mm from the opening of the lens. My simulation shows that the field penetration through the lens opening is < 2%, and we expect that the front gate has only a minor effect on the electron trajectories while all gate components are grounded.

As a rule of thumb, the penetration length through a cylindrical aperture equals its diameter [86, p. 201]. Figure 5.5 shows the field penetration from the ARTOF 10k lens [3], as it was simulated by *VG Scienta AB*. In this case there is a non-negligible potential

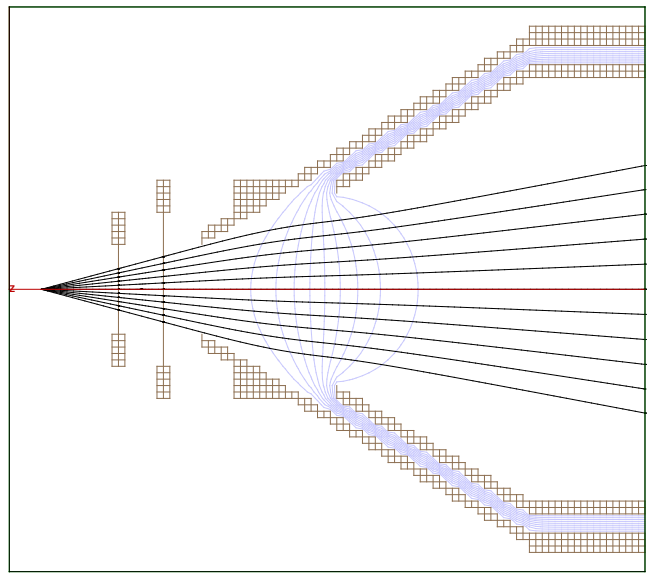

Figure 5.4. *Electrostatic simulation of the front gate mounted on the pre-lens. The isolating mounting of the gate is not included as they only have minor effect on potentials. The simulation is cylindrically symmetric. A positive potential equal to the electron kinetic energies is applied to L1. Potential surfaces are shown in blue. An electron fan with ±15° is emitted from the source position 25 mm from the lens front. The simulation shows that the electric field in this geometry hardly penetrates the lens front opening.*

contribution almost all way up to the source point. In this geometry, inclusion of a gate mesh is possibly a destructive intervention in the lens.

A recent updated design of the ARTOF includes a wide–angle lens. These new lenses will allow for a further increase in transmission and ability to record larger electron emission fans in the angle–resolved mode. An ARTOF of this type are planned to be included at the PM4 and CoESCA end-stations at BESSY. These wide–angle lenses are terminated at the nose with a mesh. A future extension of the front gating concept to this lens would mean simply adding an additional mesh with similar dimensions in front of the permanent mesh. In addition, studies with wide angle lenses have shown that spherical and ellipsoidal meshes can be used to further increase acceptance angles [87, 88]. The front gating concept could possibly be extended to these mesh shapes.

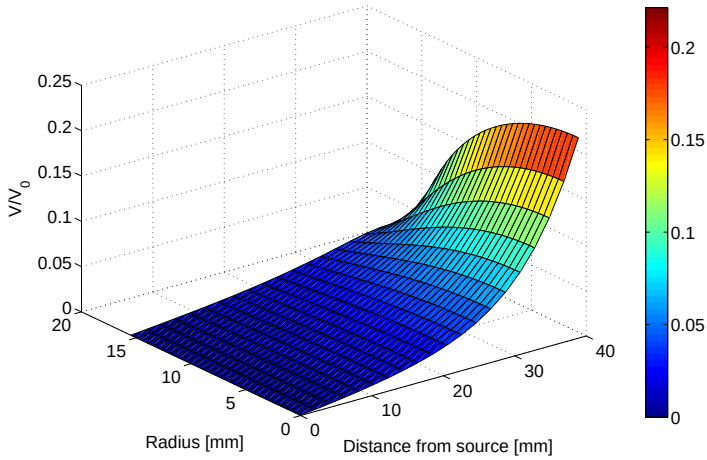

Figure 5.5. *Field penetration from ARTOF 10k lens. Source point is at (0,0) and center of lens opening is 40 mm from source. Potential is given as the fraction of the L1 potential. The lens is cylindrically symmetric. (Data courtesy of VG Scienta AB.)*

5.2 Electronic pulsing

The electronic pulsing requires a pulse generator and a suitable connection to the mesh in vacuum. In Paper II we discussed the requirements for this pulse generation. We aim to operate with ∼1 MHz repetition rate, addressing typical flight times in the ARTOF (∼ 1 μs), required fall and rise times and the overall pulse width (Fig. 5.6). High demands are put on the electronics, but solid-state switches with rise/fall–times down to a few ns sustaining 1 kV and 1 MHz repetition rate are commercially available (e.g. Refs. [89, 90]). For gating at MAX IV multi–bunch conditions or BESSY hybrid mode we have considered the *BEHLKE FSWP 51–02* MOSFET–type solid–state switch [89]. This switch can provide <50 ns pulses (rise–time 6 ns, fall–time 11 ns) with repetition rates up to 3 MHz and 5,4 kV amplitude. For BESSY hybrid mode conditions this is sufficient without adaptations. For MAX IV multi bunch, we require <20 ns pulses, and in Paper II we propose a solution with two switches providing alternating blocking pulses. This would allow for a shorter opening window if the pulse generators have a very precisely determined delay. Each switch must be synchronized to the frequency of the light pulses, which can be extracted with a photo–diode in the experimental chamber, or obtained from the ring clock. The

BEHLKE switch requires liquid cooling, which we could not provide for our initial tests of the front gate (presented in next section). Therefore, the tests we performed at BESSY used a DEI PVM-4210 pulse generator module [90], fed by a +24VDC power source and a NIM pulse with variable pulse length and repetition rate produced by a function generator. With this setup we could produce ∼100 ns pulses with 100 kHz repetition rate and amplitude just above 100 V.

To maintain good focus of the lens, it is necessary to avoid disturbances from the gating mesh while the gate is open. Ideally, we would have a zero gating potential during the time the electron passes. The signal from the system must therefore be sufficiently free from ringing[2]. Our calculations show that the capacitance of the gate can be kept below 10 pF when short wiring is used. The internal capacitance of the pulse generator is expected to be larger. Considering a maximum 500 V gating potential achieved in 3 ns, the required peak current is ∼2 A, which allows for a SHV transmission line to be used. In our tests, the gated mesh holder was connected by an impedance matched coaxial cable, while the shielding was connected to the ARTOF nose. A SHV UHV feed–trough provided the connection to vacuum.

5.3 Experimental results

The first experimental tests were performed at beamline UE52-SGM at BESSY, with the storage ring running in hybrid mode. The gate was mounted at the pre-lens, as shown in figure 5.3. A bilayer graphene sample on SiC was mounted on a manipulator arm along the ARTOF axis.

To establish if our mounting of the front gate changes the electron spectrum, we compared two sets of measurements on the valence band with and without the gate meshes mounted. The photon energy was set to 120 eV and all beamline settings were unchanged between the measurements. As the front–gate was installed, the nose-to-sample distance was increased by ~ 4 mm to allow enough room for the synchrotron beam to pass[3]. Since the ARTOF had been removed and later reinstalled at the chamber, it was not possible to establish the exact change in nose-to-sample distance[4]. Figure 5.7 show measured TOF in the region of interest. The displayed spectra are almost identical

[2] Ringing occurs in electrical circuits as an unwanted oscillation of a voltage or current, caused by stray capacitances and inductances in the circuit.

[3] As mentioned, the front gate had been mounted 10 mm further from the nose than the design value.

[4] An indirect correction for this change could have been done by a renewed t_0 calibration using scattered photons.

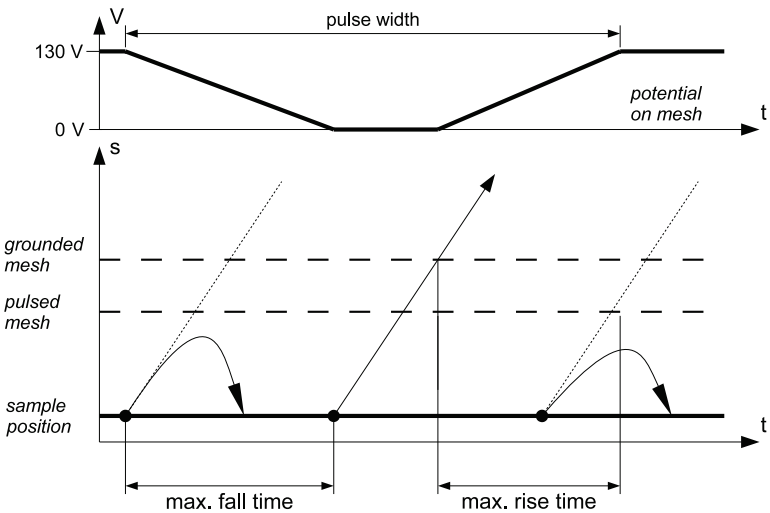

Figure 5.6. *Timing principle for the gate in a 2D time–space–diagram together with required gating potential. The tilted lines indicate propagation of mono-energetic electrons through the gate. The first and third electron should be deflected, while the second should pass the gate. Mesh potential is given for 100 eV electrons. The limits for rise time decreases as electrons become slower, while fall times can be constant.*

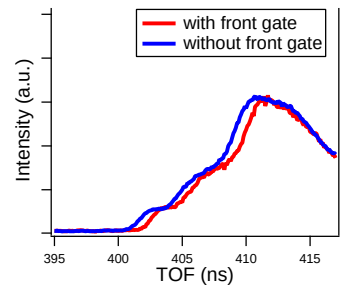

Figure 5.7. *Time-of-flight spectrum of the graphene valence bands originating from the hybrid peak. The photon energy was 120 eV. The two bands display a relative shift of 0.8 ns, which can be attributed to an error in the placement of the sample.*

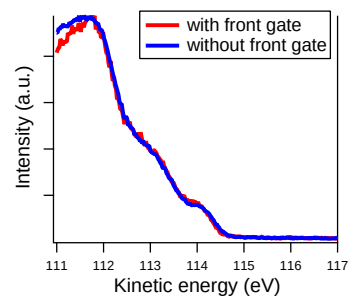

Figure 5.8. *The graphene valence bands measured at 120 eV photon energy before and after the installation of the front gate. The temporal shift noted in the previous figure has been corrected prior to energy analysis.*

apart from a 0.8 ns shift towards longer flight times for the installed front gate (red curve). From electrostatic simulations we find that this is consistent with a sample placement 5 mm further from the nose. When correcting for this temporal shift, we acquired the photoelectron spectra in Figure 5.8. The measured spectra are clearly consistent above 112 eV. Below 112 eV, there is a constant reduction of measured intensity when the front gate was installed. The shape of this edge is a consequence of the applied cut–off potential on the detector mesh, which was set to −109.25 V. We know from detector gating that the potential V_{nej} affects electrons also within the lower end of the energy window due to their transverse momentum components while flying through the instrument. The intensity difference at the edge of the energy window should therefore be disregarded. The disturbing effects of installing the front gate are thus very limited, and a valence spectrum can be completely reproduced.

To establish the effect of the front gate potential, we performed two series of measurements where a constant negative potential was applied to the gating mesh without any gating pulse. The Si 2p doublet–peak was measured with 210 eV photon energy. The doublet structure is expected at 105 eV kinetic energy. A set of measurements with different constant potentials

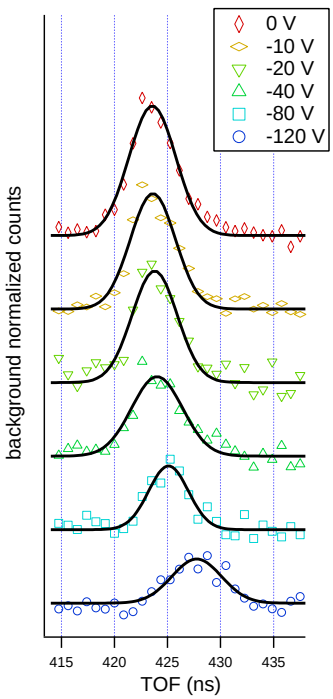

Figure 5.9. *Time-of-flight spectrum of the unresolved Si 2p peaks (expected $E_{kin} \approx 105$ eV) with applied constant potentials to the first mesh. The Si 2p peak originates from bulk SiC. The intensities have been normalized to the background level, as described in the text. Background has been subtracted in this spectrum.*

are displayed in Figure 5.9. A similar set of measurements of the graphene valence band is displayed in Figure 5.10. This spectrum was acquired at 90 eV photon energy. All spectra were normalized using a similar method: The background constituted up to 50 % of the total count in the region of interest[5]. We observed during detector gating studies that the background mainly consists of high energy electrons which are emitted from second order light. These high energy electrons are not hindered by the front gating potential and the background count rate is expected to be constant for all measurements. Therefore, the peaks were normalised to the background level at the position of the peak center of the undisturbed peak (front gate mesh at ground). For Si 2p we fitted the peak to a Gaussian line shape.

Both the Si peaks and the graphene band display a gradual reduction of intensity as the potential is increased. We also observe a peak shift towards longer flight times. Although this trend is expected due to the retardation all electrons experience at the front gate, it is striking that no clear cut–off is observed. As the potential is raised above the kinetic energy of the electrons, we still observe peaks in the region of interest both for Si 2p and graphene valence. This behaviour could be explained in two ways: Either a large fraction of the electrons manage to pass the gate following trajectories which bypasses the gate, or that a correct potential was not applied or supplied to the mesh. The behaviour of both sets of spectra points towards this solution. In particular, the sudden reduction of intensity and shift of peaks for the Si–spectra with –80 V and –120 V applied potential hints that the potential actually applied was close to the electron kinetic energy, but did not exceed it. Such a potential, my simulations show, would cause a fraction of the electrons to follow trajectories which would not be accepted by the instrument, in fact the graphene spectrum displays a shift for –100 V and –120 V, while the –140 V spectrum has been shifted towards shorter flight–times. The latter effect may be explained if the applied potential manages to block slow electrons in the measured band, while faster electrons pass through.

The experienced potential reduction has to be explained by a faulty potential source or a potential drain in the chamber. Inspection during dismounting of the instrument has given no indication of any direct problem in mounting. Therefore, the observed effect remains unexplained until further tests can be performed.

As a final test, we considered the possible disturbances on the detector read–out due to transmission of RF-frequencies. The

[5] Due to a problem with the BESSY injector during the measurements the relative intensity of the hybrid peak was smaller than in under normal hybrid operation.

outcome of our successful detector gating (Chapter 4) showed that the detector was overloaded when a gate pulse was applied close to the MCP. Tests showed that when the gating pulse contained higher frequency components, the detector tended to be overloaded[6]. The MCP read–out is particularly sensitive, but also the delay–line readings can be affected. A challenge is when noise similar to real signals stall the detector. For the front–gate, there were particular concerns that the hollow ARTOF lens would act as a wave–guide and effectively transport unattenuated RF-signals to the detector. To test this effect, we performed measurements where a sinusoidal signal with 10 V amplitude was fed to the gate mesh. The frequency was increased in steps from 100 MHz to 70 MHz while the responses on the MCP and the delay–lines were monitored. The reference count-rate at zero frequency was 400 kcounts/s in the MCP channel and 60 kcounts/s (complete events) in the DLD-channel. At 60 MHz the MCP count had increased to 600 kcounts/s and DLD-count to 100 kcounts/s. At 68 MHz a sudden detector overload occurred independently in both the MCP and DLD-channel.

We proceeded by applying regular 100 ns long pulses from the DEI pulser to the gating mesh, gradually increasing their amplitude. We could increase the amplitude from zero to 300 V without overloading the detector; higher amplitudes were not permitted by the pulse generator.

The pulse generator used was a severe limitation. Creation of the required pulse frequency could not be achieved when its duration was reduced to 100 ns. Therefore we could not create a pulse with required characteristics fro gating. While a 100 ns pulse could be created, it could only be delivered with 50 kHz repetition rate, thus only picking 1 in 25 hybrid pulses. We established through an oscilloscope observation that ring clock synchronization was achieved. We could also create a precisely determined delay to center our pulse to the hybrid window. However, we could not distinguish any "true" spectrum or peak from the comparatively large high–energy electron background presumably created by second and third order light, as well as scattered photons. Actual gating of the hybrid peak thus remain to be achieved.

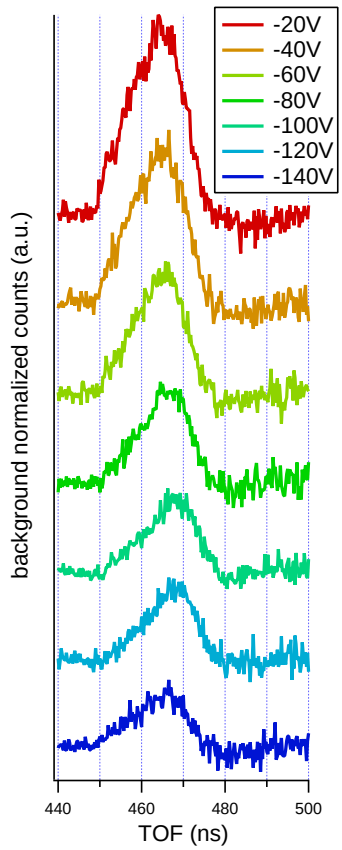

Figure 5.10. *Time-of-flight spectrum of the graphene valence band with applied constant potentials to the first mesh. The photon energy was 90 eV. The intensities have been normalized to the background level, as described in the text.*

5.4 Discussion

Electrostatic simulations and experimental verification has shown that a front gate can be installed without severe distur-

[6] It should be noted that overload due to stray frequency components is different from overload due to intense electron impact. The latter causes large currents to pass through the MCP which may cause the detector to burn. Frequency overloads cause only signal errors and are not harmful to the detector.

bances to electron trajectories at the ARTOF pre–lens. The effects still need to be studied for other lens designs. We also saw that electric pulses of the required length and amplitude could be applied to the gate without overloading the detector. These findings support the front–gate scheme.

The further development should be focused on a more suitable pulse generator together with a renewed gate design. For the physical design, the gate must be changed to allow a closer mount relative to the spectrometer. Simulations have shown that a close mount does not significantly disturb electron trajectories for the pre–lens. If the front–gating scheme is to be extended to other versions of the ARTOF, gate designs should be further discussed in collaboration with the manufacturer.

For gating, a setup containing a high frequency solid–state switch should be developed. As mentioned, such switches with suitable characteristics are commercially available, but will require a liquid cooling system.

Further tests are planned upon completion of the new CoESCA end–station at BESSY, which will include two ARTOF instruments of different designs. This end–station will be operational in 2015.

CHAPTER 6

SUMMARY AND OUTLOOK

This thesis has addressed how timing–based electron spectroscopies can be best used at storage ring light sources. I have shown how important developments in accelerator technology and beamline instrumentation will simplify the use of timing-based instruments . Some of these solutions are particularly interesting for high-brilliance light sources, such as MAX IV, and could prove valuable for the future course of electron spectroscopy instrumentation at the facility.

Since the beginning of my studies in 2011, an increasing interest in timing–based experiments at MAX IV has been expressed both by the user community and the accelerator staff at MAX IV. Initial meetings with relevant stakeholders have taken place to discuss requirements for timing at the facility. These discussions are likely to continue. This work could form part of a framework for discussion on these issues.

My experimental contribution to the field has been in the area of ARTOF gating, aimed at allowing us to use the most efficient electron spectrometer at MAX IV. This project is ongoing and further tests and development are planned. Detector gating has proven successful under the timing requirements set by the hybrid mode at BESSY. Further development of this scheme will include continued impedance matching of the gate electronics and attempts to achieve gating where higher demands are put on energy resolution. This development should be done in dialogue with *VG Scienta AB*. In particular, new transformation matrices which accounts for the inclusion of the detector gate should be calculated.

Currently, two new permanent end–stations including ARTOF are built at BESSY—PM4 and CoESCA. These will be operational in 2015. PM4 will feature the MHz chopper solution discussed in Chapter 2. Thus, single–bunch operation will be available (almost) all–year. Nevertheless, detector gating

may still prove valuable to gate stray electrons which might be present. The same goes for the application of resonant pulse–picking at BESSY. Therefore, further refinement of the detector gate should be pursued.

The front–gate scheme has not yet achieved its projected performance. Areas for improvement has been outlined in Chapter 5. New attempts to achieve front–gating is expected as the Co-ESCA station is commissioned in 2015.

I mentioned in Chapter 2 how experiments using HDA in coincidence with eTOF instruments can benefit from the temporal properties of MAX IV, particularly the 100 MHz RF system. It is my intention to pursue this timing scheme. As a proof–of–principle, plans have been made to test the timing scheme at MAX II using a setup containing an electron–TOF and a hemispherical analyser. If proven successful, a case will be put forward to implement such a coincidence scheme at MAX IV using a state-of-the-art high–transmission ARTOF spectrometer. Beamtime at I411 has been granted and experiments are planned for spring 2015.

ACKNOWLEDGMENTS

My supervisor Rami Sankari is greatly acknowledged for his firm guidance, our many interesting discussions and all the moral support throughout this project. My assistant supervisor Ralf Nyholm is likewise acknowledged for this support and feedback on my work.

All people involved in the ArTOF project; especially Torsten Leitner, Ruslan Ovsyannikov, Svante Svensson, Nils Mårtensson, Andreas Lindblad, Mihaela Gorgoi and Melanie Mucke; are acknowledge for their participation and support for realizing the gating schemes and for teaching me a lot of practical skills related to beamline instrumentation.

I have had valuable discussions on timing related issues with Teresia Olsson, Walan Grizolli and Simon C. Leemann. This has contributed greatly to the chapter on timing based instrumentation.

VG Scienta AB has kindly provided me with relevant data on the ArTOF lens. They are also acknowledged for providing figures for this thesis. Johan Winqvist is acknowledged for his contributions to the graphics of this thesis.

Funding for travels to BESSY was provided by Ångpanneföreningens forskningsstiftelse, Westlings minnesfond, and Bokelunds resestipendiefond.

REFERENCES

1. Fadley C. *X-ray photoelectron spectroscopy: Progress and perspectives.* J. Electron Spectrosc. Relat. Phenom., **178–179**:2–32 (2010). doi:10.1016/j.elspec.2010.01.006.

2. Wannberg B. *Electron optics development for photo-electron spectrometers.* Nucl. Instrum. Methods Phys. Res. A, **601**(1-2):182–194 (2009). doi:10.1016/j.nima.2008.12.156.

3. Öhrwall G, Karlsson P, Wirde M, Lundqvist M, Andersson P et al. *A new energy and angle resolving electron spectrometer — First results.* J. Electron Spectrosc. Relat. Phenom., **183**(1-3):125–131 (2011). doi:10.1016/j.elspec.2010.09.009.

4. Ovsyannikov R, Karlsson P, Lundqvist M, Lupulescu C, Eberhardt W, Föhlisch A, Svensson S, and Mårtensson N. *Principles and operation of a new type of electron spectrometer - ArTOF.* J. Electron Spectrosc. Relat. Phenom., **191**:92–103 (2013). doi:10.1016/j.elspec.2013.08.005.

5. *Time of Flight spectrometers THEMIS 1000 / THEMIS 600 — Technical note.* `http://www.specs.de/cms/upload/PDFs/ApplNotes/THEMIS/TNote_THEMIS_performance_overview.pdf` (2014-04-11).

6. Eland JHD, Vieuxmaire O, Kinugawa T, Lablanquie P, Hall RI, and Penent F. *Complete two-electron spectra in double photoionization: The rare gases Ar, Kr, and Xe.* Phys. Rev. Lett., **90**:053003 (2003). doi:10.1103/PhysRevLett.90.053003.

7. Reinert F and Hüfner S. *Photoemission spectroscopy — from early days to recent applications.* New J. Phys., **7**(1):97 (2005). doi:10.1088/1367-2630/7/1/097.

8. Jozwiak C, Graf J, Lebedev G, Andresen N, Schmid AK, Fedorov AV, El Gabaly F, Wan W, Lanzara A, and Hussain Z. *A high-efficiency spin-resolved photoemission spectrometer combining time-of-flight spectroscopy with exchange-scattering polarimetry.* Rev. Sci. Instrum., **81**(5):053904 (2010). doi:10.1063/1.3427223.

9. Bachrach RZ, Brown FC, and Hagström SBM. *Photoelectron spectroscopy by time-of-flight technique using synchrotron radiation.* J. Vac. Sci. Technol., **12**(1):309–312 (1975). doi:10.1116/1.568772.

10. Hemmers O, Whitfield SB, Glans P, Wang H, Lindle DW, Wehlitz R, and Sellin IA. *High-resolution electron time-of-flight apparatus for the soft x-ray region.* Rev. Sci. Instrum., **69**(11):3809 (1998). doi:10.1063/1.1149183.

11. Ulrich V, Barth S, Lischke T, Joshi S, Arion T, Mucke M, Förstel M, Bradshaw AM, and Hergenhahn U. *Photoelectron–Auger electron coincidence spectroscopy of free molecules: New experiments.* J. Electron Spectrosc. Relat. Phenom., **183**(1–3):70–79 (2011). doi:10.1016/j.elspec.2010.03.001.

12. Bostedt C, Bozek JD, Bucksbaum PH, Coffee RN, Hastings JB et al. *Ultrafast and ultra-intense X-ray sciences: first results from the Linac Coherent Light Source free-electron laser.* J. Phys. B: At., Mol. Opt. Phys., **46**(16):164003 (2013). doi:10.1088/0953-4075/46/16/164003.

13. Vollmer A, Ovsyannikov R, Gorgoi M, Krause S, Oehzelt M et al. *Two dimensional band structure mapping of organic single crystals using the new generation electron energy analyzer ARTOF.* J. Electron Spectrosc. Relat. Phenom., **185**(3-4):55–60 (2012). doi:10.1016/j.elspec.2012.01.003.

14. Eland J, Linusson P, Mucke M, and Feifel R. *Homonuclear site-specific photochemistry by an ion-electron multi-coincidence spectroscopy technique.* Chem. Phys. Lett., **548**(0):90–94 (2012). doi:10.1016/j.cplett.2012.08.018.

15. Penent F, Lablanquie P, Hall R, Palaudoux J, Ito K, Hikosaka Y, Aoto T, and Eland J. *Coincidence Auger spectroscopy.* J. Electron Spectrosc. Relat. Phenom., **144-147**:7–11 (2005). doi:10.1016/j.elspec.2005.01.187.

16. Mucke M, Förstel M, Lischke T, Arion T, Bradshaw AM, and Hergenhahn U. *Performance of a short "magnetic bottle" electron spectrometer.* Rev. Sci. Instrum., **83**(6):063106 (2012). doi:10.1063/1.4729256.

17. Mirsaleh-Kohan N, Robertson WD, and Compton RN. *Electron ionization time-of-flight mass spectrometry: Historical review and current applications.* Mass Spectrom. Rev., **27**(3):237–285 (2008). doi:10.1002/mas.20162.

18. Ueda K and Eland JHD. *Molecular photodissociation studied by VUV and soft x-ray radiation.* J. Phys. B: At., Mol. Opt. Phys., **38**(9):S839 (2005). doi:10.1088/0953-4075/38/9/025.

19. Wille K. *The Physics of Particle Accelerators: An Introduction.* Oxford University Press, USA (2001). ISBN 0198505493.

20. Eriksson M. *The accelerator system MAX.* Nucl. Instrum. Methods Phys. Res., **196**(2–3):331–340 (1982). doi:10.1016/0029-554X(82)90096-9.

21. Andersson Å, Eriksson M, Lindgren LJ, Röjsel P, and Werin S. *The MAX II synchrotron radiation storage ring.* Nucl. Instrum. Methods Phys. Res. A, **343**(2-3):644 – 649 (1994). doi:10.1016/0168-9002(94)90248-8.

22. Sjöström M, Wallén E, Eriksson M, and Lindgren LJ. *The MAX III storage ring.* Nucl. Instrum. Methods Phys. Res. A, **601**(3):229–244 (2009). doi:10.1016/j.nima.2008.12.195.

23. Byrd JM and Georgsson M. *Lifetime increase using passive harmonic cavities in synchrotron light sources.* Phys. Rev. ST Accel. Beams, **4**:030701 (2001). doi:10.1103/PhysRevSTAB.4.030701.

24. Georgsson M. *Landau cavities in third generation synchrotron light sources.* In *Particle Accelerator Conference, 2001. PAC 2001.*, volume 4, pp. 2689–2691 vol.4 (2001). doi:10.1109/PAC.2001.987874.

25. Bassi G, Blednykh A, Krinsky S, and Rose J. *Self-consistent simulations of passive Landau cavity effects.* Proceedings of PAC2013, Pasadena, CA USA (2013).

26. Andersson Å, Bergqvist M, Eriksson M, Malmgren L, and Thånell L. *The 100 MHz RF system for MAX-II and MAX-III.* In *Proceedings of the 8th European Particle Accelerator Conference*, pp. 2118–2120. European Physical Society Interdivisional Group on Accelerators (EPS-IGA) and CERN (2002).

27. *Detailed Design Report on the MAX IV Facility.* `http://www.maxlab.lu.se/maxlab/max4/DDR_public/index.html` (2012).

28. Abo-Bakr M, Anders W, Kuske P, and Wustefeld G. *Bunch length measurements at BESSY.* In *Proceedings of the Particle Accelerator Conference, 2003. PAC 2003.*, volume 5, pp. 3020–3022 (2003). doi:10.1109/PAC.2003.1289800.

29. *ALS storage ring parameters.* `http://www-als.lbl.gov/index.php/beamlines/storage-ring-parameters.html%5D/` (2014-05-12).

30. Hertel N and Vrønning Hoffmann S. *ASTRID2: A new Danish low-emittance SR source.* Synchrotron Radiat. News, **24**(1):19–23 (2011). doi:10.1080/08940886.2011.550553.

31. *ESRF performance.* `http://www.esrf.eu/Accelerators/Performance/` (2014-05-12).

32. Bergeard N, Silly MG, Krizmancic D, Chauvet C, Guzzo M et al. *Time-resolved photoelectron spectroscopy using synchrotron radiation time structure.* J. Synchrotron Rad., **18**(2):245–250 (2011). doi:10.1107/S0909049510052301.

33. *SPring-8 storage ring.* `http://www.spring8.or.jp/en/facilities/accelerators/storage_ring/` (2014-05-12).

34. Milas N and Stingelin L. *Impact of filling patterns on bunch length and lifetime at the SLS.* In *Proceedings of IPAC2011, San Sebastian, Spain*, p. THPE084 (2010).

35. Bocchetta C, Goryl P, Kró las K, Mł ynarczyk M, Stankiewicz MJ et al. *Project status of the Polish synchrotron radiation facility SOLARIS.* In *Proceedings of IPAC2011, San Sebastian, Spain*, pp. 3014–3016 (2011). ISBN 978-92-9083-366-6.

36. *Operating modi BESSY II.* `http://www.helmholtz-berlin.de/forschung/grossgeraete/betrieb-beschleuniger/betriebsmodi_en.html` (2012-05-07).

37. Sun C, Portmann G, Hertlein M, Kirz J, and Robin DS. *Pseudo-single-bunch with adjustable frequency: A new operation mode for synchrotron light sources.* Phys. Rev. Lett., **109**:264801 (2012). doi:10.1103/PhysRevLett.109.264801.

38. Sun C, Portmann G, Hertlein M, Kirz J, Marcus MA, and Robin DS. *Pseudo-single-bunch with adjustable frequency.* Synchrotron Radiat. News, **26**(3):9–13 (2013). doi:10.1080/08940886.2013.791209.

39. Nadolski LS, Lavieville JP, Lebasque P, Nadji A, Ricaud JP, Silly M, and Sirotti F. *First measurements with a kicked off axis bunch for Pseudo Single Bunch mode studies at SOLEIL.* In *Proceedings of IPAC2011, San Sebastian, Spain*, p. 2912 (2011).

40. Couprie ME, Nadolski LS, Nagaoka R, Brunelle P, Loulergue A, Tordeux MA, Lamarre JF, and Nadji A. *Versatile modes of operation to meet user needs at SOLEIL.* Synchrotron Radiat. News, **26**(3):14–18 (2013). doi:10.1080/08940886.2013.791210.

41. Holldack K, Ovsyannikov R, Kuske P, Müller R, Schälicke A et al. *Single bunch X-ray pulses on demand from a multi–bunch synchrotron radiation source.* Nat. Commun., **5**:4010 (2014). doi:10.1038/ncomms5010.

42. Murphy JB. *Synchrotron light source data book*. AIP Conference Proceedings, **249**(2):1939–2011 (1992). doi:10.1063/1.41969.

43. Yamamoto S and Matsuda I. *Time-resolved photoelectron spectroscopies using synchrotron radiation: Past, present, and future*. J. Phys. Soc. Jpn., **82**(2):021003 (2013). doi:10.7566/JPSJ.82.021003.

44. Müller AS. *Short-pulse operation of storage ring light sources*. In *Proceedings of IPAC2013, Shanghai, China*, p. 1129 (2013).

45. Abo-Bakr M, Feikes J, Holldack K, Wüstefeld G, and Hübers HW. *Steady-state far-infrared coherent synchrotron radiation detected at BESSY II*. Phys. Rev. Lett., **88**:254801 (2002). doi:10.1103/PhysRevLett.88.254801.

46. Wüstefeld G, Jankowiak A, Knobloch J, and Ries M. *Simultaneous long and short electron bunches in the BESSY II storage ring*. In *Proceedings of IPAC2011, San Sebastian, Spain*, p. 2936 (2011).

47. Schoenlein R, Chattopadhyay S, Chong H, Glover T, Heimann P, Leemans W, Shank C, Zholents A, and Zolotorev M. *Generation of femtosecond X-ray pulses via laser–electron beam interaction*. Appl. Phys. B, **71**(1):1–10 (2000). doi:10.1007/PL00021152.

48. Khan S, Holldack K, Kachel T, Mitzner R, and Quast T. *Femtosecond undulator radiation from sliced electron bunches*. Phys. Rev. Lett., **97**:074801 (2006). doi:10.1103/PhysRevLett.97.074801.

49. Werin S, Thorin S, Eriksson M, and Larsson J. *Short pulse facility for MAX–lab*. Nucl. Instrum. Methods Phys. Res. A, **601**(1-2):98–107 (2009). doi:10.1016/j.nima.2008.12.106.

50. Husheer SLG, Cole JM, d' Almeida T, and Teat SJ. *A prototype chopper for synchrotron time-resolved crystallographic measurements*. Rev. Sci. Instrum., **81**(4):043905 (2010). doi:10.1063/1.3358939.

51. McPherson A, Lee WK, and Mills DM. *A synchronized rotating crystal x-ray beam chopper*. Rev. Sci. Instrum., **73**(8):2852–2855 (2002). doi:10.1063/1.1485780.

52. Kosciesza D and Bartunik HD. *Extraction of single bunches of synchrotron radiation from storage rings with an X-ray chopper based on a rotating mirror*. J. Synchrotron Rad., **6**(5):947–952 (1999). doi:10.1107/S0909049599003404.

53. Plogmaker S, Linusson P, Eland JHD, Baker N, Johansson EMJ, kan Rensmo H, Feifel R, and Siegbahn H. *Versatile high-repetition-rate phase-locked chopper system for fast timing experiments in the vacuum ultraviolet and x-ray spectral region*. Rev. Sci. Instrum., **83**(1):013115 (2012). doi:10.1063/1.3677329.

54. Ito K, Penent F, Hikosaka Y, Shigemasa E, Suzuki IH, Eland JHD, and Lablanquie P. *Application of a simple asynchronous mechanical light chopper to multielectron coincidence spectroscopy*. Rev. Sci. Instrum., **80**(12):123101 (2009). doi:10.1063/1.3258200.

55. Cammarata M, Eybert L, Ewald F, Reichenbach W, Wulff M et al. *Chopper system for time resolved experiments with synchrotron radiation*. Rev. Sci. Instrum., **80**(1):015101 (2009). doi:10.1063/1.3036983.

56. Gembicky M, Oss D, Fuchs R, and Coppens P. *A fast mechanical shutter for submicrosecond time-resolved synchrotron experiments*. J. Synchrotron Rad., **12**(5):665–669 (2005). doi:10.1107/S090904950501770X.

57. McPherson A, Wang J, Lee PL, and Mills DM. *A new high-speed beam chopper for time-resolved X-ray studies.* J. Synchrotron Radiat., **7**(1):1–4 (2000). doi:10.1107/S0909049599014582.

58. *Chopper for synchrotron radiation.* `http://www.fz-juelich.de/zea/zea-1/EN/Research/ChopperSynchrotron/choppersynchrotron_node.html` (2014-05-12).

59. Lindenau B, Janssen F, and Leyendecker M. *1.25 MHz light chopper dedicated for operation at BESSY.* In *Presentation given at MEDSI/Pan-American SRI 2008 Meeting* (2008).

60. Gembicky M and Coppens P. *On the design of ultrafast shutters for time-resolved synchrotron experiments.* J. Synchrotron Rad., **14**(1):133–137 (2007). doi:10.1107/S0909049506041835.

61. Glover TE, Ackermann GD, Hussain Z, and Padmore HA. *Laser pump and X-ray probe surface photovoltage spectroscopy on si(111).* J. Mod. Opt., **51**(16–18):2805–2811 (2004). doi:10.1080/09500340408231839.

62. Tanaka S, Dylan Moré S, Takahashi K, and Kamada M. *Dynamics of surface photovoltage effects on clean and negative electron affinity surfaces of p-GaAs (100).* J. Phys. Soc. Jpn., **72**(3):659–663 (2003). doi:10.1143/JPSJ.72.659.

63. Takahashi K, Kondo Y, Azuma J, and Kamada M. *Beamline for high-resolution angle-resolved photoemission at Saga Light Source.* J. Electron Spectrosc. Relat. Phenom., **144–147**(0):1093–1096 (2005). doi:10.1016/j.elspec.2005.01.184. Proceeding of the Fourteenth International Conference on Vacuum Ultraviolet Radiation Physics.

64. Takahashi K, Azuma J, Tokudomi S, and Kamada M. *Development of the experimental system for time– and angle–resolved photoemission spectroscopy.* AIP Conference Proceedings, **879**(1):1218–1221 (2007). doi:10.1063/1.2436283.

65. Eland J. *Photoelectron–photoion coincidence spectroscopy: I. Basic principles and theory.* Int. J. Mass spectrom., **8**(2):143–151 (1972). doi:10.1016/0020-7381(72)80004-4.

66. Danby C and Eland J. *Photoelectron–photoion coincidence spectroscopy: II. Design and performance of a practical instrument.* Int. J. Mass spectrom., **8**(2):153–161 (1972). doi:http://dx.doi.org/10.1016/0020-7381(72)80005-6.

67. Laksman J, Céolin D, Månsson EP, Sorensen SL, and Gisselbrecht M. *Development and characterization of a multiple-coincidence ion-momentum imaging spectrometer.* Rev. Sci. Instrum., **84**(12):123113 (2013). doi:10.1063/1.4853435.

68. Kukk E, Sankari R, Huttula M, Sankari A, Aksela H, and Aksela S. *New electron-ion coincidence setup: Fragmentation of acetonitrile following N 1s core excitation.* J. Electron Spectrosc. Relat. Phenom., **155**(1–3):141–147 (2007). doi:10.1016/j.elspec.2006.10.011.

69. Kugeler O, Marburger S, and Hergenhahn U. *Calculation and measurement of the time-of-flight spread in a hemispherical electron energy analyzer.* Rev. Sci. Instrum., **74**(9):3955–3961 (2003). doi:10.1063/1.1599060.

70. Arion T, Püttner R, Lupulescu C, Ovsyannikov R, Förstel M et al. *New insight into the Auger decay process in O_2: The coincidence perspective.* J. Electron Spectrosc. Relat. Phenom., **185**(8-9):234–243 (2012). doi:10.1016/j.elspec.2012.06.010.

71. Leemann SC, Andersson A, Eriksson M, Lindgren LJ, Wallén E, Bengtsson J, and Streun A. *Beam dynamics and expected performance of sweden's new storage-ring light source: MAX IV.* Phys. Rev. ST Accel. Beams, **12**:120701 (2009). doi:10.1103/PhysRevSTAB.12.120701.

72. Leemann SC. *MAX-lab internal note 20120313: Updates to the MAX IV 1.5 GeV storage ring lattice.* `http://www.maxlab.lu.se/node/999/` (2012-03-13, revised 2012-06-11).

73. Leemann SC. *MAX-lab internal note 20121107: Updates to the MAX IV 3 GeV storage ring lattice.* `http://www.maxlab.lu.se/node/999/` (2012-11-07, revised 2014-01-29).

74. Leemann SC. *Interplay of Touschek scattering, intrabeam scattering, and rf cavities in ultralow-emittance storage rings.* Phys. Rev. ST Accel. Beams, **17**:050705 (2014). doi:10.1103/PhysRevSTAB.17.050705.

75. *FinEstBeaMS.* `https://www.maxlab.lu.se/sv/finestbeams` (2014-05-14).

76. Lupulescu C, Arion T, Hergenhahn U, Ovsyannikov R, Förstel M, Gavrila G, and Eberhardt W. *iDEEAA: A novel, versatile apparatus for electron spectroscopy.* J. Electron Spectrosc. Relat. Phenom., **191**:104–111 (2013). doi:10.1016/j.elspec.2013.09.002.

77. Dörner R, Mergel V, Jagutzki O, Spielberger L, Ullrich J, Moshammer R, and Schmidt-Böcking H. *Cold target recoil ion momentum spectroscopy: a "momentum microscope" to view atomic collision dynamics.* Phys. Rep., **330**(2-3):95–192 (2000). doi:10.1016/S0370-1573(99)00109-X.

78. Kruit P and Read FH. *Magnetic field paralleliser for 2π electron-spectrometer and electron-image magnifier.* J. Phys. E: Sci. Instrum., **16**(4):313 (1983). doi:10.1088/0022-3735/16/4/016.

79. Cha CY, Ganteför G, and Eberhardt W. *New experimental setup for photoelectron spectroscopy on cluster anions.* Rev. Sci. Instrum., **63**(12):5661–5666 (1992). doi:10.1063/1.1143397.

80. Gelius U, Wannberg B, Baltzer P, Fellner-Feldegg H, Carlsson G, Johansson CG, Larsson J, Münger P, and Vegerfors G. *A new ESCA instrument with improved surface sensitivity, fast imaging properties and excellent energy resolution.* J. Electron Spectrosc. Relat. Phenom., **52**(0):747–785 (1990). doi:10.1016/0368-2048(90)85063-F.

81. Mårtensson N, Baltzer P, Brühwiler P, Forsell JO, Nilsson A, Stenborg A, and Wannberg B. *A very high resolution electron spectrometer.* J. Electron Spectrosc. Relat. Phenom., **70**(2):117–128 (1994). doi:10.1016/0368-2048(94)02224-N.

82. King PDC, Hatch RC, Bianchi M, Ovsyannikov R, Lupulescu C et al. *Large tunable Rashba spin splitting of a two-dimensional electron gas in Bi_2Si_3.* Phys. Rev. Lett., **107**:096802 (2011). doi:10.1103/PhysRevLett.107.096802.

83. Ogawa M, Yamamoto S, Kousa Y, Nakamura F, Yukawa R et al. *Development of soft x-ray time-resolved photoemission spectroscopy system with a two-dimensional angle-resolved time-of-flight analyzer at SPring-8 BL07LSU.* Rev. Sci. Instrum., **83**(2):023109 (2012). doi:10.1063/1.3687428.

84. Guilhaus M. *Special feature: Tutorial. Principles and instrumentation in time-of-flight mass spectrometry. Physical and instrumental concepts.* J. Mass Spectrom., **30**(11):1519–1532 (1995). doi:10.1002/jms.1190301102.

85. *SIMION.* `http://simion.com/`.

86. King GC. *Electron and ion optics.* In F Dunning and RG Hulet, editors, *Atomic, Molecular, and Optical Physics: Charged Particles*, volume 29, Part A of *Methods in Experimental Physics*, pp. 189 – 207. Academic Press (1995). doi:10.1016/S0076-695X(08)60656-0.

87. Kato M and Sekine T. *Spherical aberration correction of electrostatic lenses using spherical meshes.* J. Vac. Sci. Technol. A, **13**(4):2255–2260 (1995). doi:10.1116/1.579504.

88. Matsuda H, Daimon H, Kato M, and Kudo M. *Approach for simultaneous measurement of two-dimensional angular distribution of charged particles: Spherical aberration correction using an ellipsoidal mesh.* Phys. Rev. E, **71**:066503 (2005). doi:10.1103/PhysRevE.71.066503.

89. *BEHLKE FSWP 51-02 product sheet.* `http://www.behlke.com/pdf/fswp%2091-01_rs.pdf` (2012-11-27).

90. *DEI Scientific Instruments, PVM-4210.* `http://www.directedenergy.com/index.php?option=com_joomdoc&task=document.download&path=dei-scientific/datasheets/PVM-4210_Datasheet_RevB.pdf` (2014-05-27).

Papers

PAPER I

Using Detector Gating to Operate an ArTOF Time-of-Flight Electron Spectrometer in Hybrid Mode at Storage Ring SR-Facilities

R. Ovsyannikov, T. Leitner, C. Stråhlman, P. Karlsson, M. Lundqvist, M. Gorgoi, R. Sankari, S. Svensson, N. Mårtensson, A. Föhlisch.

In preparation, .

Using Detector Gating to Operate an ArTOF Time–of–Flight Electron Spectrometer in Hybrid Mode at Storage Ring SR-Facilities

R. Ovsyannikov[a,b,*], T. Leitner[a,c], C. Stråhlman[d], P. Karlsson[e], M. Lundqvist[e], M. Gorgoi[a,b], R. Sankari[d], S. Svensson[a,c], N. Mårtensson[a,c], A. Föhlisch[a,b,f]

[a] *Uppsala-Berlin joint Laboratory for next generation photoelectron spectroscopy, Albert-Einstein-Str. 15, 12489 Berlin, Germany*
[b] *Helmholtz-Zentrum Berlin, BESSY II, Albert-Einstein-Str. 15, 12489, Berlin, Germany*
[c] *Dept. of Physics and Astronomy, Uppsala University, Box 516, SE-751 20 Uppsala, Sweden*
[d] *MAX IV Laboratory, Lund University, Box 118, SE-221 00 Lund, Sweden*
[e] *VG Scienta AB, P.O. Box 151 20, SE-750 15, Uppsala, Sweden*
[f] *Institut für Physik und Astronomie, Universität Potsdam, Karl-Liebknecht-Strasse 24/25, 14476 Potsdam, Germany*

Abstract

The angular resolved time-of-flight electron analyzers show excellent performance concerning energy resolution, transmission and time resolved angular resolved electron spectroscopy. However, these instruments need an external trigger which has implied that until recently only single bunch mode operated storage rings could be used to generate the necessary x-ray pulses. In this paper we show that gating of the detector in such an instrument can be used to make the ArTOF to operate also when the storage ring is operated in hybrid mode. In combination with e.g. resonant pulse-picking or with mechanical choppers the gating opens up for a very general use of the ArTOF technology.

Keywords:
ARPES, Time of Flight, Electron Spectroscopy, Synchrotron radiation, Hybrid filling mode

1. Introduction

A new type of time-of-flight electron spectrometer, ArTOF, has recently been developed [1, 2]. It is based on the properties of the angular resolved mode of the electron lens originally developed for the Scienta SES-200 type hemispherical spectrometers [3, 4]. In this mode of operation, electrons are dispersed in one direction on the two dimensional detector of the spectrometer according to their kinetic energies. The other direction of the detector is used for the determination of the emission angles in one direction.

In the ArTOF, the energy analysis is instead made directly in the electron lens by measuring the time-of-flight of the electrons. In this way one can use the full acceptance cone of the electron lens. A time resolved two dimensional detector is placed at the end of the lens where the angular pattern is projected. This allows the simultaneous measurement of two coordinates (x and y) and the arrival time of the electrons at the detector. With this information, the trajectories, and the velocity distribution along these, can be calculated with high precision. In this way it is possible to determine the electrons' kinetic energies as well as their emission angles [1].

The time-of-flight technique requires a pulsed photon source. The maximum repetition rate that can be handled by the ArTOF spectrometer is a few MHz. This fits excellently to the revolution frequency of a single electron bunch in a third generation synchrotron radiation storage ring. A synchrotron radiation source is pulsed since the operation of the accelerating cavity will force all stored electrons into equally spaced bunches. The allowed positions are referred to as electron buckets. To achieve maximum stored current, all such buckets are filled with electrons. With a typical RF system used at synchrotron radiation facilities this leads to a repetition rate of 500 MHz, much too fast for most timing experiments. However, it is also possible to fill only selected buckets. One possibility is

*e-mail: ovsyannikov@helmholtz-berlin.de

to store only one bunch in the storage ring. In the case of the BESSY II storage ring at the Helmholtz-Zentrum Berlin (HZB) in Berlin this leads to a repetition frequency of 1.25 MHz, ideally suited for many types of experiments. However, this mode of operation leads to a very small total electron current and hence to a much reduced average photon flux making most other types of experiments impractical. Single-bunch operation is therefore only available at very few facilities in the world and in that case only for a very limited fraction of the time.

The ArTOF has a number of valuable characteristics. The full band structure of a solid can be monitored in real time without moving the sample or the analyzer [5]. This is important for e.g. time resolved studies. The very high transmission of the ArTOF also gives new opportunities to study X-ray sensitive samples like organic crystals. We have shown that it is possible to study the band structure of such systems at a photon flux of only 10^7 photons/s and that the full band structure of an organic crystal can be recorded in only a few minutes [6]. Another area where the excellent transmission of the ArTOF creates new opportunities is coincidence spectroscopy. The crucial factor for such experiments is the ratio of true to random coincidences and hence the transmission of the spectrometers. In Ref. [7] such a set-up is described, where a VG Scienta 4000 hemispherical electron spectrometer is used together with an ArTOF. We have also started to build a set-up where two ArTOF spectrometers can be used in coincidence.

However, the need for single-bunch operation of the synchrotron radiation facility represents a major restriction for the technique. An urgent development is therefore to make the ArTOF set-up compatible with the so called hybrid mode operation of the storage ring. In such a mode, most of the electron buckets in the storage ring are filled with electrons. In one section of the filling pattern, however, there is a single bunch which is surrounded by a number of empty buckets. In this way it is possible to combine a high overall circulating current with the characteristics of single-bunch operation. This mode of operation can therefore be chosen as the regular mode for any synchrotron radiation facility.

In order to use hybrid bunch operation one must be able to remove the influence from all bunches except the isolated single bunch. One can think of a number of different ways to achieve this for the ArTOF experiment, each being connected with their specific advantages, disadvantages and technical challenges. One way is to introduce a sufficiently rapid mechanical chopper that blocks all X-ray photons except those generated by the separated single bunch. Another possibility is to modify the single electron bunch by a kicker magnet or stripline kicker arrangement in the accelerator lattice such that it emits X-ray photons in a different direction or spatially separated from the multi bunch light. It is then possible to set up a beam-line which accepts only photons from this modified bunch. Operation with Pulse Picking by Resonant Excitation has been demonstrated at BESSY [8]. Here one selected bunch is resonantly excited in order to emit single bunch light with an angular separation. Operation with Pseudo-Single-Bunch, where one bunch is displaced from the ideal orbit by a kicker magnet, has been demonstrated at ALS [9]. Another possibility is to use repulsive voltages to block those photoelectrons that are emitted from the sample due to the multi-bunch part of the bunch train. One option is to apply a rapidly switched repulsive voltage close to the sample [10]. Still another option is to gate the detector using a set of meshes put on suitable switched potentials.

We have recently implemented the technique of detector gating and in this report will show that this indeed allows hybrid mode operation of the ArTOF. The basic idea behind this scheme is that the spectrometer combines the function of a flight tube and an electron lens which allows only electrons in a certain kinetic energy range to reach the detector. By introducing a properly controlled repulsive voltage in front of the detector it is then possible to create a time window when the detector is open such that only electrons originating from the hybrid bunch will be detected.

The gating arrangement has also a number of additional advantages for the operation of the ArTOF. The introduction of additional meshes in front of the detector makes it possible to equalize the energies of the electrons before entering the Multi Channel Plate (MCP) detector, hence creating a more uniform MCP response for the detected events. The mesh arrangement can also be used to remove the low energy electrons that can otherwise reach the detector close to the lens axis. The arrival of each such electron will otherwise lead to a dead-time for the MCP plates which reduces the count-rate for the real events. The gating can also be used to reduce the MCP load for those applications where the ArTOF is used in multi bunch mode. Addition-

ally, it allows removing the background due to any remaining multi bunch intensity if a pulse picking scheme is used to achieve pseudo-single-bunch operation. In pump-probe experiments with a slower pump than the 1.25 MHz probe presently used at BESSY II, the gating can also be used to open the detector only when the relevant electrons are emitted.

A difference when operating the ArTOF in hybrid bunch mode with detector gating as compared to single-bunch or pseudo single-bunch operation is that the sample is experiencing the full X-ray load of the multi-bunch train. In this way one cannot explore one of the advantages of the ArTOF, namely that it allows measurements for very X-ray sensitive samples, i.e. the research field of low-dose photoelectron spectroscopy. A consequence of the gating scheme is also that it makes it difficult to determine the arrival time of the electrons using the MCP signal, which is sensitive to the rapidly changing gate pulse. However, this information can also be retrieved using the signals from the Delay Line Detector (DLD). The gating scheme also introduces some restrictions when studying core-levels due to the possible overlap with much faster electrons, e.g. from the valence band, emitted by later bunches in the multi-bunch part of the filling pattern.

In the present paper we describe the gating scheme and how it has been implemented in the ArTOF spectrometer. We show results from the BESSY II storage ring at HZB in Berlin operating in the hybrid mode.

2. Results and Discussion

The purpose of ArTOF detector gating is to reduce the number of detected unresolvable electrons in order to increase the detection efficiency in hybrid mode. This implies blocking a large number of electrons with low kinetic energies as well as those unresolvable electrons emitted as a result of the multi-bunch train.

The standard operation mode of BESSY II is shown in Fig. 1. It features four distinct camshaft bunches residing in a 224 ns ion clearing gap. The remaining part of the 800 ns long filling pattern features a multibunch train with 2 ns pulse separation. The camshaft bunches have ∼10 times higher bunch charge than the standard multibunches. In the case where four camshaft bunches are injected, the acceptable time window for gating is 36 ns before and

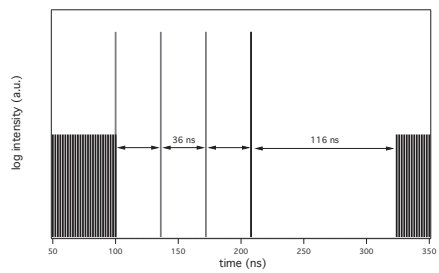

Figure 1: The two hybrid modes at BESSY II. A camshaft bunch (black) resides in a 224 ns ion clearing gap with a distance to the multi bunches of 108 ns before and 116 ns after. Three additional camshaft bunches (grey) might be injected equidistantly before for experiments at other beam lines. For the experiments presented in this paper, only one camshaft bunch was injected. The camshafts have ∼10 times higher bunch charge than the standard multi bunch. Light from the center camshaft bunch arrives at the sample with 1.25 MHz repetition rate.

116 ns after the last camshaft bunch. For the experiments presented in this paper, BESSY was injected with a special hybrid mode with only one camshaft bunch. Fig. 2 shows a typical 2D time-of-flight spectrum acquired with the ArTOF in hybrid mode. It can be clearly seen that a majority of electrons are unresolvable since they are originating from the multibunch train. On the other hand, the electrons originating from the camshaft bunch are resolvable since their temporal dispersion is lower than half of the size of the ion clearing gap. Under these circumstances, the electron spectrum can be analysed from the camshaft electrons and all other electrons can be disregarded. However, it is disadvantageous to have a large background of undesired electron detections since these overload the MCP detector. Hence, the acquisition time for an electron spectrum increases by more than one order of magnitude compared to single–bunch operation.

The gate we present in this paper filters the electrons in two steps. The ArTOF lens system is designed to analyse electrons in a certain energy window defined by the user [1]. Electrons with higher or lower energies should be disregarded by the analysis software. Thus, any detection outside of the energy window is an unnecessary load on the detector and acquisition. In a photoemission measurement there will most often be photoelectrons with lower energies. In our gating system, these electrons are

deflected by means of a constant potential V_{nej}. In the next step, we use a pulsed electric potential V_{gate} to block electrons with an analysable energy, but which are emitted from the multibunch train and hence of undefined time-of-flight. In addition we have high energy electrons, which originate from valence ionisations (in a core or inner valence experiment) or from higher order light. These electrons are not filtered by our gate. They will be detected and remain as artefacts in the spectrum. However, if the total temporal dispersion of electrons in the analysable window and higher energy contributions are smaller than the preceding time gap, they do not interfere with the analysis.

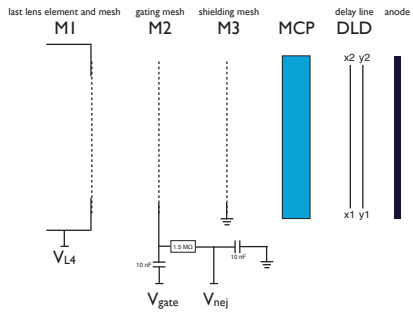

Figure 3: The functional principle of the GAME.

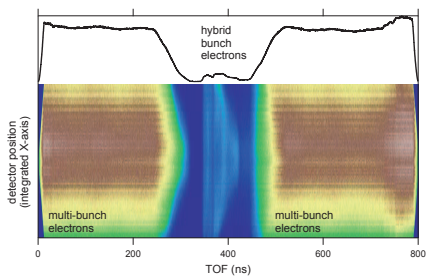

Figure 2: Typical TOF spectrum acquired in hybrid mode at BESSY. The graphene valence band is measured with $h\nu = 180\,\mathrm{eV}$ and the instrument optimized for recording $E_{kin} = 175\,\mathrm{eV}$. Electrons generated by the hybrid bunch are clearly separated from the multi–bunch electrons.

2.1. Detection scheme

The ArTOF uses a commercially available delay-line detector from *Roentdek GmbH*, consisting of two Chevron stacked MCP plates followed by two delay lines and an anode. An electron hitting the detector therefore generates five signals, one from the MCP stack and one signal from each end of the two delay-lines. In non-gated operation, the MCP signal provides for the arrival time of the electron, while the hit coordinates are deduced from the delay-line signals. Knowing arrival time and therefore the flight time of the electron, and knowing the position of the hit on the detector, allows calculating both the kinetic energy and the emission angle of the electron.

In standard non-gated operation the MCP stack is preceded by a gold mesh kept at the same potential as the last lens element of the electron lens. We developed a modular extension to the standard ArTOF, which allows multibunch operation using an electronic gating scheme. Within this *Gated Artof Modular Extension* (GAME), we have introduced two more meshes between the last lens element of the analyser and the MCP. With additional electronics we can apply a high constant deflection potential together with a low voltage gate pulse to the mesh in the middle. Fig. 3 depicts a principal sketch of the ArTOF detector system, equipped with the GAME.

A high voltage source feeds a tuneable negative potential V_{nej} to the M2 mesh. This potential acts as an energy filter and allows passage of electrons with kinetic energies higher than V_{nej} [eV]. To achieve gating, we add a pulsed gating potential V_{gate} sufficient to deflect all electrons. The gate characteristics is altered by changing the filter potential V_{nej} as well as the length, amplitude and frequency of the gating pulse.

For pulsing we use a ± 10 V function generator which is coupled to M2 through a high–capacitance coupling capacitor. The function generator is coupled to M2 through a high-capacitance coupling capacitor. When the filter potential has been set to deflect all electrons with energies lower than the region of interest, the function generator signal is fed through the coupling capacitor. As the gate poten-

tial is added to the filter potential, full deflection is achieved.

The gate should only be open for the time when electrons originating from the center camshaft bunch are expected to reach the detector. The required opening time of the gate is governed by the length of the ion clearing gap and the temporal dispersion of the electrons in the region of interest.

Higher energy electrons will have higher speeds, and thus arrive earlier to the gate. These unwanted electrons contribute strongly to the load on the MCP stack and decrease the detection efficiency. Furthermore, due to a dead-time of the detector stack following each hit, in the order of 200 ns or more, electrons arriving just before the region of interest lead to a perturbation of the electron distribution, and hence to false relative intensities in the resulting photoelectron spectra. This restriction is particularly hindering in core-level measurements where fast valence electrons are emitted together with the slower core electrons.

In our results we have a strong contribution of high energy electrons associated with second order light. As will be seen, these cannot be gated with our present scheme. We prove however a large reduction in detection of unwanted electrons.

One problem which has been encountered is the possible interference posed on the MCP by the gating pulse. A set of stacked meshes has the internal capacitance of a parallel plate capacitor. Naturally, there will be a signal propagation between meshes and between mesh and MCP. We have acknowledged this problem by introducing the third mesh M3, which is set to ground and is used as a shield to avoid crosstalk between the gate mesh M2 and the MCP and DLD. This crosstalk cannot be completely avoided, and some signal disturbance is still seen on the MCP, imposing a noise on the MCP potential which undermines a precise timing measurement. For this reason, we have changed the original detector signal handling scheme so that the timing information is taken from the DLD signals. This reduces the accuracy for the measurement of the arrival time by a factor of 2.5 to around 500 ps, compared to 200 ps when using the MCP signal. Consequently, in a linear approximation, the energy resolution is reduced by the same factor. However, increasing the accuracy of the DLD timing signal is on-going development; by introducing new electronics and additional correction algorithms, we are expecting to obtain similar resolutions for MCP and DLD timing.

We shaped the gating pulse to minimize the crosstalk between M2 and neighbouring meshes. Fig. 4 shows the function with its maximum amplitude. To make a long time window we want to keep the rise and fall times as short as possible. On the other hand, the pulse should have as few as possible high frequency components to avoid transmission of high frequency signals to the MCP. After a trial including up to eight Fourier components of the pulse function, we settled with a function only including first and third order components. The highest frequency component in this function is 10 MHz, and it has approximately 10 ns rise and fall time. A trial function including eight Fourier components was also investigated, but did not prove successful at full 20 V amplitude.

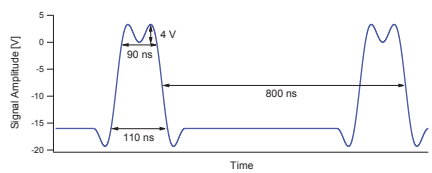

Figure 4: Custom made gate pulse with 20 V amplitude. Each pulse start is triggered by the 1.25 MHz ring clock signal. As indicated, we achieve a 90 ns fully open window with 10 ns rise and fall times. The oscillation of the gate function has a 4 V amplitude at 20 V gate potential.

2.2. Experimental conditions

The experiments were performed at the BESSY II storage ring in Berlin, Germany. Our spectrometer chamber was mounted on beamline UE52-SGM. The beamline operates in the 90–1500 eV photon energy range using a monochromator with three spherical gratings. Our test sample was bilayer graphene on SiC (001) manufactured at Linköping University. The ArTOF was mounted on our APEX chamber [1], which is equipped with all necessary devices for sample cleaning, heating and manipulation. The data were downloaded in a database on a hard disc and have been analysed using our in-house developed software.

2.3. Results

Fig. 5 shows the acquired TOF-spectrum of the graphene valence band with and without the active gate. The electrons originating from the camshaft

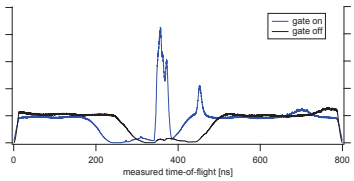

Figure 5: Full measured time-of-flight spectrum on graphene valence band with (blue) and without (black, identical to spectrum in Fig. 2) gate enabled. The spectra have been normalised to the (apparent) background level of the multibunch electrons. The gate pulse was delayed to match the desired temporal window for gating the electrons originating from the hybrid bunch. The graph clearly shows how the analysable electrons originating from the camshaft bunch are enhanced.

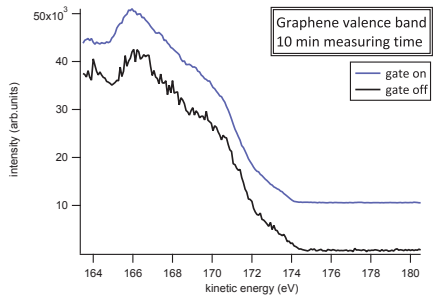

Figure 6: The graphene valence band spectrum obtained with and without gating during 10 minutes.

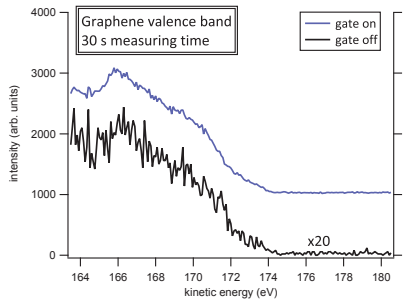

Figure 7: The graphene valence band spectrum obtained with and without gating during 30 s.

bunch are clearly separated from the multibunch electrons. The expected flight times of the desired electrons can be calculated from the lens settings. By introducing a corresponding fixed delay to the gate pulse, we can set the opening of the gate to the desired temporal window. The gated spectrum shows a clear enhancement of the electron signal for the desired temporal window and demonstrates the feasibility of our gating scheme.

The main figure of merit for detector gating is the detection efficiency; defined as the number of detected electrons originating from the selected camshaft bunch and arriving in the analysis time window, hence electrons within the selected energy window. These electrons represent the effective counts, which is compared to the total number of all detector counts. The detection efficiency is increased in two steps; by introducing the constant potential V_{nej} and by the gate pulse. To quantify this effect, we made three sets of measurements at 180 eV photon energy and the lens centred on 175 eV kinetic energy and with 10 % energy window, thus measuring parts of the graphene valence band. The first measurement had no constant voltage applied, resulting in 300 effective counts/s out of a total count rate of 90,000 counts/s (efficiency: 0.3%). The application of a constant potential $V_{\mathrm{nej}} = 164\,\mathrm{eV}$ gives 600 effective counts/s at a 72,000 counts/s total (efficiency: 0.8%). Finally, the application of the gate pulse at 20 V amplitude gives 5,000 compared to 65,000 counts/s (efficiency: 8%), increasing the efficiency by an order of magnitude. This is expected at BESSY, since roughly 10% of the total current in the ring is due to the camshaft bunch.

Since no high energy electrons are gated, the scheme is very sensitive to higher order light. This is mirrored in the fairly low effective count rate even with gating applied. To further increase the efficiency of the gating, the amount of second order light must be reduced.

Fig. 6 shows an energy analysed spectrum of the graphene valence band with and without gating. The match is very good and shows that the electron spectrum is not affected by the gate pulse. Both spectra were measured during 10 minutes. To further show the effect of increased efficiency, Fig. 7 show the same spectrum after 30 s of measuring time; the difference in signal-to-noise ratio is clear.

A concern is the effect on electrons with ener-

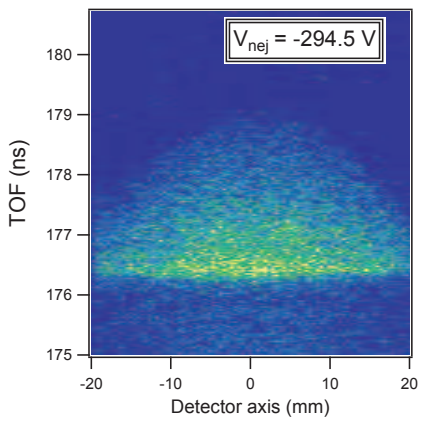

Figure 8: Graphene valence spectra measured during five minutes with 320 eV photon energy and the lens focused at 310 eV electron kinetic energy. The analysable window of the spectrometer is 30 eV and extends from 168 ns to 192 ns. The spectra clearly shows the cone–shape of the cut-off, which has been shown to move towards shorter flight times as the cut-off voltage is increased.

gies close to the cut off potential. Electrons in the lower end of the energy window will be decelerated to very low kinetic energies, thus decreasing their speeds much more than higher energy electrons. We have observed a cone–shaped cut off in the measured spectra (see Fig. 8). It is shown that electrons with longer flight times are detected close to the center of the detector, while electrons further towards the periphery are cut off earlier. We have not conclusively established why this phenomenon appears. It is known from the properties of the lens that electrons hitting the detector in the periphery will have lesser impinging angles towards the mesh ensemble. One can therefore expect that electrons with higher kinetic energies will be deflected at the periphery than at the center of the detector. We can conclusively state that the cone shape is an effect of the constant potential since its edge is moving proportionally with the magnitude of the potential.

3. Conclusion and Outlook

In conclusion we have shown that it is possible to gate the multibunch electron pulses in an ArTOF spectrometer, thus allowing to use effectively the signal originating from the camshaft pulse(s). The method involves a series of meshes, as well as a careful generation of the gating pulses with very few Fourier components of as low frequency as possible. The efficiency of the detection has been shown to increase with at least an order of magnitude and we foresee that this gating scheme will be very useful, notably in combination with the use of a mechanical chopper or resonant pulse picking. Plans to utilize this combination is currently pursued at BESSY. Several issues however remain for the future: We aim to reduce the influence of the high energy electrons excited by higher orders in the x-ray beam. This could for example be done with a photon energy filter in the beamline. The parameters of the lens should be further optimized to account for focusing conditions at relevant gating potentials, in order to fully preserve the resolution of the instrument. We intend to study the influence of the the gating pulse to the detector to allow for a higher gate amplitude. In connection to this, we have investigated the option to move the gate mesh closer to the front of the ArTOF spectrometer, as outlined in Ref. [10]. This in order to allow for a much higher gate amplitude and also to allow for gate operation with smaller ion clearing gaps. These development tracks are under further investigation and will be pursued as part of our continuous development of the ArTOF instrument.

[1] G. Ohrwall, P. Karlsson, M. Wirde, M. Lundqvist, P. Andersson, D. Ceolin, B. Wannberg, T. Kachel, H. Duerr, W. Eberhardt, S. Svensson, Journal of Electron Spectroscopy and Related Phenomena 183 (2011) 125–131.

[2] R. Ovsyannikov, P. Karlsson, M. Lundqvist, C. Lupulescu, W. Eberhardt, A. Föhlisch, S. Svensson, N. Mårtensson, Principles and operation of a new type of electron spectrometer - ArTOF, J. Electron Spectrosc. Relat. Phenom. 191 (2013) 92–103.

[3] N. Martensson, P. Baltzer, P. Bruhwiler, J. Forsell, A. Nilsson, A. Stenborg, B. Wannberg, J. Electron Spectrosc. Rel. Phen. 70 (1994) 117–128.

[4] B. Wannberg, Nuclear Instruments and Methods in Physics Research Section A: Accelerators, Spectrometers, Detectors and Associated Equipment 601 (2009) 182 – 194.

[5] P. D. C. King, R. C. Hatch, M. Bianchi, R. Ovsyannikov, C. Lupulescu, G. Landolt, B. Slomski, J. H. Dil, D. Guan, J. L. Mi, E. D. L. Rienks, J. Fink, A. Lindblad, S. Svensson, S. Bao, G. Balakrishnan, B. B. Iversen, J. Osterwalder, W. Eberhardt, F. Baumberger, P. Hofmann, Physical Review Letters 107 (2011) 096802.

[6] A. Vollmer, R. Ovsyannikov, M. Gorgoi, S. Krause, M. Oehzelt, A. Lindblad, N. Mårtensson, S. Svensson, P. Karlsson, M. Lundqvist, T. Schmeiler, J. Pflaum, N. Koch, Journal of Electron Spectroscopy and Related Phenomena 185 (2012) 55 – 60.

[7] T. Arion, R. Püttner, C. Lupulescu, R. Ovsyannikov, M. Förstel, G. Öhrwall, A. Lindblad, K. Ueda, S. Svensson, A. Bradshaw, et al., Journal of Electron Spectroscopy and Related Phenomena 185 (2012) 234–243.

[8] K. Holldack, R. Ovsyannikov, P. Kuske, R. Müller, A. Schälicke, M. Scheer, M. Gorgoi, D. Kühn, T. Leitner, S. Svensson, N. Mårtensson, A. Föhlisch, Single bunch X-ray pulses on demand from a multi–bunch synchrotron radiation source, Nat. Commun. 5 (2014) 4010.

[9] C. Sun, G. Portmann, M. Hertlein, J. Kirz, D. S. Robin, Pseudo-single-bunch with adjustable frequency: A new operation mode for synchrotron light sources, Phys. Rev. Lett. 109 (2012) 264801.

[10] C. Stråhlman, R. Sankari, M. Lundqvist, G. Öhrwall, R. Ovsyannikov, S. Svensson, N. Mårtensson, R. Nyholm, Angle-resolved time-of-flight spectroscopy applied to multi-bunch operation at max-lab: a design study, Journal of Physics: Conference Series 425 (9) (2013) 092011.

PAPER II

Angle-resolved time-of-fight spectroscopy applied to multi-bunch operation at MAX-lab: a design study

C. Stråhlman, R. Sankari, M. Lundqvist, G. Öhrwall, R. Ovsyannikov, S. Svensson, N. Mårtensson, R. Nyholm.

Journal of Physics: Conference Series **425**, 092011 (2013).

11th International Conference on Synchrotron Radiation Instrumentation (SRI 2012) IOP Publishing
Journal of Physics: Conference Series **425** (2013) 092011 doi:10.1088/1742-6596/425/9/092011

Angle-resolved time-of-flight spectroscopy applied to multi-bunch operation at MAX-lab: a design study

C Stråhlman[1], R Sankari[1], M Lundqvist[2], G Öhrwall[1], R Ovsyannikov[3], S Svensson[3,4], N Mårtensson[4], R Nyholm[1]

[1] MAX IV Laboratory, Lund University, P.O. Box 118, SE-22100 Lund, Sweden
[2] VG Scienta AB, P.O. Box 15120, SE-750 15 Uppsala, Sweden
[3] Helmholtz–Zentrum Berlin, Albert-Einstein-Straße 15, D-12489 Berlin, Germany
[4] Dept. of Physics and Astronomy, Uppsala University, P.O. Box 521, SE-75121 Uppsala, Sweden

E-mail: Christian.Strahlman@maxlab.lu.se

Abstract. Angle-resolved time-of-flight (ARTOF) spectrometers have found use in a number of applications, including ARPES. However, the fundamental requirement of an external start trigger matching the read-out time of the instrument limits its usability at many storage rings. Hitherto all reported experiments have been performed at storage rings capable of running in single-bunch mode. To eliminate this restriction, we propose a method where a pulsed electronic gate is introduced to allow for ARTOF usage at normal multi-bunch operation of the MAX II storage ring. This paper will show the working principle and outline the design for this technique.

1. Introduction

Angular resolved photoelectron spectroscopy (ARPES) has become a powerful tool in many applications. In the field of band–mapping of materials, the technique has had particular impact. The dominating instrument for such experiments has been the hemispherical deflector electron energy analyzer (HDA). Recent development of electron time-of-flight (TOF) type analyzers have made them cover ground in this area [1]. Both types have proven high energy resolution, thus allowing detailed studies of electronic structure. A significant trend has been the extension to simultaneous measurements of all momentum components of the electron, via the energy and angular distribution. In this spirit, a new energy and angle resolving electron spectrometer, the Scienta ARTOF 10k, has been recently developed based on angle-resolved electron time-of-flight (ARTOF) [2]. The principles behind this detection system have been described in detail by Wannberg [1]. The ARTOF spectrometer consists of a many-element electron lens and a position–sensitive detector. With the aid of simulations, the lens can be set up so that each combination of TOF and hit position can be determined to correspond to a point in 3D momentum space.

ARTOF instruments have so far been designed to operate at pulsed sources of X-rays and VUV–radiation with a pulse frequency in the order of 1 MHz, corresponding to 1 μs spacing between light pulses. This prerequisite poses a fundamental restriction compared to the HDA, namely that the start trigger must be external [1]. So far the use of electron TOF at synchrotrons has been restricted to facilities with single–bunch operation. Still, multi–bunch operation

11th International Conference on Synchrotron Radiation Instrumentation (SRI 2012) IOP Publishing
Journal of Physics: Conference Series **425** (2013) 092011 doi:10.1088/1742-6596/425/9/092011

is far more common at synchrotron radiation facilities, as most users exploit the light as a high intensity quasi-continuous beam. Following demands for time resolved experiments, some facilities are able to operate in more exotic modes, such as single–bunch and hybrid modes (see e.g. BESSY II [3]). The availability of single–bunch operations is however quite limited. To enable for increased use of TOF-based techniques, it is necessary to develop a method where the ARTOF spectrometer can be used under normal multi–bunch operation. The most common approach to decrease the undesired repetition rates in storage rings has been mechanical choppers which filter out a certain fraction of the light pulses (see e.g. [4]). However, no chopping setup has been fast enough to filter out single pulses from the multi–bunch light pulse pattern.

We propose instead a method where an electronic gate is implemented to protect the spectrometer from undesired electrons. The setup should allow for the electrons originating from one single light pulse to reach the spectrometer and propagate undisturbed to the spectrometer detector. All other electrons should be deflected. In the following we shall show that an electronic gate can mimic single–bunch temporal structure under normal multi–bunch operation.

2. 100 MHz multi–bunch operation at MAX II

The MAX II storage ring has been in operation since 1997. Since 2002, it has operated on a 100 MHz RF system [5]. The filling pattern of MAX II today is homogeneous with equal and equidistant electron bunches (10 ns). The 100 MHz concept has been preserved for the new MAX IV synchrotron light facility, which is now been built in Lund, Sweden. The MAX IV project will utilize a time structure in normal operation equal to that of MAX II [6]. The operating frequency of MAX II (and MAX IV) provides us with an advantage compared to storage rings with 500 MHz RF systems since we have a relatively long 10 ns intermediate time between light pulses.

3. Design considerations

The conceptual design of our gate is showed in Fig. 1. In simulations we have used the ARTOF 10k [2] as a reference instrument, although the principle stands for all electron spectrometers with timing constraints. For this spectrometer, the focal distance of the lens is 40 mm. Our proposed gate consists of two consecutive high transmission meshes placed in front of the first lens element. A sufficient negative potential is applied to the mesh closest to the sample. The purpose of this gating potential is to deflect all electrons away from the lens when the gate is 'closed'. Simulations performed with the SIMION software [7] predict a required gating potential given by $V_{\mathrm{gate}}[\mathrm{V}] = 1.3 \cdot E_{\mathrm{elec,max}}[\mathrm{eV}]$, where $E_{\mathrm{elec,max}}$ is the highest expected electron kinetic energy. The second mesh, which is grounded, has two functions: Firstly, it protects the spectrometer from the gating potential, whereas otherwise the gating potential would leak into the lens and disturb the focus. Secondly, as shall be shown, it increases the available ramp-up time of the gating potential. When the gate is closed, no electrons from the interaction region are able to reach the spectrometer. To open the gate, the potential is reduced to zero, thus allowing for undisturbed passage of electrons.

The optimal timing scheme of the gate depends heavily on the electron energy to be measured. With the 100 MHz pulsing of light, energetic electrons are ejected from the sample every 10 ns. The distance traveled by a non-relativistic electron in free space is given by the equation $d[\mathrm{mm}] = 0.59 \cdot t[\mathrm{ns}] \cdot \sqrt{E_{\mathrm{elec}}[\mathrm{eV}]}$. Fig. 2 show the restrictions on gate timing. The maximum fall time equals the pulse separation 10 ns, while the rise time depend mainly on the energies of the electrons. Fast electrons (>100 eV) will pass the gate quickly and the available rise time is 9 ns. For 10 eV electrons, the required passing time is longer and available rise time is reduced to 7 ns. Hence, spectroscopy with low electron energies put a tougher constraint on the rise time than higher energies. At the same time, lower electron energies require lower shielding potential, which is easier to reach in shorter time.

11th International Conference on Synchrotron Radiation Instrumentation (SRI 2012) IOP Publishing
Journal of Physics: Conference Series **425** (2013) 092011 doi:10.1088/1742-6596/425/9/092011

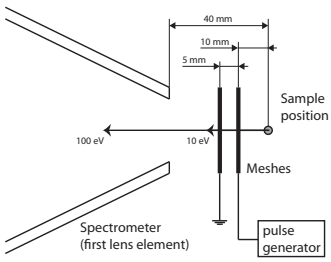

Figure 1. The conceptual design of the electronic gate for ARTOF 10k focusing conditions. The mesh closest to the sample is fed by fast pulse generation. The second mesh shields the entrance to the spectrometer from the gating potential. We have indicated the distance traveled by a 10 eV and a 100 eV electron in 10 ns.

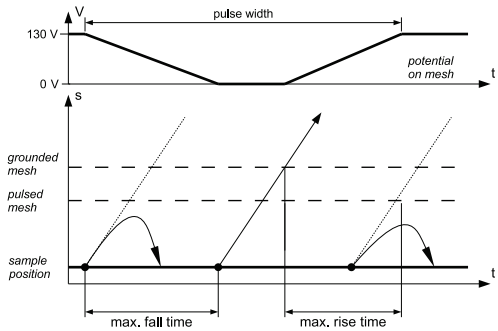

Figure 2. Timing principle for the gate in a 2D time-space-diagram together with required gating potential. The tilted lines indicate propagation of mono-energetic electrons through the gate. The first and third electron should be deflected, while the second should pass the gate. Mesh potential is given for 100 eV electrons.

There is a practical lower limit for the electron energies which can be gated. Below 10 eV, temporal overlapping of adjacent electron bursts start to become an issue. For MAX II standard operation the practical lower limit should thus be slightly below 10 eV. One should in this case make use of the ARTOF 10k low energy cut-off, which will filter out low-energy electrons and any secondary electron which would reside in the chamber [2].

In present simulations the gating meshes are separated by 5mm, whereas the pulsed mesh is placed 10 mm from the sample. It is preferential to put the gate as close to the sample as possible. The first reason for this is that a wider energy range of electrons is allowed, since the time separation of electrons are smaller. This is particularly relevant for low energy electrons. The second reason is that the usability of electron spectrometers, and particular ARTOF spectrometers, fully relies on our ability to predict the electron trajectories through the lens. The inclusion of the second mesh constitutes a disturbance to the lens focus which decreases with increasing distance.

4. Pulse generation

The use of pulse generators to gate electrons and ions is very common in spectroscopy. However, they are normally operated in the kHz regime. Here, we should operate in 1 MHz frequency, addressing the dead time of the ARTOF (1 μs), required fall and rise times and the overall pulse width (Fig. 2). To maintain good focus of the lens, it is necessary to avoid disturbances from the gating mesh while the gate is open. Ideally, we would have a zero gating potential during the time the electron passes. The signal from the system must thus be sufficiently free from ringing.

High demands are put on the electronic switches. Switches with rise/fall-times down to a few ns sustaining 1 kV and 1 MHz repetition rate are commercially available (see e.g. [8]). The difficulty is to find a device which can provide pulse lengths <20 ns, which is a demand of our setup. We have therefore explored a solution where two parallel switches are deployed, as seen in Fig. 3. Each switch is set up to provide a pulse every 2 μs. This frequency is

11th International Conference on Synchrotron Radiation Instrumentation (SRI 2012) IOP Publishing
Journal of Physics: Conference Series **425** (2013) 092011 doi:10.1088/1742-6596/425/9/092011

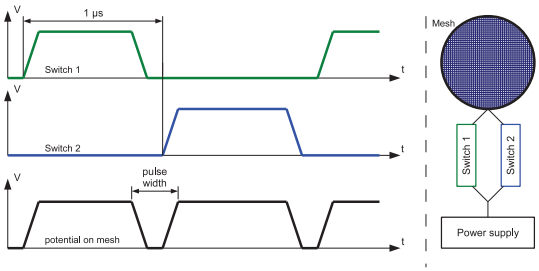

Figure 3. Two parallel switches feed the pulser mesh. Each blocking pulse is started by an external trigger determined by the ring frequency. The pulse is set to end after a predetermined time, just before the start of the next blocking pulse. (Graphs are not to scale.)

synchronized to the frequency of the light pulses, which can be extracted with a photo-diode in the experimental chamber, or obtained from a bunch marker from the ring. The switch is set up to close after a predetermined time just long enough to create the <20 ns time-window needed for the application. With this solution, a short time-window can be created without reducing the pulse length of the switch.

Our calculations have shown that the capacitance of the system can be kept below 10 pF when short wiring is utilized. Considering a maximum 500 V gating potential achieved in 3 ns, the peak current is 2 A, which can be well transferred by available feedthroughs. Considerations must also be given to the potential fall of the device to minimize ringing during the time which the gate is open. The length of the blocking pulse must be defined within a few ns margin of error.

5. Conclusions

We have in this paper shown how an electronic gate can be constructed to allow for time-resolving spectrometers to be used at multi-bunch storage rings. We have discussed how one can mimic single-bunch operation not only by chopping light, but also by blocking ejected electrons from reaching the spectrometer. A setup with a mesh with an applied pulsed blocking potential, in conjunction with a second shielding mesh, have been studied in electrostatic simulations. We have further suggested an electronic setup with two fast switches to overcome inherent restrictions in terms of achieving very short electronic pulses.

References

[1] B. Wannberg, Nucl. Instrum. Methods Phys. Res. A **601**, 182 (2009).
[2] G. Öhrwall *et al.*, J. Electron Spectrosc. Relat. Phenom. **183**, 125 (2011).
[3] *Operating Modi BESSY II* (`http://www.helmholtz-berlin.de/forschung/grossgeraete/betrieb-beschleuniger/betriebsmodi_en.html`).
[4] S. Plogmaker *et al.*, Rev. Sci. Instrum. **83**, 013115 (2012).
[5] Å. Andersson, M. Bergqvist, M. Eriksson, L. Malmgren, and L. Thånell, The 100 mhz rf system for max-ii and max-iii, in *Proceedings of the 8th European Particle Accelerator Conference*, pp. 2118–2120, European Physical Society Interdivisional Group on Accelerators (EPS-IGA) and CERN, 2002.
[6] *Detailed Design Report on the MAX IV Facility*, 1 ed. (`https://www.maxlab.lu.se/node/1136`, 2012).
[7] `http://simion.com/`.
[8] *BEHLKE FSWP 51-02 product sheet* (`http://www.behlke.com/pdf/fswp%2091-01_rs.pdf`, 2012-11-27).